

Neutrino Mixing and Leptonic CP Violation from S_4 Flavour and Generalised CP Symmetries

J. T. Penedo ^{a,1}, S. T. Petcov ^{a,b,2} and A. V. Titov ^{a,3}

^a *SISSA/INFN, Via Bonomea 265, 34136 Trieste, Italy*

^b *Kavli IPMU (WPI), University of Tokyo, 5-1-5 Kashiwanoha, 277-8583 Kashiwa, Japan*

Abstract

We consider a class of models of neutrino mixing with S_4 lepton flavour symmetry combined with a generalised CP symmetry, which are broken to residual Z_2 and $Z_2 \times H_{\text{CP}}^\nu$ symmetries in the charged lepton and neutrino sectors, respectively, H_{CP}^ν being a remnant CP symmetry of the neutrino Majorana mass term. In this set-up the neutrino mixing angles and CP violation (CPV) phases of the neutrino mixing matrix depend on three real parameters — two angles and a phase. We classify all phenomenologically viable mixing patterns and derive predictions for the Dirac and Majorana CPV phases. Further, we use the results obtained on the neutrino mixing angles and leptonic CPV phases to derive predictions for the effective Majorana mass in neutrinoless double beta decay.

¹E-mail: jpenedo@sissa.it

²Also at: Institute of Nuclear Research and Nuclear Energy, Bulgarian Academy of Sciences, 1784 Sofia, Bulgaria.

³E-mail: atitov@sissa.it

1 Introduction

Understanding the origin of the pattern of neutrino mixing that emerged from the neutrino oscillation data in the recent years (see, e.g., [1]) is one of the most challenging problems in neutrino physics. It is part of the more general fundamental problem in particle physics of understanding the origins of flavour in the quark and lepton sectors, i.e., of the patterns of quark masses and mixing, and of the charged lepton and neutrino masses and of neutrino mixing.

The idea of extending the Standard Model (SM) with a non-Abelian discrete flavour symmetry has been widely exploited in attempts to make progress towards the understanding the origin(s) of flavour (for reviews on the discrete symmetry approach to the flavour problem see, e.g., [2–4]). In this approach it is assumed that at a certain high-energy scale the theory possesses a flavour symmetry, which is broken at lower energies to residual symmetries of the charged lepton and neutrino sectors, yielding certain predictions for the values of, and/or correlations between, the low-energy neutrino mixing parameters. In the reference 3-neutrino mixing scheme we are going to consider in what follows (see, e.g., [1]), i) the values of certain pairs of, or of all three, neutrino mixing angles are predicted to be correlated, and/or ii) there is a correlation between the value of the Dirac CP violation (CPV) phase δ in the neutrino mixing matrix and the values of the three neutrino mixing angles¹, θ_{12} , θ_{13} and θ_{23} , which includes also symmetry dependent fixed parameter(s) (see, e.g., [5–12] and references quoted therein). These correlations are usually referred to as “neutrino mixing sum rules”. As we have already indicated, the sum rules for the Dirac phase δ , in particular, depend on the underlying symmetry form of the PMNS matrix [5–9] (see also, e.g., [10–12]), which in turn is determined by the assumed lepton flavour symmetry that typically has to be broken, and by the residual unbroken symmetries in the charged lepton and neutrino sectors (see, e.g., [2–4, 7, 9]). They can be tested experimentally (see, e.g., [6, 10, 13, 14]). These tests can provide unique information about the possible existence of a new fundamental symmetry in the lepton sector, which determines the pattern of neutrino mixing [5]. Sufficiently precise experimental data on the neutrino mixing angles and on the Dirac CPV phase can also be used to distinguish between different possible underlying flavour symmetries leading to viable patterns of neutrino mixing.

While in the discrete flavour symmetry approach at least some of the neutrino mixing angles and/or the Dirac phase are determined (directly or indirectly via a sum rule) by the flavour symmetry, the Majorana CPV phases α_{21} and α_{31} [15] remain unconstrained. The values of the Majorana CPV phases are instead constrained to lie in certain narrow intervals, or are predicted, in theories which in addition to a flavour symmetry possess at a certain high-energy scale a generalised CP (GCP) symmetry [16]. The GCP symmetry should be implemented in a theory based on a discrete flavour symmetry in a way that is consistent with the flavour symmetry [17, 18]. At low energies the GCP symmetry is broken, in general, to residual CP symmetries of the charged lepton and neutrino sectors.

In the scenarios involving a GCP symmetry, which were most widely explored so far (see, e.g., [17, 19–23]), a non-Abelian flavour symmetry G_f consistently combined with a GCP symmetry H_{CP} is broken to residual Abelian symmetries $G_e = Z_n$, $n > 2$, or $Z_m \times Z_k$, $m, k \geq 2$, and $G_\nu = Z_2 \times H'_{\text{CP}}$ of the charged lepton and neutrino mass terms, respectively².

¹Throughout the present study we use the standard parametrisation of the Pontecorvo, Maki, Nakagawa and Sakata (PMNS) neutrino mixing matrix (see, e.g., [1]).

²We note that in refs. [20, 21] the residual symmetry G_e of the charged lepton mass term is augmented with

The factor H_{CP}^ν in G_ν stands for a remnant GCP symmetry of the neutrino mass term. In such a set-up, G_e fixes completely the form of the unitary matrix U_e which diagonalises the product $M_e M_e^\dagger$ and enters into the expression of the PMNS matrix, M_e being the charged lepton mass matrix (in the charged lepton mass term written in the left-right convention). At the same time, G_ν fixes the unitary matrix U_ν , diagonalising the neutrino Majorana mass matrix M_ν up to a single free real parameter — a rotation angle θ^ν . Given the fact that the PMNS neutrino mixing matrix U_{PMNS} is given by the product

$$U_{\text{PMNS}} = U_e^\dagger U_\nu, \quad (1.1)$$

all three neutrino mixing angles are expressed in terms of this rotation angle. In this class of models one obtains specific correlations between the values of the three neutrino mixing angles, while the leptonic CPV phases are typically predicted to be exactly 0 or π , or else $\pi/2$ or $3\pi/2$. For example, in the set-up considered in [17] (see also [19]), based on $G_f \times H_{\text{CP}} = S_4 \times H_{\text{CP}}$ broken to $G_e = Z_3^T$ and $G_\nu = Z_2^S \times H_{\text{CP}}^\nu$ with $H_{\text{CP}}^\nu = \{U, SU\}$ ³, the authors find:

$$\sin^2 \theta_{13} = \frac{2}{3} \sin^2 \theta^\nu, \quad \sin^2 \theta_{12} = \frac{1}{2 + \cos 2\theta^\nu} = \frac{1}{3(1 - \sin^2 \theta_{13})}, \quad \sin^2 \theta_{23} = \frac{1}{2}, \quad (1.2)$$

$$|\sin \delta| = 1, \quad \sin \alpha_{21} = \sin \alpha_{31} = 0. \quad (1.3)$$

It follows, in particular, from the results on the neutrino oscillation parameters — best fit values, 2σ and 3σ allowed ranges — obtained in the latest global fit of neutrino oscillation data [24] and summarised in Table 1, to be used in our further analysis⁴, that the predictions quoted in eq. (1.2) for $\sin^2 \theta_{12}$ and $\sin^2 \theta_{23}$ lie outside of their respective currently allowed 2σ ranges⁵.

Another example of one-parametric models is the extensive study performed in [26], in which the authors have considered two different residual symmetry patterns. The first pattern is the one described above, and the second pattern has $G_e = Z_2 \times H_{\text{CP}}^e$ and $G_\nu = Z_2 \times Z_2 \times H_{\text{CP}}^\nu$ as residual symmetries in the charged lepton and neutrino sectors, respectively. The authors have performed an exhaustive scan over discrete groups of order less than 2000, which admit faithful 3-dimensional irreducible representations, and classified phenomenologically viable mixing patterns.

Theoretical models based on the approach to neutrino mixing that combines discrete symmetries and GCP invariance, in which the neutrino mixing angles and the leptonic CPV phases are functions of two or three parameters have also been considered in the literature (see, e.g., [27–30]). In these models the residual symmetry G_e of the charged lepton mass term is typically assumed to be a Z_2 symmetry or to be fully broken. In spite of the larger number of parameters in terms of which the neutrino mixing angles and the leptonic CPV phases are expressed, the values of the CPV phases are still predicted to be correlated with the values of

a remnant CP symmetry H_{CP}^e as well.

³ S , T and U are the generators of S_4 in the basis for its 3-dimensional representation we employ in this work (see subsection 3.2).

⁴The results on the neutrino oscillation parameters obtained in the global fit performed in [25] differ somewhat from, but are compatible at 1σ confidence level (C.L.) with, those found in [24] and given in Table 1.

⁵We have used the best fit value of $\sin^2 \theta_{13}$ to obtain the prediction of $\sin^2 \theta_{12}$ leading to the quoted conclusion. Using the 2σ allowed range for $\sin^2 \theta_{13}$ leads to a minimal value of $\sin^2 \theta_{12} = 0.340$, which is above the maximal allowed value of $\sin^2 \theta_{12}$ at 2σ C.L., but inside its 3σ range.

Parameter	Best fit value	2σ range	3σ range
$\sin^2 \theta_{12}/10^{-1}$	2.97	2.65 – 3.34	2.50 – 3.54
$\sin^2 \theta_{13}/10^{-2}$ (NO)	2.15	1.99 – 2.31	1.90 – 2.40
$\sin^2 \theta_{13}/10^{-2}$ (IO)	2.16	1.98 – 2.33	1.90 – 2.42
$\sin^2 \theta_{23}/10^{-1}$ (NO)	4.25	3.95 – 4.70	3.81 – 6.15
$\sin^2 \theta_{23}/10^{-1}$ (IO)	5.89	$3.99 - 4.83 \oplus 5.33 - 6.21$	3.84 – 6.36
δ/π (NO)	1.38	1.00 – 1.90	$0 - 0.17 \oplus 0.76 - 2$
δ/π (IO)	1.31	0.92 – 1.88	$0 - 0.15 \oplus 0.69 - 2$
$\Delta m_{21}^2/10^{-5} \text{ eV}^2$	7.37	7.07 – 7.73	6.93 – 7.96
$\Delta m_{31}^2/10^{-3} \text{ eV}^2$ (NO)	2.56	2.49 – 2.64	2.45 – 2.69
$\Delta m_{23}^2/10^{-3} \text{ eV}^2$ (IO)	2.54	2.47 – 2.62	2.42 – 2.66

Table 1: The best fit values, 2σ and 3σ ranges of the neutrino oscillation parameters obtained in the global analysis of the neutrino oscillation data performed in [24].

the three neutrino mixing angles. A set-up with $G_e = Z_2 \times H_{\text{CP}}^e$ and $G_\nu = Z_2 \times H_{\text{CP}}^\nu$ has been considered in [30]. The resulting PMNS matrix in such a scheme depends on two free real parameters — two angles θ^ν and θ^e . The authors have obtained several phenomenologically viable neutrino mixing patterns from $G_f = S_4$ combined with H_{CP} , broken to all possible residual symmetries of the type indicated above. Models allowing for three free parameters have been investigated in [27–29]. In, e.g., [28], the author has considered $G_f = A_5$ combined with H_{CP} , which are broken to $G_e = Z_2$ and $G_\nu = Z_2 \times H_{\text{CP}}^\nu$. In this case, the matrix U_e depends on an angle θ^e and a phase δ^e , while the matrix U_ν depends on an angle θ^ν . In these two scenarios the leptonic CPV phases possess non-trivial values.

The specific correlations between the values of the three neutrino mixing angles, which characterise the one-parameter models based on $G_e = Z_n$, $n > 2$, or $Z_m \times Z_k$, $m, k \geq 2$, and $G_\nu = Z_2 \times H_{\text{CP}}^\nu$, do not hold in the two- and three-parameter models. In addition, the Dirac CPV phase in the two- and three-parameter models is predicted to have non-trivial values which are correlated with the values of the three neutrino mixing angles and differ from 0 , π , $\pi/2$ and $3\pi/2$, although the deviations from, e.g., $3\pi/2$ can be relatively small. The indicated differences between the predictions of the models based on $G_e = Z_n$, $n > 2$, or $Z_m \times Z_k$, $m, k \geq 2$, and on $G_e = Z_2$ symmetries make it possible to distinguish between them experimentally by improving the precision on each of the three measured neutrino mixing angles θ_{12} , θ_{23} and θ_{13} , and by performing a sufficiently precise measurement of the Dirac phase δ .

In the present article, we investigate the possible neutrino mixing patterns generated by a $G_f = S_4$ symmetry combined with an H_{CP} symmetry when these symmetries are broken down to $G_e = Z_2$ and $G_\nu = Z_2 \times H_{\text{CP}}^\nu$. In Section 2, we describe a general framework for deriving the form of the PMNS matrix, dictated by the chosen residual symmetries. Then, in Section 3, we apply this framework to $G_f = S_4$ combined with H_{CP} and obtain all phenomenologically viable mixing patterns. Next, in Section 4, using the obtained predictions for the neutrino mixing angles and the Dirac and Majorana CPV phases, we derive predictions for the neutrinoless double beta decay effective Majorana mass. Section 5 contains the

conclusions of the present study.

2 The Framework

We start with a non-Abelian flavour symmetry group G_f , which admits a faithful irreducible 3-dimensional representation ρ . The three generations of left-handed (LH) leptons are assigned to this representation. Apart from that, the high-energy theory respects also the GCP symmetry H_{CP} , which is implemented consistently along with the flavour symmetry. At some flavour symmetry breaking scale $G_f \times H_{\text{CP}}$ gets broken down to residual symmetries G_e and G_ν of the charged lepton and neutrino mass terms, respectively. The residual flavour symmetries are Abelian subgroups of G_f . The symmetries G_e and G_ν significantly constrain the form of the neutrino mixing matrix U_{PMNS} , as we demonstrate below.

2.1 The PMNS Matrix from $G_e = Z_2$ and $G_\nu = Z_2 \times H_{\text{CP}}^\nu$

We choose G_e to be a Z_2 symmetry. We will denote it as $Z_2^{g_e} \equiv \{1, g_e\}$, $g_e^2 = 1$ being an element of G_f of order two, generating the $Z_2^{g_e}$ subgroup. The invariance of the charged lepton mass term under G_e implies

$$\rho(g_e)^\dagger M_e M_e^\dagger \rho(g_e) = M_e M_e^\dagger. \quad (2.1)$$

Below we show how this invariance constrains the form of the unitary matrix U_e , diagonalising $M_e M_e^\dagger$:

$$U_e^\dagger M_e M_e^\dagger U_e = \text{diag}(m_e^2, m_\mu^2, m_\tau^2). \quad (2.2)$$

Lets Ω_e be a diagonalising unitary matrix of $\rho(g_e)$, such that

$$\Omega_e^\dagger \rho(g_e) \Omega_e = \rho(g_e)^d \equiv \text{diag}(1, -1, -1). \quad (2.3)$$

This result is obtained as follows. The diagonal entries of $\rho(g_e)^d$ are constrained to be ± 1 , since this matrix must still furnish a representation of Z_2 and hence its square is the identity. We have assumed that the trace of $\rho(g_e)$ is -1 , for the relevant elements g_e , as it is the case for the 3-dimensional representation of S_4 we will consider later on ⁶. Note that we can take the order of the eigenvalues of $\rho(g_e)$ as given in eq. (2.3) without loss of generality, as will become clear later.

Expressing $\rho(g_e)$ from eq. (2.3) and substituting it in eq. (2.1), we obtain

$$\rho(g_e)^d \Omega_e^\dagger M_e M_e^\dagger \Omega_e \rho(g_e)^d = \Omega_e^\dagger M_e M_e^\dagger \Omega_e. \quad (2.4)$$

This equation implies that $\Omega_e^\dagger M_e M_e^\dagger \Omega_e$ has the block-diagonal form

$$\begin{pmatrix} \times & 0 & 0 \\ 0 & \times & \times \\ 0 & \times & \times \end{pmatrix}, \quad (2.5)$$

⁶ For the other 3-dimensional irreducible representation of S_4 the trace can be either -1 or $+1$, depending on g_e . Choosing $+1$ would simply imply a change of sign of $\rho(g_e)^d$, which however does not lead to new constraints. The conclusions we reach in what follows are then independent of the choice of 3-dimensional representation.

and, since this matrix is hermitian, it can be diagonalised by a unitary matrix with a $U(2)$ transformation acting on the 2-3 block. In the general case, the $U(2)$ transformation can be parametrised as follows:

$$\begin{pmatrix} \cos \theta^e & -\sin \theta^e e^{-i\delta^e} \\ \sin \theta^e e^{i\delta^e} & \cos \theta^e \end{pmatrix} \begin{pmatrix} e^{i\beta_1^e} & 0 \\ 0 & e^{i\beta_2^e} \end{pmatrix}. \quad (2.6)$$

The diagonal phase matrix is, however, unphysical, since it can be eliminated by rephasing of the charged lepton fields, and we will not keep it in the future. Thus, we arrive to the conclusion that the matrix U_e diagonalising $M_e M_e^\dagger$ reads

$$U_e = \Omega_e U_{23}(\theta^e, \delta^e)^\dagger P_e^T, \quad (2.7)$$

with

$$U_{23}(\theta^e, \delta^e) = \begin{pmatrix} 1 & 0 & 0 \\ 0 & \cos \theta^e & \sin \theta^e e^{-i\delta^e} \\ 0 & -\sin \theta^e e^{i\delta^e} & \cos \theta^e \end{pmatrix}, \quad (2.8)$$

and P_e being one of six permutation matrices, which need to be taken into account, since in the approach under consideration the order of the charged lepton masses is unknown. The six permutation matrices read:

$$P_{123} = \begin{pmatrix} 1 & 0 & 0 \\ 0 & 1 & 0 \\ 0 & 0 & 1 \end{pmatrix}, \quad P_{132} = \begin{pmatrix} 1 & 0 & 0 \\ 0 & 0 & 1 \\ 0 & 1 & 0 \end{pmatrix}, \quad P_{213} = \begin{pmatrix} 0 & 1 & 0 \\ 1 & 0 & 0 \\ 0 & 0 & 1 \end{pmatrix}, \quad (2.9)$$

$$P_{231} = \begin{pmatrix} 0 & 1 & 0 \\ 0 & 0 & 1 \\ 1 & 0 & 0 \end{pmatrix}, \quad P_{312} = \begin{pmatrix} 0 & 0 & 1 \\ 1 & 0 & 0 \\ 0 & 1 & 0 \end{pmatrix}, \quad P_{321} = \begin{pmatrix} 0 & 0 & 1 \\ 0 & 1 & 0 \\ 1 & 0 & 0 \end{pmatrix}. \quad (2.10)$$

Note that the order of indices in P_{ijk} stands for the order of rows, i.e., when applied from the left to a matrix, it gives the desired order, i - j - k , of the matrix rows. The same is also true for columns, when P_{ijk} is applied from the right, except for P_{231} which leads to the 3-1-2 order of columns and P_{312} yielding the 2-3-1 order.

In the neutrino sector we have a $G_\nu = Z_2 \times H_{\text{CP}}^\nu$ residual symmetry. We will denote the Z_2 symmetry of the neutrino mass matrix as $Z_2^{g_\nu} \equiv \{1, g_\nu\}$, with $g_\nu^2 = 1$ being an element of G_f , generating the $Z_2^{g_\nu}$ subgroup. $H_{\text{CP}}^\nu = \{X_\nu\}$ is the set of remnant GCP unitary transformations X_ν forming a residual CP symmetry of the neutrino mass matrix. H_{CP}^ν is contained in $H_{\text{CP}} = \{X\}$ which is the GCP symmetry of the high-energy theory consistently defined along with the flavour symmetry G_f ⁷. The invariance under G_ν of the neutrino mass

⁷It is worth to comment here on the notation H_{CP}^ν we use. When we write in what follows $H_{\text{CP}}^\nu = \{X_{\nu 1}, X_{\nu 2}\}$, we mean a set of GCP transformations ($X_{\nu 1}$ and $X_{\nu 2}$) compatible with the residual flavour $Z_2^{g_\nu}$ symmetry (see eq. (2.13)). However, when writing $G_\nu = Z_2^{g_\nu} \times H_{\text{CP}}^\nu$, H_{CP}^ν is intended to be a group generated by $X_{\nu 1}$. Namely, following Appendix B in [17], H_{CP}^ν is isomorphic to $\{\mathcal{I}, \mathcal{X}_{\nu 1}\}$, where \mathcal{I} is the unit matrix and

$$\mathcal{X}_{\nu 1} = \begin{pmatrix} 0 & X_{\nu 1} \\ X_{\nu 1}^* & 0 \end{pmatrix},$$

both of them acting on $(\varphi, \varphi^*)^T$. Then, $Z_2^{g_\nu}$ is isomorphic to $\{\mathcal{I}, \mathcal{G}_\nu\}$, where

$$\mathcal{G}_\nu = \begin{pmatrix} \rho(g_\nu) & 0 \\ 0 & \rho^*(g_\nu) \end{pmatrix}$$

matrix implies that the following two equations hold:

$$\rho(g_\nu)^T M_\nu \rho(g_\nu) = M_\nu, \quad (2.11)$$

$$X_\nu^T M_\nu X_\nu = M_\nu^*. \quad (2.12)$$

In addition, the consistency condition between $Z_2^{g_\nu}$ and H_{CP}^ν has to be respected:

$$X_\nu \rho^*(g_\nu) X_\nu^{-1} = \rho(g_\nu). \quad (2.13)$$

To derive the form of the unitary matrix U_ν diagonalising the neutrino Majorana mass matrix M_ν as

$$U_\nu^T M_\nu U_\nu = \text{diag}(m_1, m_2, m_3), \quad (2.14)$$

$m_j > 0$ being the neutrino masses, we will follow the method presented in [30].

Lets $\Omega_{\nu 1}$ be a diagonalising unitary matrix of $\rho(g_\nu)$, such that

$$\Omega_{\nu 1}^\dagger \rho(g_\nu) \Omega_{\nu 1} = \rho(g_\nu)^{\text{d}} \equiv \text{diag}(1, -1, -1). \quad (2.15)$$

Expressing $\rho(g_\nu)$ from this equation and substituting it in the consistency condition, eq. (2.13), we find

$$\rho(g_\nu)^{\text{d}} \Omega_{\nu 1}^\dagger X_\nu \Omega_{\nu 1}^* \rho(g_\nu)^{\text{d}} = \Omega_{\nu 1}^\dagger X_\nu \Omega_{\nu 1}^*, \quad (2.16)$$

meaning that $\Omega_{\nu 1}^\dagger X_\nu \Omega_{\nu 1}^*$ is a block-diagonal matrix, having the form of eq. (2.5). Moreover, this matrix is symmetric, since the GCP transformations X_ν have to be symmetric in order for all the three neutrino masses to be different [17, 19], as is required by the data. In Appendix A we provide a proof of this. Being a complex (unitary) symmetric matrix, it is diagonalised by a unitary matrix $\Omega_{\nu 2}$ via the transformation:

$$\Omega_{\nu 2}^\dagger (\Omega_{\nu 1}^\dagger X_\nu \Omega_{\nu 1}^*) \Omega_{\nu 2}^* = (\Omega_{\nu 1}^\dagger X_\nu \Omega_{\nu 1}^*)^{\text{d}}. \quad (2.17)$$

The matrix $(\Omega_{\nu 1}^\dagger X_\nu \Omega_{\nu 1}^*)^{\text{d}}$ is, in general, a diagonal phase matrix. However, we can choose $(\Omega_{\nu 1}^\dagger X_\nu \Omega_{\nu 1}^*)^{\text{d}} = \text{diag}(1, 1, 1)$ as the phases of $(\Omega_{\nu 1}^\dagger X_\nu \Omega_{\nu 1}^*)^{\text{d}}$ can be moved to the matrix $\Omega_{\nu 2}$. With this choice we obtain the Takagi factorisation of the X_ν (valid for unitary symmetric matrices):

$$X_\nu = \Omega_\nu \Omega_\nu^T, \quad (2.18)$$

with $\Omega_\nu = \Omega_{\nu 1} \Omega_{\nu 2}$.

Since, as we have noticed earlier, $\Omega_{\nu 1}^\dagger X_\nu \Omega_{\nu 1}^*$ has the form of eq. (2.5), the matrix $\Omega_{\nu 2}$ can be chosen without loss of generality to have the form of eq. (2.5) with a unitary 2×2 matrix in the 2-3 block. This implies that the matrix $\Omega_\nu = \Omega_{\nu 1} \Omega_{\nu 2}$ also diagonalises $\rho(g_\nu)$. Indeed,

$$\Omega_\nu^\dagger \rho(g_\nu) \Omega_\nu = \Omega_{\nu 2}^\dagger \rho(g_\nu)^{\text{d}} \Omega_{\nu 2} = \rho(g_\nu)^{\text{d}}, \quad (2.19)$$

where we have used eq. (2.15).

We substitute next X_ν from eq. (2.18) in the GCP invariance condition of the neutrino mass matrix, eq. (2.12), and find that the matrix $\Omega_\nu^T M_\nu \Omega_\nu$ is real. Furthermore, this is a

acts again on $(\varphi, \varphi^*)^T$. Finally, it is not difficult to convince oneself that the full residual symmetry group G_ν is given by a direct product $Z_2^{g_\nu} \times H_{\text{CP}}^\nu$, and the second GCP transformation $X_{\nu 2} = \rho(g_\nu) X_{\nu 1}$ is contained in it. The same logic applies to the notation H_{CP} , and, as has been shown in Appendix B of [17], the full symmetry group is a semi-direct product $G_f \rtimes H_{\text{CP}}$. Note that these notations are widely used in the literature.

symmetric matrix, since the neutrino Majorana mass matrix M_ν is symmetric. A real symmetric matrix can be diagonalised by a real orthogonal transformation. Employing eqs. (2.19) and (2.11), we have

$$\rho(g_\nu)^d \Omega_\nu^T M_\nu \Omega_\nu \rho(g_\nu)^d = \Omega_\nu^T M_\nu \Omega_\nu, \quad (2.20)$$

implying that $\Omega_\nu^T M_\nu \Omega_\nu$ is a block-diagonal matrix as in eq. (2.5). Thus, the required orthogonal transformation is a rotation in the 2-3 plane on an angle θ^ν :

$$R_{23}(\theta^\nu) = \begin{pmatrix} 1 & 0 & 0 \\ 0 & \cos \theta^\nu & \sin \theta^\nu \\ 0 & -\sin \theta^\nu & \cos \theta^\nu \end{pmatrix}. \quad (2.21)$$

Finally, the matrix U_ν diagonalising M_ν reads

$$U_\nu = \Omega_\nu R_{23}(\theta^\nu) P_\nu Q_\nu, \quad (2.22)$$

where P_ν is one of the six permutation matrices, which accounts for different order of m_j , and the matrix Q_ν renders them positive. Without loss of generality Q_ν can be parametrised as follows:

$$Q_\nu = \text{diag}(1, i^{k_1}, i^{k_2}), \quad \text{with } k_{1,2} = 0, 1. \quad (2.23)$$

Assembling together the results for U_e and U_ν , eqs. (2.7) and (2.22), we obtain for the form of the PMNS matrix:

$$U_{\text{PMNS}} = P_e U_{23}(\theta^e, \delta^e) \Omega_e^\dagger \Omega_\nu R_{23}(\theta^\nu) P_\nu Q_\nu. \quad (2.24)$$

Thus, in the approach we are following the PMNS matrix depends on three free real parameters⁸ — the two angles θ^e and θ^ν and the phase δ^e . One of the elements of the PMNS matrix is fixed to be a constant by the employed residual symmetries. We note finally that, since $R_{23}(\theta^\nu + \pi) = R_{23}(\theta^\nu) \text{diag}(1, -1, -1)$, where the diagonal matrix can be absorbed into Q_ν , and $U_{23}(\theta^e + \pi, \delta^e) = \text{diag}(1, -1, -1) U_{23}(\theta^e, \delta^e)$, where the diagonal matrix contributes to the unphysical charged lepton phases, it is sufficient to consider θ^e and θ^ν in the interval $[0, \pi)$.

2.2 Conjugate Residual Symmetries

In this subsection we briefly recall why the residual symmetries G'_e and G'_ν conjugate to G_e and G_ν , respectively, under the same element of the flavour symmetry group G_f lead to the same PMNS matrix (see, e.g., [17, 20]). Two pairs of residual symmetries $\{Z_2^{g_e}, Z_2^{g_\nu}\}$ and $\{Z_2^{g'_e}, Z_2^{g'_\nu}\}$ are conjugate to each other under $h \in G_f$ if

$$h g_e h^{-1} = g'_e \quad \text{and} \quad h g_\nu h^{-1} = g'_\nu. \quad (2.25)$$

At the representation level this means

$$\rho(h) \rho(g_e) \rho(h)^\dagger = \rho(g'_e) \quad \text{and} \quad \rho(h) \rho(g_\nu) \rho(h)^\dagger = \rho(g'_\nu). \quad (2.26)$$

⁸It should be noted that the matrix $\Omega_{\nu 2}$ in eq. (2.17) with $(\Omega_{\nu 1}^\dagger X_\nu \Omega_{\nu 1}^*)^d = \text{diag}(1, 1, 1)$, and thus the matrix $\Omega_\nu = \Omega_{\nu 1} \Omega_{\nu 2}$ in eq. (2.18), is determined up to a multiplication by an orthogonal matrix O on the right. The matrix $\Omega_{\nu 2} O$ must be unitary since it diagonalises a complex symmetric matrix, which implies that O must be unitary in addition of being orthogonal, and therefore must be a real matrix. Equation (2.19) restricts further this real orthogonal matrix O to have the form of a real rotation in the 2-3 plane, which can be “absorbed” in the $R_{23}(\theta^\nu)$ matrix in eq. (2.24).

Substituting $\rho(g_e)$ and $\rho(g_\nu)$ from these equalities to eqs. (2.1) and (2.11), respectively, we obtain

$$\rho(g_e)^\dagger M'_e M_e'^\dagger \rho(g_e) = M'_e M_e'^\dagger \quad \text{and} \quad \rho(g_\nu)^T M'_\nu \rho(g_\nu) = M'_\nu, \quad (2.27)$$

where the primed mass matrices are related to the original ones as

$$M'_e M_e'^\dagger = \rho(h) M_e M_e^\dagger \rho(h)^\dagger \quad \text{and} \quad M'_\nu = \rho(h)^* M_\nu \rho(h)^\dagger. \quad (2.28)$$

As can be understood from eq. (2.12) (or eq. (2.13)), the matrix M'_ν will respect a remnant CP symmetry $H'_{\text{CP}} = \{X'_\nu\}$, which is related to $H_{\text{CP}} = \{X_\nu\}$ as follows:

$$X'_\nu = \rho(h) X_\nu \rho(h)^T. \quad (2.29)$$

Obviously, the unitary transformations U'_e and U'_ν diagonalising the primed mass matrices are given by

$$U'_e = \rho(h) U_e \quad \text{and} \quad U'_\nu = \rho(h) U_\nu, \quad (2.30)$$

thus yielding

$$U'_{\text{PMNS}} = U_e'^\dagger U'_\nu = U_e^\dagger U_\nu = U_{\text{PMNS}}. \quad (2.31)$$

2.3 Phenomenologically Non-Viable Cases

Here we demonstrate that at least two types of residual symmetries $\{G_e, G_\nu\} = \{Z_2^{g_e}, Z_2^{g_\nu} \times H_{\text{CP}}^\nu\}$, characterised by certain g_e and g_ν , cannot lead to phenomenologically viable form of the PMNS matrix.

• **Type I:** $g_e = g_\nu$. In this case, we can choose $\Omega_e = \Omega_\nu P$, with P_{123} or P_{132} . Then, eq. (2.24) yields

$$U_{\text{PMNS}} = P_e U_{23}(\theta^e, \delta^e) P R_{23}(\theta^\nu) P_\nu Q_\nu. \quad (2.32)$$

This means that up to permutations of the rows and columns U_{PMNS} has the form of eq. (2.5), i.e., contains four zero entries, which are ruled out by neutrino oscillation data [24, 25].

• **Type II:** $g_e, g_\nu \in Z_2 \times Z_2 \subset G_f$. Now we consider two different order two elements $g_e \neq g_\nu$, which belong to the same $Z_2 \times Z_2 = \{1, g_e, g_\nu, g_e g_\nu\}$ subgroup of G_f . In this case, since g_e and g_ν commute, there exists a unitary matrix simultaneously diagonalising both $\rho(g_e)$ and $\rho(g_\nu)$. Note, however, that the order of eigenvalues in the resulting diagonal matrices will be different. Namely, lets $\Omega_{\nu 1}$ be a diagonalising matrix of $\rho(g_\nu)$ and $\rho(g_e)$, and lets $\Omega_{\nu 1}$ diagonalise $\rho(g_\nu)$ as in eq. (2.15). Then, $\Omega_{\nu 1}^\dagger \rho(g_e) \Omega_{\nu 1}$ can yield either $\text{diag}(-1, 1, -1)$ or $\text{diag}(-1, -1, 1)$, but not $\text{diag}(1, -1, -1)$. Hence, Ω_e diagonalising $\rho(g_e)$ as in eq. (2.3), must read

$$\Omega_e = \Omega_{\nu 1} P, \quad \text{with} \quad P = P_{213} \text{ or } P_{312} \quad \text{if} \quad \Omega_{\nu 1}^\dagger \rho(g_e) \Omega_{\nu 1} = \text{diag}(-1, 1, -1), \quad (2.33)$$

$$\text{and} \quad P = P_{231} \text{ or } P_{321} \quad \text{if} \quad \Omega_{\nu 1}^\dagger \rho(g_e) \Omega_{\nu 1} = \text{diag}(-1, -1, 1). \quad (2.34)$$

Taking into account that $\Omega_\nu = \Omega_{\nu 1} \Omega_{\nu 2}$, with $\Omega_{\nu 2}$ of the block-diagonal form given in eq. (2.5), we obtain

$$U_{\text{PMNS}} = P_e U_{23}(\theta^e, \delta^e) P^T \Omega_{\nu 2} R_{23}(\theta^\nu) P_\nu Q_\nu, \quad (2.35)$$

where $P^T \Omega_{\nu 2}$, depending on P , can take one of the following forms:

$$\begin{pmatrix} 0 & \times & \times \\ \times & 0 & 0 \\ 0 & \times & \times \end{pmatrix} \quad \text{or} \quad \begin{pmatrix} 0 & \times & \times \\ 0 & \times & \times \\ \times & 0 & 0 \end{pmatrix}. \quad (2.36)$$

As a consequence, U_{PMNS} up to permutations of the rows and columns has the form

$$\begin{pmatrix} 0 & \times & \times \\ \times & \times & \times \\ \times & \times & \times \end{pmatrix}, \quad (2.37)$$

containing one zero element, which is ruled out by the data.

3 Mixing Patterns from $G_f \rtimes H_{\text{CP}} = S_4 \rtimes H_{\text{CP}}$ Broken to $G_e = Z_2$ and $G_\nu = Z_2 \times H_{\text{CP}}^\nu$

3.1 Group S_4 and Residual Symmetries

S_4 is the symmetric group of permutations of four objects. This group is isomorphic to the group of rotational symmetries of the cube. S_4 can be defined in terms of three generators S , T and U , satisfying [31]

$$S^2 = T^3 = U^2 = (ST)^3 = (SU)^2 = (TU)^2 = (STU)^4 = 1. \quad (3.1)$$

From 24 elements of the group there are nine elements of order two, which belong to two of five conjugacy classes of S_4 (see, e.g., [19]):

$$3\mathcal{C}_2 : \{S, TST^2, T^2ST\}, \quad (3.2)$$

$$6\mathcal{C}'_2 : \{U, TU, SU, T^2U, STSU, ST^2SU\}. \quad (3.3)$$

Each of these nine elements generates a corresponding Z_2 subgroup of S_4 . Each subgroup can be the residual symmetry of $M_e M_e^\dagger$, and, combined with compatible CP transformations, yield the residual symmetry of M_ν . Hence, we have 81 possible pairs of only residual flavour symmetries (taking into account remnant CP symmetries increases the number of possibilities). Many of them, however, being conjugate to each other, will lead to the same form of the PMNS matrix, as explained in subsection 2.2. Thus, we first identify the pairs of elements $\{g_e, g_\nu\}$, which are not related by the similarity transformation given in eq. (2.25). We find nine distinct cases for which $\{g_e, g_\nu\}$ can be chosen as

$$\{S, S\}, \quad \{U, U\}, \quad \{T^2ST, S\}, \quad \{S, U\}, \quad \{U, S\}, \quad \{SU, U\}, \quad (3.4)$$

$$\{S, TU\}, \quad \{TU, S\}, \quad \{TU, U\}. \quad (3.5)$$

The pair $\{S, S\}$ is obviously conjugate to $\{TST^2, TST^2\}$ and $\{T^2ST, T^2ST\}$, while $\{U, U\}$ is conjugate to $\{g_e, g_\nu\}$ with $g_e = g_\nu$ being one of the remaining five elements from conjugacy class $6\mathcal{C}'_2$ given in eq. (3.3). The pairs $\{T^2ST, S\}$, $\{S, U\}$, $\{U, S\}$ and $\{SU, U\}$ are conjugate to five pairs each, and $\{S, TU\}$ and $\{TU, S\}$ to eleven pairs each. Finally, $\{TU, U\}$ is conjugate to 23 pairs. As it should be, the total number of pairs yields 81. The complete lists of pairs of elements which are conjugate to each of these nine pairs are given in Appendix B.

The cases in eq. (3.4) do not lead to phenomenologically viable results. The first two of them belong to the cases of Type I (see subsection 2.3). The remaining four belong to Type II, since S_4 contains $Z_2^S \times Z_2^{TST^2} = \{1, S, TST^2, T^2ST\}$ and $Z_2^S \times Z_2^U = \{1, S, U, SU\}$ subgroups (see, e.g., [32]). Thus, we are left with three cases in eq. (3.5).

We have chosen g_ν in such a way that it is S, U or TU for all the cases in eq. (3.5). Now we need to identify the remnant CP transformations X_ν compatible with each of these three elements. It is known that the GCP symmetry $H_{\text{CP}} = \{X\}$ compatible with $G_f = S_4$ is of the same form of G_f itself [18], i.e.,

$$X = \rho(g), \quad g \in S_4. \quad (3.6)$$

Thus, to find X_ν compatible with g_ν of interest, we need to select those $X = \rho(g)$, which i) satisfy the consistency condition in eq. (2.13) and ii) are symmetric in order to avoid partially degenerate neutrino mass spectrum, as was noted earlier. The result reads ⁹:

$$X_\nu = 1, (S), U, (SU), TST^2U, (T^2STU) \quad \text{for } g_\nu = S; \quad (3.7)$$

$$X_\nu = 1, (U), S, (SU) \quad \text{for } g_\nu = U; \quad (3.8)$$

$$X_\nu = U, (T), STS, (T^2STU) \quad \text{for } g_\nu = TU. \quad (3.9)$$

A GCP transformation in parentheses appears automatically to be a remnant CP symmetry of M_ν , if X_ν which precedes this in the list is a remnant CP symmetry. This is a consequence of eqs. (2.11) and (2.12), which imply that if X_ν is a residual CP symmetry of M_ν , then $\rho(g_\nu)X_\nu$ is a residual CP symmetry as well. Therefore, we have three sets of remnant CP transformations compatible with Z_2^S , namely, $H_{\text{CP}}^\nu = \{1, S\}$, $\{U, SU\}$ and $\{TST^2U, T^2STU\}$, two sets compatible with Z_2^U , which are $H_{\text{CP}}^\nu = \{1, U\}$ and $\{S, SU\}$, and two sets consistent with Z_2^{TU} , which read $H_{\text{CP}}^\nu = \{U, T\}$ and $\{STS, T^2STU\}$. Taking them into account, we end up with seven possible pairs of residual symmetries $\{G_e, G_\nu\} = \{Z_2^{g_e}, Z_2^{g_\nu} \times H_{\text{CP}}^\nu\}$, with $\{g_e, g_\nu\}$ as in eq. (3.5). In what follows, we will consider them case by case and classify all phenomenologically viable mixing patterns they lead to.

Before starting, however, let us recall the current knowledge on the absolute values of the PMNS matrix elements, which we will use in what follows. The 3σ ranges of the absolute values of the PMNS matrix elements read [33]

$$|U_{\text{PMNS}}|_{3\sigma} = \begin{pmatrix} 0.796 \rightarrow 0.855 & 0.497 \rightarrow 0.587 & 0.140 \rightarrow 0.153 \\ 0.245 \rightarrow 0.513 & 0.543 \rightarrow 0.709 & 0.614 \rightarrow 0.768 \\ 0.244 \rightarrow 0.510 & 0.456 \rightarrow 0.642 & 0.624 \rightarrow 0.776 \end{pmatrix} \quad (3.10)$$

for the neutrino mass spectrum with normal ordering (NO), and

$$|U_{\text{PMNS}}|_{3\sigma} = \begin{pmatrix} 0.796 \rightarrow 0.855 & 0.497 \rightarrow 0.587 & 0.140 \rightarrow 0.153 \\ 0.223 \rightarrow 0.503 & 0.452 \rightarrow 0.703 & 0.614 \rightarrow 0.783 \\ 0.257 \rightarrow 0.526 & 0.464 \rightarrow 0.712 & 0.605 \rightarrow 0.775 \end{pmatrix} \quad (3.11)$$

for the neutrino mass spectrum with inverted ordering (IO). The ranges in eqs. (3.10) and (3.11) differ a little from the results obtained in [25].

⁹For notation simplicity we will not write the representation symbol ρ , keeping in mind that $X_\nu = g$ means $X_\nu = \rho(g)$ with $g \in G_f$.

3.2 Explicit Forms of the PMNS Matrix

First, we present an explicit example of constructing the PMNS matrix in the case of $g_e = S$, $g_\nu = TU$ and $H_{\text{CP}}^\nu = \{U, T\}$, which is the first case out of the seven potentially viable cases indicated above. We will work in the basis for S_4 from [34], in which the matrices for the generators S , T and U in the 3-dimensional representation read

$$S = \frac{1}{3} \begin{pmatrix} -1 & 2 & 2 \\ 2 & -1 & 2 \\ 2 & 2 & -1 \end{pmatrix}, \quad T = \begin{pmatrix} 1 & 0 & 0 \\ 0 & \omega^2 & 0 \\ 0 & 0 & \omega \end{pmatrix} \quad \text{and} \quad U = - \begin{pmatrix} 1 & 0 & 0 \\ 0 & 0 & 1 \\ 0 & 1 & 0 \end{pmatrix}, \quad (3.12)$$

where $\omega = e^{2\pi i/3}$. For simplicity we use the same notation (S , T and U) for the generators and their 3-dimensional representation matrices. We will follow the procedure described in subsection 2.1. The matrix Ω_e which diagonalises $\rho(g_e) = S$ (see eq. (2.3)) is given by

$$\Omega_e = \frac{1}{\sqrt{6}} \begin{pmatrix} \sqrt{2} & -\sqrt{3} & -1 \\ \sqrt{2} & 0 & 2 \\ \sqrt{2} & \sqrt{3} & -1 \end{pmatrix}. \quad (3.13)$$

The matrix Ω_ν , such that $\Omega_\nu \Omega_\nu^T = U$ (see eq. (2.18)), reads

$$\Omega_\nu = \frac{1}{\sqrt{2}} \begin{pmatrix} 0 & 0 & \sqrt{2}i \\ e^{\frac{2\pi i}{3}} & -e^{\frac{i\pi}{6}} & 0 \\ e^{\frac{i\pi}{3}} & e^{-\frac{i\pi}{6}} & 0 \end{pmatrix}. \quad (3.14)$$

Using the master formula in eq. (2.24), we obtain that up to permutations of the rows and columns U_{PMNS} has the form

$$\begin{pmatrix} \frac{i}{\sqrt{2}} & \times & \times \\ \times & \times & \times \\ \times & \times & \times \end{pmatrix}, \quad (3.15)$$

where “ \times ” entries are functions of the free parameters θ^ν , θ^e and δ^e . Taking into account the current data, eqs. (3.10) and (3.11), the fixed element with the absolute value of $1/\sqrt{2} \approx 0.707$ can be $(U_{\text{PMNS}})_{\mu 2}$, $(U_{\text{PMNS}})_{\mu 3}$, $(U_{\text{PMNS}})_{\tau 2}$ or $(U_{\text{PMNS}})_{\tau 3}$. Note that $|(U_{\text{PMNS}})_{\tau 2}| = 0.707$ is outside the 3σ range in the case of the NO neutrino mass spectrum, while $|(U_{\text{PMNS}})_{\mu 2}| = 0.707$ is at the border of the 3σ allowed ranges for both the NO and IO spectra.

Let us consider as an example the first possibility, i.e., $P_e = P_\nu = P_{213}$, leading to $|(U_{\text{PMNS}})_{\mu 2}| = 1/\sqrt{2}$. In this case the mixing angles of the standard parametrisation of the PMNS matrix are related to the free parameters θ^ν , θ^e and δ^e as follows:

$$\begin{aligned} \sin^2 \theta_{13} &= |(U_{\text{PMNS}})_{e3}|^2 = \frac{1}{24} \left[\cos 2\theta^\nu \left(\sin 2\theta^e \left(3 \sin \delta^e + 4\sqrt{3} \cos \delta^e \right) + 4 \cos 2\theta^e - 1 \right) \right. \\ &\quad \left. + \sqrt{2} \sin 2\theta^\nu \left(\sin 2\theta^e \left(\sqrt{3} \cos \delta^e - 6 \sin \delta^e \right) + \cos 2\theta^e + 2 \right) - 3 \sin \delta^e \sin 2\theta^e + 9 \right], \end{aligned} \quad (3.16)$$

$$\sin^2 \theta_{23} = \frac{|(U_{\text{PMNS}})_{\mu 3}|^2}{1 - |(U_{\text{PMNS}})_{e3}|^2} = \frac{3 - 2\sqrt{2} \sin 2\theta^\nu + \cos 2\theta^\nu}{12 \cos^2 \theta_{13}}, \quad (3.17)$$

$$\sin^2 \theta_{12} = \frac{|(U_{\text{PMNS}})_{e2}|^2}{1 - |(U_{\text{PMNS}})_{e3}|^2} = \frac{1 + \sin \delta^e \sin 2\theta^e}{4 \cos^2 \theta_{13}}. \quad (3.18)$$

Moreover, from $|(U_{\text{PMNS}})_{\mu 2}| = 1/\sqrt{2}$ we obtain a sum rule for $\cos \delta$:

$$\cos \delta = \frac{2 \cos^2 \theta_{12} \cos^2 \theta_{23} + 2 \sin^2 \theta_{12} \sin^2 \theta_{23} \sin^2 \theta_{13} - 1}{\sin 2\theta_{12} \sin 2\theta_{23} \sin \theta_{13}}. \quad (3.19)$$

Let us comment now on the following issue. Once one of the elements of the PMNS matrix is fixed to be a constant, we still have four possible configurations, namely, a permutation of two remaining columns, a permutation of two remaining rows and both of them. For instance, in the case considered above, except for $P_e = P_\nu = P_{213}$, we can have a fixed $(U_{\text{PMNS}})_{\mu 2}$ with $(P_e, P_\nu) = (P_{213}, P_{231})$, (P_{312}, P_{213}) and (P_{312}, P_{231}) . These combinations of the permutation matrices will not lead, however, to different mixing patterns by virtue of the following relations:

$$R_{23}(\theta^\nu) P_{231} = R_{23}(\theta^\nu + \pi/2) P_{213} \text{diag}(-1, 1, 1), \quad (3.20)$$

$$P_{312} U_{23}(\theta^e, \delta^e) = \text{diag}(e^{i\delta^e}, 1, -e^{-i\delta^e}) P_{213} U_{23}(\theta^e + \pi/2, \delta^e). \quad (3.21)$$

Indeed, e.g., in the case of $(P_e, P_\nu) = (P_{312}, P_{231})$, defining $\hat{\theta}^\nu = \theta^\nu + \pi/2$, $\hat{\theta}^e = \theta^e + \pi/2$ and absorbing the matrix $\text{diag}(-1, 1, 1)$ in the matrix Q_ν , we obtain the same PMNS matrix as in the case of $(P_e, P_\nu) = (P_{213}, P_{213})$:

$$U_{\text{PMNS}} = P_{213} U_{23}(\hat{\theta}^e, \delta^e) \Omega_e^\dagger \Omega_\nu R_{23}(\hat{\theta}^\nu) P_{213} Q_\nu. \quad (3.22)$$

The phases in the matrix $\text{diag}(e^{i\delta^e}, 1, -e^{-i\delta^e})$ are unphysical, and we have disregarded them.

We list in Table 2 the matrices Ω_e and Ω_ν for all seven phenomenologically viable pairs of residual symmetries $\{G_e, G_\nu\} = \{Z_2^{g_e}, Z_2^{g_\nu} \times H_{\text{CP}}^\nu\}$. It turns out, however, that four of these seven pairs, namely, $\{G_e, G_\nu\} = \{Z_2^S, Z_2^{TU} \times H_{\text{CP}}^\nu\}$ with $H_{\text{CP}}^\nu = \{U, T\}$ and $\{STS, T^2STU\}$, and $\{G_e, G_\nu\} = \{Z_2^{TU}, Z_2^S \times H_{\text{CP}}^\nu\}$ with $H_{\text{CP}}^\nu = \{U, SU\}$ and $\{TST^2U, T^2STU\}$, lead to the same predictions for the mixing parameters. We demonstrate this in Appendix C.

3.3 Extracting Mixing Parameters and Statistical Analysis

In this subsection we perform a statistical analysis of the predictions for the neutrino mixing angles and CPV phases for each of the four distinctive sets of the residual flavour and CP symmetries, which are $\{G_e, G_\nu\} = \{Z_2^{TU}, Z_2^S \times H_{\text{CP}}^\nu\}$ with $H_{\text{CP}}^\nu = \{1, S\}$ and $\{U, SU\}$, and $\{G_e, G_\nu\} = \{Z_2^{TU}, Z_2^U \times H_{\text{CP}}^\nu\}$ with $H_{\text{CP}}^\nu = \{1, U\}$ and $\{S, SU\}$. This allows us to derive predictions for the three neutrino mixing angles and the three leptonic CPV phases, which, in many of the cases analysed in the present study is impossible to obtain purely analytically.

Once a pair of residual symmetries and the permutation matrices P_e and P_ν are specified, we have the expressions for $\sin^2 \theta_{ij}$ in terms of θ^ν , θ^e and δ^e of the type of eqs. (3.16)–(3.18). Moreover, employing a sum rule for $\cos \delta$ analogous to that in eq. (3.19) and computing the rephasing invariant

$$J_{\text{CP}} = \text{Im} \left\{ (U_{\text{PMNS}})_{e1}^* (U_{\text{PMNS}})_{\mu 3}^* (U_{\text{PMNS}})_{e3} (U_{\text{PMNS}})_{\mu 1} \right\}, \quad (3.23)$$

which determines the magnitude of CPV effects in neutrino oscillations [35] and which in the standard parametrisation of the PMNS matrix is proportional to $\sin \delta$,

$$J_{\text{CP}} = \frac{1}{8} \sin 2\theta_{12} \sin 2\theta_{23} \sin 2\theta_{13} \cos \theta_{13} \sin \delta, \quad (3.24)$$

g_e	Ω_e	g_ν	H_{CP}^ν	Ω_ν
S	$\frac{1}{\sqrt{6}} \begin{pmatrix} \sqrt{2} & -\sqrt{3} & -1 \\ \sqrt{2} & 0 & 2 \\ \sqrt{2} & \sqrt{3} & -1 \end{pmatrix}$	TU	$\{U, T\}$	$\frac{1}{\sqrt{2}} \begin{pmatrix} 0 & 0 & \sqrt{2}i \\ e^{\frac{2\pi i}{3}} & -e^{\frac{i\pi}{6}} & 0 \\ e^{\frac{i\pi}{3}} & e^{-\frac{i\pi}{6}} & 0 \end{pmatrix}$
			$\{STS, T^2STU\}$	$\frac{1}{\sqrt{6}} \begin{pmatrix} 0 & 2i & \sqrt{2} \\ \sqrt{3}e^{\frac{i\pi}{6}} & e^{\frac{i\pi}{6}} & -\sqrt{2}e^{-\frac{i\pi}{3}} \\ \sqrt{3}e^{-\frac{i\pi}{6}} & -e^{-\frac{i\pi}{6}} & -\sqrt{2}e^{\frac{i\pi}{3}} \end{pmatrix}$
TU	$\frac{1}{\sqrt{2}} \begin{pmatrix} 0 & 0 & \sqrt{2} \\ e^{\frac{i\pi}{3}} & e^{-\frac{2\pi i}{3}} & 0 \\ 1 & 1 & 0 \end{pmatrix}$	S	$\{1, S\}$	$\frac{1}{\sqrt{6}} \begin{pmatrix} \sqrt{2} & -\sqrt{3} & -1 \\ \sqrt{2} & 0 & 2 \\ \sqrt{2} & \sqrt{3} & -1 \end{pmatrix}$
			$\{U, SU\}$	$\frac{i}{\sqrt{6}} \begin{pmatrix} \sqrt{2} & -2 & 0 \\ \sqrt{2} & 1 & -\sqrt{3}i \\ \sqrt{2} & 1 & \sqrt{3}i \end{pmatrix}$
			$\{TST^2U, T^2STU\}$	$\frac{1}{\sqrt{3}} \begin{pmatrix} 1 & i & 1 \\ 1 & e^{-\frac{i\pi}{6}} & -e^{-\frac{i\pi}{3}} \\ 1 & -e^{\frac{i\pi}{6}} & -e^{\frac{i\pi}{3}} \end{pmatrix}$
		U	$\{1, U\}$	$\frac{1}{\sqrt{2}} \begin{pmatrix} 0 & 0 & \sqrt{2} \\ -1 & 1 & 0 \\ 1 & 1 & 0 \end{pmatrix}$
			$\{S, SU\}$	$-\frac{i}{\sqrt{6}} \begin{pmatrix} 0 & \sqrt{2}i & -2 \\ \sqrt{3} & \sqrt{2}i & 1 \\ -\sqrt{3} & \sqrt{2}i & 1 \end{pmatrix}$

Table 2: The matrices Ω_e and Ω_ν dictated by the residual symmetries $G_e = Z_2^{g_e}$ and $G_\nu = Z_2^{g_\nu} \times H_{\text{CP}}^\nu$ for all seven phenomenologically viable pairs of G_e and G_ν . For each pair $H_{\text{CP}}^\nu = \{X_{\nu 1}, X_{\nu 2}\}$ of remnant GCP transformations, the given matrix Ω_ν provides the Takagi factorisation of the first element, i.e., $X_{\nu 1} = \Omega_\nu \Omega_\nu^T$ ¹⁰.

we know the value of δ for any θ^ν , θ^e and δ^e . Similarly, making use of the two charged lepton

¹⁰ $X_{\nu 2}$ is instead factorised as $X_{\nu 2} = \tilde{\Omega}_\nu \tilde{\Omega}_\nu^T$, with $\tilde{\Omega}_\nu = \Omega_\nu \text{diag}(1, i, i)$, as follows from $X_{\nu 2} = \rho(g_\nu) X_{\nu 1} = \Omega_\nu \Omega_\nu^\dagger \rho(g_\nu) \Omega_\nu \Omega_\nu^T = \Omega_\nu \rho(g_\nu)^d \Omega_\nu^T$, with $\rho(g_\nu)^d$ defined in eq. (2.15).

rephasing invariants¹¹, associated with the Majorana phases [36–39],

$$I_1 = \text{Im} \{ (U_{\text{PMNS}})_{e1}^* (U_{\text{PMNS}})_{e2} \} \quad \text{and} \quad I_2 = \text{Im} \{ (U_{\text{PMNS}})_{e1}^* (U_{\text{PMNS}})_{e3} \} , \quad (3.25)$$

and the corresponding real parts

$$R_1 = \text{Re} \{ (U_{\text{PMNS}})_{e1}^* (U_{\text{PMNS}})_{e2} \} \quad \text{and} \quad R_2 = \text{Re} \{ (U_{\text{PMNS}})_{e1}^* (U_{\text{PMNS}})_{e3} \} , \quad (3.26)$$

which in the standard parametrisation of the PMNS matrix read:

$$I_1 = \sin \theta_{12} \cos \theta_{12} \cos^2 \theta_{13} \sin(\alpha_{21}/2) , \quad I_2 = \cos \theta_{12} \sin \theta_{13} \cos \theta_{13} \sin(\alpha_{31}/2 - \delta) , \quad (3.27)$$

$$R_1 = \sin \theta_{12} \cos \theta_{12} \cos^2 \theta_{13} \cos(\alpha_{21}/2) , \quad R_2 = \cos \theta_{12} \sin \theta_{13} \cos \theta_{13} \cos(\alpha_{31}/2 - \delta) , \quad (3.28)$$

we also obtain the values of α_{21} and α_{31} for any θ^ν , θ^e and δ^e .

Further, we scan randomly over $\theta^\nu \in [0, \pi)$, $\theta^e \in [0, \pi)$ and $\delta^e \in [0, 2\pi)$ and calculate the values of $\sin^2 \theta_{ij}$ and the CPV phases. We require $\sin^2 \theta_{ij}$ to lie in the corresponding 3σ ranges given in Table 1. The obtained values of $\sin^2 \theta_{ij}$ and δ can be characterised by a certain value of the χ^2 function constructed as follows:

$$\chi^2(\vec{x}) = \sum_{i=1}^4 \chi_i^2(x_i) , \quad (3.29)$$

where $\vec{x} = \{x_i\} = (\sin^2 \theta_{12}, \sin^2 \theta_{13}, \sin^2 \theta_{23}, \delta)$ and χ_i^2 are one-dimensional projections for NO and IO taken from [24]¹². Thus, we have a list of points $(\sin^2 \theta_{12}, \sin^2 \theta_{13}, \sin^2 \theta_{23}, \delta, \alpha_{21}, \alpha_{31}, \chi^2)$. To see the restrictions on the mixing parameters imposed by flavour and CP symmetries we consider all 15 different pairs (a, b) of the mixing parameters. For each pair we divide the plane (a, b) into bins and find a minimum of the χ^2 function in each bin. We present results in terms of heat maps with colour representing a minimal value of χ^2 in each bin. The results obtained in each case are discussed in the following subsection.

3.4 Results and Discussion

In this subsection we systematically go through all different potentially viable cases and summarise their particular features. All these cases can be divided in four groups corresponding to a particular pair of residual symmetries $\{G_e, G_\nu\}$.

In each case we concentrate on results for the ordering for which a better compatibility with the global data is attained. Note that results for NO and IO differ only i) due to the fact that the 3σ ranges of $\sin^2 \theta_{13}$ and $\sin^2 \theta_{23}$ depend slightly on the ordering and ii) in the respective χ^2 landscapes. Moreover, we present numerical results for the Majorana phases obtained for $k_1 = k_2 = 0$, where k_1 and k_2 are defined in eq. (2.23). However, one should keep in mind that all four (k_1, k_2) pairs, where $k_i = 0, 1$, are allowed. Whenever $k_{1(2)} = 1$, the predicted range for $\alpha_{21(31)}$ shifts by π . The values of the k_i are important for the predictions

¹¹In their general form, when one keeps explicit the unphysical phases ξ_j in the Majorana condition $C \bar{\nu}_j^T = \xi_j \nu_j$, $j = 1, 2, 3$, the rephasing invariants related to the Majorana phases involve ξ_j and are invariant under phase transformations of both the charged lepton and neutrino fields (see, for example, eqs. (22)–(28) in [36]). We have set $\xi_j = 1$.

¹²We note that according to the latest global oscillation data, there is an overall preference for NO over IO of $\Delta\chi_{\text{IO-NO}}^2 \approx 3.6$. Nevertheless, we take a conservative approach and treat both orderings on an equal footing. A discussion on this issue can be found in [24].

of the neutrinoless double beta decay effective Majorana mass (see, e.g., [36, 40, 41]), which we obtain in Section 4.

Group A: $\{G_e, G_\nu\} = \{Z_2^{TU}, Z_2^S \times H_{\text{CP}}^\nu\}$ with $H_{\text{CP}}^\nu = \{\mathbf{1}, S\}$. Using the corresponding matrices Ω_e and Ω_ν from Table 2 and the master formula for the PMNS matrix in eq. (2.24), we find the following form of the PMNS matrix (up to permutations of rows and columns and the phases in the matrix Q_ν):

$$U_{\text{PMNS}}^A = \frac{1}{2\sqrt{3}} \begin{pmatrix} \sqrt{6} e^{-\frac{i\pi}{6}} & \sqrt{3} e^{i\theta^\nu} & \sqrt{3} e^{-i\theta^\nu} \\ \sqrt{2} c^e e^{\frac{i\pi}{3}} + 2 s^e e^{-i\delta^e} & a_1(\theta^\nu, \theta^e, \delta^e) & a_2(\theta^\nu, \theta^e, \delta^e) \\ 2 c^e - \sqrt{2} s^e e^{\frac{i\pi}{3}} e^{i\delta^e} & a_3(\theta^\nu, \theta^e, \delta^e) & a_4(\theta^\nu, \theta^e, \delta^e) \end{pmatrix}, \quad (3.30)$$

with $c^e \equiv \cos \theta^e$, $s^e \equiv \sin \theta^e$, $c^\nu \equiv \cos \theta^\nu$, $s^\nu \equiv \sin \theta^\nu$ and

$$a_1(\theta^\nu, \theta^e, \delta^e) = \left[\sqrt{3} c^\nu + (2 - i\sqrt{3}) s^\nu \right] c^e + \sqrt{2} (s^\nu - \sqrt{3} c^\nu) s^e e^{-i\delta^e}, \quad (3.31)$$

$$a_2(\theta^\nu, \theta^e, \delta^e) = \left[\sqrt{3} s^\nu - (2 - i\sqrt{3}) c^\nu \right] c^e - \sqrt{2} (c^\nu + \sqrt{3} s^\nu) s^e e^{-i\delta^e}, \quad (3.32)$$

$$a_3(\theta^\nu, \theta^e, \delta^e) = \sqrt{2} (s^\nu - \sqrt{3} c^\nu) c^e - \left[\sqrt{3} c^\nu + (2 - i\sqrt{3}) s^\nu \right] s^e e^{i\delta^e}, \quad (3.33)$$

$$a_4(\theta^\nu, \theta^e, \delta^e) = -\sqrt{2} (c^\nu + \sqrt{3} s^\nu) c^e - \left[\sqrt{3} s^\nu - (2 - i\sqrt{3}) c^\nu \right] s^e e^{i\delta^e}. \quad (3.34)$$

From eq. (3.30), we see that the absolute values of the elements of the first row are fixed. Namely, the modulus of the first element is equal to $1/\sqrt{2}$, while the moduli of the second and third elements equal $1/2$. Taking into account the current knowledge of the mixing parameters, eqs. (3.10) and (3.11), this implies that there are only two potentially viable cases: i) with $|(U_{\text{PMNS}})_{\mu 1}| = |(U_{\text{PMNS}})_{\mu 2}| = 1/2$ and $|(U_{\text{PMNS}})_{\mu 3}| = 1/\sqrt{2}$, and ii) with $|(U_{\text{PMNS}})_{\tau 1}| = |(U_{\text{PMNS}})_{\tau 2}| = 1/2$ and $|(U_{\text{PMNS}})_{\tau 3}| = 1/\sqrt{2}$.

• **Case A1:** $|(U_{\text{PMNS}})_{\mu 1}| = |(U_{\text{PMNS}})_{\mu 2}| = 1/2$, $|(U_{\text{PMNS}})_{\mu 3}| = 1/\sqrt{2}$ ($P_e = P_{213}$, $P_\nu = P_{321}$). In this case we obtain

$$\sin^2 \theta_{23} = \frac{1}{2(1 - \sin^2 \theta_{13})} \quad (3.35)$$

$$= \frac{1}{2} (1 + \sin^2 \theta_{13}) + \mathcal{O}(\sin^4 \theta_{13}). \quad (3.36)$$

This means that only a narrow interval $\sin^2 \theta_{23} \in [0.510, 0.512]$ is allowed using the 3σ region for $\sin^2 \theta_{13}$. From the equality $|(U_{\text{PMNS}})_{\mu 1}| = 1/2$, which we find to hold in this case, it follows that $\cos \delta$ satisfies the following sum rule:

$$\cos \delta = \frac{1 - 4 \sin^2 \theta_{12} \cos^2 \theta_{23} - 4 \cos^2 \theta_{12} \sin^2 \theta_{23} \sin^2 \theta_{13}}{2 \sin 2\theta_{12} \sin 2\theta_{23} \sin \theta_{13}}, \quad (3.37)$$

where the mixing angles in addition are correlated among themselves. We find that $\sin^2 \theta_{13}$ is constrained to lie in the interval $(0.0213, 0.0240(2))$ for NO (IO) and, hence, $\sin^2 \theta_{23}$ in $[0.5109, 0.5123(4)]$. This range of values of $\sin^2 \theta_{23}$ is not compatible with its current 2σ range. Moreover, $\sin^2 \theta_{12}$ is found to be between approximately 0.345 and 0.354, which is

outside its current 2σ range as well. What concerns the CPV phases, the predicted values of δ are distributed around 0, namely, $\delta \in [-0.11\pi, 0.11\pi]$, of α_{21} around π , $\alpha_{21} \in (0.93\pi, 1.07\pi)$, while the values of α_{31} fill the whole range, i.e., $\alpha_{31} \in [0, 2\pi)$. These numbers, presented for the NO spectrum, remain practically unchanged for the IO spectrum. However, the global minimum χ_{\min}^2 of the χ^2 function, defined in eq. (3.29), yields approximately 22 (19) for NO (IO), which implies that this case is disfavoured by the global data at more than 4σ .

• **Case A2:** $|(U_{\text{PMNS}})_{\tau 1}| = |(U_{\text{PMNS}})_{\tau 2}| = 1/2$, $|(U_{\text{PMNS}})_{\tau 3}| = 1/\sqrt{2}$ ($P_e = P_\nu = P_{321}$). This case shares the predicted ranges for $\sin^2 \theta_{12}$, $\sin^2 \theta_{13}$, α_{21} and α_{31} with case A1, but differs in the predictions for $\sin^2 \theta_{23}$ and δ . Again, there is a correlation between $\sin^2 \theta_{13}$ and $\sin^2 \theta_{23}$:

$$\sin^2 \theta_{23} = \frac{1 - 2 \sin^2 \theta_{13}}{2(1 - \sin^2 \theta_{13})} \quad (3.38)$$

$$= \frac{1}{2}(1 - \sin^2 \theta_{13}) + \mathcal{O}(\sin^4 \theta_{13}), \quad (3.39)$$

which, in particular, implies that $\sin^2 \theta_{23} \in [0.4877(6), 0.4891]$, which is not compatible with its present 2σ range. We also find that $|(U_{\text{PMNS}})_{\tau 1}| = 1/2$. This equality leads to the following sum rule:

$$\cos \delta = \frac{4 \sin^2 \theta_{12} \sin^2 \theta_{23} + 4 \cos^2 \theta_{12} \cos^2 \theta_{23} \sin^2 \theta_{13} - 1}{2 \sin 2\theta_{12} \sin 2\theta_{23} \sin \theta_{13}}. \quad (3.40)$$

It is worth noting that we should always keep in mind the correlations between the mixing angles in expressions of this type. The values of δ in this case lie around π , in the interval $[0.89\pi, 1.11\pi]$. As in the previous case, the global minimum of χ^2 is somewhat large, $\chi_{\min}^2 \approx 18.5$ (15) for NO (IO), meaning that this case is also disfavoured.

Group B: $\{G_e, G_\nu\} = \{Z_2^{TU}, Z_2^S \times H_{\text{CP}}^\nu\}$ with $H_{\text{CP}}^\nu = \{U, SU\}$. For this choice of the residual symmetries, the PMNS matrix reads (up to permutations of rows and columns and the phases in the matrix Q_ν):

$$U_{\text{PMNS}}^{\text{B}} = \frac{1}{2\sqrt{3}} \begin{pmatrix} \sqrt{6} e^{\frac{i\pi}{3}} & \sqrt{3}(c^\nu + s^\nu) e^{\frac{i\pi}{3}} & \sqrt{3}(s^\nu - c^\nu) e^{\frac{i\pi}{3}} \\ -\sqrt{2} c^e e^{-\frac{i\pi}{6}} + 2i s^e e^{-i\delta^e} & b_1(\theta^\nu, \theta^e, \delta^e) & b_2(\theta^\nu, \theta^e, \delta^e) \\ 2i c^e + \sqrt{2} s^e e^{-\frac{i\pi}{6}} e^{i\delta^e} & b_3(\theta^\nu, \theta^e, \delta^e) & b_4(\theta^\nu, \theta^e, \delta^e) \end{pmatrix}, \quad (3.41)$$

with

$$b_1(\theta^\nu, \theta^e, \delta^e) = (3s^\nu - c^\nu) c^e e^{-\frac{i\pi}{6}} - 2\sqrt{2} i c^\nu s^e e^{-i\delta^e}, \quad (3.42)$$

$$b_2(\theta^\nu, \theta^e, \delta^e) = -(3c^\nu + s^\nu) c^e e^{-\frac{i\pi}{6}} - 2\sqrt{2} i s^\nu s^e e^{-i\delta^e}, \quad (3.43)$$

$$b_3(\theta^\nu, \theta^e, \delta^e) = -2\sqrt{2} i c^\nu c^e - (3s^\nu - c^\nu) s^e e^{-\frac{i\pi}{6}} e^{i\delta^e}, \quad (3.44)$$

$$b_4(\theta^\nu, \theta^e, \delta^e) = -2\sqrt{2} i s^\nu c^e + (3c^\nu + s^\nu) s^e e^{-\frac{i\pi}{6}} e^{i\delta^e}. \quad (3.45)$$

Equation (3.41) implies that the absolute value of one element of the PMNS matrix is predicted to be $1/\sqrt{2}$. Thus, we have four potentially viable cases.

• **Case B1:** $|(U_{\text{PMNS}})_{\mu 2}| = 1/\sqrt{2}$ ($P_e = P_\nu = P_{213}$). Note that from eqs. (3.10) and (3.11) it follows that this magnitude of the fixed element is inside its 3σ range for NO, but

slightly outside the corresponding range for IO. Hence, we will focus on the results for NO. The characteristic feature of this case is the following sum rule for $\cos \delta$:

$$\cos \delta = \frac{2 \cos^2 \theta_{12} \cos^2 \theta_{23} + 2 \sin^2 \theta_{12} \sin^2 \theta_{23} \sin^2 \theta_{13} - 1}{\sin 2\theta_{12} \sin 2\theta_{23} \sin \theta_{13}}, \quad (3.46)$$

which arises from the equality of $|(U_{\text{PMNS}})_{\mu 2}|$ to $1/\sqrt{2}$. The pair correlations between the mixing parameters in this case are summarised in Fig. 1. The colour palette corresponds to values of χ^2 for NO. As can be seen, while all values of $\sin^2 \theta_{13}$ in its 3σ range are allowed, the parameters $\sin^2 \theta_{12}$ and $\sin^2 \theta_{23}$ are found to lie in $[0.250, 0.308]$ and $[0.381, 0.425]$ intervals, respectively. The predicted values of δ span the range $[0.68\pi, 1.32\pi]$. Thus, CPV effects in neutrino oscillations due to the phase δ can be suppressed. The Majorana phases instead are distributed in relatively narrow regions around 0, so the magnitude of the neutrinoless double beta decay effective Majorana mass (see Section 4 and, e.g., [36, 40, 41]) is predicted (for $k_1 = k_2 = 0$) to have a value close to the maximal possible for the NO spectrum. Namely, $\alpha_{21} \in [-0.16\pi, 0.16\pi]$ and $\alpha_{31} \in (-0.13\pi, 0.13\pi)$. In addition, δ is strongly correlated with α_{21} and α_{31} , which in turn exhibit a strong correlation between themselves. Finally, $\chi_{\text{min}}^2 \approx 7$ for both NO and IO, i.e., this case is compatible with the global data at less than 3σ ¹³.

• **Case B2:** $|(U_{\text{PMNS}})_{\tau 2}| = 1/\sqrt{2}$ ($P_e = P_{321}$, $P_\nu = P_{213}$). Note that this value of $|(U_{\text{PMNS}})_{\tau 2}|$ is compatible at 3σ with the global data in the case of IO spectrum, but not in the case of NO spectrum, as can be seen from eqs. (3.10) and (3.11). Thus, below we present results for the IO spectrum only. As in case B1, the whole 3σ range for $\sin^2 \theta_{13}$ is allowed. The obtained ranges of values of α_{21} and α_{31} are the same of the preceding case. The range for $\sin^2 \theta_{12}$ differs somewhat from that obtained in case B1, and it reads $\sin^2 \theta_{12} \in [0.250, 0.328]$ ¹⁴. The predictions for $\sin^2 \theta_{23}$ and δ are different. Now the following sum rule, derived from $|(U_{\text{PMNS}})_{\tau 2}| = 1/\sqrt{2}$, holds:

$$\cos \delta = \frac{1 - 2 \cos^2 \theta_{12} \sin^2 \theta_{23} - 2 \sin^2 \theta_{12} \cos^2 \theta_{23} \sin^2 \theta_{13}}{\sin 2\theta_{12} \sin 2\theta_{23} \sin \theta_{13}}. \quad (3.47)$$

The values of δ are concentrated in $[-0.38\pi, 0.38\pi]$. For $\sin^2 \theta_{23}$ we find the range $(0.575, 0.636]$. The correlations between the phases are of the same type as in case B1. We summarise the results in Fig. 2. Finally, $\chi_{\text{min}}^2 \approx 6$ in the case of IO and $\chi_{\text{min}}^2 \approx 12.5$ for NO, which reflects incompatibility of this case at more than 3σ for the NO spectrum. This occurs mainly due to the predicted values of $\sin^2 \theta_{23}$, which are outside its current 2σ range for NO.

• **Case B3:** $|(U_{\text{PMNS}})_{\mu 3}| = 1/\sqrt{2}$ ($P_e = P_{213}$, $P_\nu = P_{321}$). Since $|(U_{\text{PMNS}})_{\mu 3}| = 1/\sqrt{2}$, the angles θ_{13} and θ_{23} are correlated as in case A1, i.e., according to eq. (3.35). For IO this leads to $\sin^2 \theta_{23} \in [0.5097, 0.5124]$ due to the fact that the whole 3σ range of $\sin^2 \theta_{13}$ is found to be allowed, as can be seen from Fig. 3. Note that this range is outside the current 2σ range of $\sin^2 \theta_{23}$. In addition, we find that the whole 3σ range of the values of $\sin^2 \theta_{12}$ can

¹³The apparent contradiction between the obtained value of $\chi_{\text{min}}^2 \approx 7$, which suggests compatibility also for IO, and the expectation of $\chi_{\text{min}}^2 \gtrsim 9$, according to eq. (3.11), arises from the way we construct the χ^2 function (see eq. (3.29)), which does not explicitly include covariances between the oscillation parameters.

¹⁴This difference is related to the fact that the current 3σ range of $\sin^2 \theta_{23}$ for IO, which reads $[0.384, 0.636]$, is not symmetric with respect to 0.5. The asymmetry of 0.02 translates to increase of the allowed range of $\sin^2 \theta_{12}$ by approximately 0.02. This can be better understood from the top right plots in Figs. 1 and 2.

be reproduced. In contrast to case A1, $|(U_{\text{PMNS}})_{\mu 1}|$ does not equal 1/2, but depends on θ^ν in the following way:

$$|(U_{\text{PMNS}})_{\mu 1}|^2 = \frac{1 - \sin 2\theta^\nu}{4}. \quad (3.48)$$

From this equation we find

$$\cos \delta = \frac{1 - 4 \sin^2 \theta_{12} \cos^2 \theta_{23} - 4 \cos^2 \theta_{12} \sin^2 \theta_{23} \sin^2 \theta_{13} - \sin 2\theta^\nu}{2 \sin 2\theta_{12} \sin 2\theta_{23} \sin \theta_{13}}, \quad (3.49)$$

i.e., $\cos \delta$ depends on θ^ν explicitly (not only via θ_{12} , θ_{23} and θ_{13}). With this relation, any value of δ between 0 and 2π is allowed (see Fig. 3). The Majorana phases, however, are constrained to lie around 0 in the following intervals: $\alpha_{21} \in [-0.23\pi, 0.23\pi]$ and $\alpha_{31} \in (-0.18\pi, 0.18\pi)$. Moreover, both phases α_{21} and α_{31} are correlated in one and the same peculiar way with the phase δ . The correlation between α_{21} and α_{31} is similar to those in cases B1 and B2 (cf. Figs. 1 and 2). Due to the predicted values of $\sin^2 \theta_{23}$, which belong to the upper octant, IO is preferred over NO, the corresponding χ_{min}^2 being approximately 5 and 8.5.

• **Case B4:** $|(U_{\text{PMNS}})_{\tau 3}| = 1/\sqrt{2}$ ($P_e = P_\nu = P_{321}$). The predicted ranges of all the mixing parameters are the same of case B3, except for $\sin^2 \theta_{23}$, which respects the relation in eq. (3.38), and thus belongs to $[0.4876, 0.4903]$ in the case of IO spectrum. As in the previous case, this interval falls outside the 2σ range of $\sin^2 \theta_{23}$. The results obtained in this case for the IO spectrum are presented in Fig. 4. Similarly to the preceding case, we find

$$|(U_{\text{PMNS}})_{\tau 1}|^2 = \frac{1 - \sin 2\theta^\nu}{4}, \quad (3.50)$$

which leads to

$$\cos \delta = \frac{\sin 2\theta^\nu + 4 \sin^2 \theta_{12} \sin^2 \theta_{23} + 4 \cos^2 \theta_{12} \cos^2 \theta_{23} \sin^2 \theta_{13} - 1}{2 \sin 2\theta_{12} \sin 2\theta_{23} \sin \theta_{13}}. \quad (3.51)$$

The correlation between the Majorana phases is similar to that in the previous case. Also in this case, $\chi_{\text{min}}^2 \approx 4.5$ for IO is lower than that of approximately 6.5 for NO, the reason being again the predicted range of $\sin^2 \theta_{23}$.

Group C: $\{G_e, G_\nu\} = \{Z_2^{TU}, Z_2^U \times H_{\text{CP}}^\nu\}$ with $H_{\text{CP}}^\nu = \{\mathbf{1}, U\}$. Using the corresponding matrices Ω_e and Ω_ν given in Table 2 and eq. (2.24), we obtain the following form of the PMNS matrix (up to permutations of rows and columns and the phases in the matrix Q_ν):

$$U_{\text{PMNS}}^{\text{C}} = \frac{1}{2} \begin{pmatrix} e^{i\frac{\pi}{3}} & \sqrt{3} c^\nu e^{-\frac{i\pi}{6}} & \sqrt{3} s^\nu e^{-\frac{i\pi}{6}} \\ \sqrt{3} c^e e^{-\frac{i\pi}{6}} & c^\nu c^e e^{\frac{i\pi}{3}} - 2 s^\nu s^e e^{-i\delta^e} & s^\nu c^e e^{\frac{i\pi}{3}} + 2 c^\nu s^e e^{-i\delta^e} \\ -\sqrt{3} s^e e^{-\frac{i\pi}{6}} e^{i\delta^e} & -2 s^\nu c^e - c^\nu s^e e^{\frac{i\pi}{3}} e^{i\delta^e} & 2 c^\nu c^e - s^\nu s^e e^{\frac{i\pi}{3}} e^{i\delta^e} \end{pmatrix}. \quad (3.52)$$

Thus, this pair of residual symmetries leads the absolute value of the fixed element to be 1/2. Taking into account the current uncertainties in the values of the neutrino mixing parameters, eqs. (3.10) and (3.11), we have to consider five potentially viable cases corresponding to $(U_{\text{PMNS}})_{e2}$, $(U_{\text{PMNS}})_{\mu 1}$, $(U_{\text{PMNS}})_{\tau 1}$, $(U_{\text{PMNS}})_{\mu 2}$ or $(U_{\text{PMNS}})_{\tau 2}$ being the fixed element.

• **Case C1:** $|(U_{\text{PMNS}})_{e2}| = 1/2$ ($P_e = P_{123}$, $P_\nu = P_{213}$). Fixing $(U_{\text{PMNS}})_{e2}$ leads to the following relation between $\sin^2 \theta_{13}$ and $\sin^2 \theta_{12}$:

$$\sin^2 \theta_{12} = \frac{1}{4(1 - \sin^2 \theta_{13})} \quad (3.53)$$

$$= \frac{1}{4} (1 + \sin^2 \theta_{13}) + \mathcal{O}(\sin^4 \theta_{13}) . \quad (3.54)$$

Since this case allows for the whole 3σ range of $\sin^2 \theta_{13}$ (see Fig. 5), we find $\sin^2 \theta_{12} \in (0.2548, 0.2562)$. Note that this narrow interval is outside the current 2σ range of $\sin^2 \theta_{12}$. At the same time, this case reproduces the whole 3σ range of the values of $\sin^2 \theta_{23}$. From

$$|(U_{\text{PMNS}})_{\mu 2}|^2 = \frac{3 \cos^2 \theta^e}{4} , \quad (3.55)$$

we obtain

$$\cos \delta = \frac{4 \cos^2 \theta_{12} \cos^2 \theta_{23} + 4 \sin^2 \theta_{12} \sin^2 \theta_{23} \sin^2 \theta_{13} - 3 \cos^2 \theta^e}{2 \sin 2\theta_{12} \sin 2\theta_{23} \sin \theta_{13}} , \quad (3.56)$$

i.e., $\cos \delta$ explicitly depends on θ^e , and eventually this relation does not constrain δ . Instead the Majorana phase α_{21} is predicted to be exactly π (exactly 0) for $k_1 = 0$ ($k_1 = 1$). While the second Majorana phase α_{31} itself remains unconstrained, the difference $\alpha_{31} - 2\delta = 0$ (π) for $k_2 = 0$ ($k_2 = 1$), i.e., we have a strong linear correlation between δ and α_{31} (see Fig. 5). The reason for these trivial values of α_{21} and $\alpha_{31} - 2\delta$ is the following. In the standard parametrisation of the PMNS matrix, α_{21} and the combination $(\alpha_{31} - 2\delta)$ may be extracted from the phases of the first row of the PMNS matrix, as can be seen from eqs. (3.25)–(3.28). In case C1, none of the phases of the first row elements of the PMNS matrix depend (mod π) on the free parameters θ^ν , θ^e and δ^e . Namely, the phases of $(U_{\text{PMNS}})_{e1}$, $(U_{\text{PMNS}})_{e2}$ and $(U_{\text{PMNS}})_{e3}$ are fixed (mod π and up to a global phase) to be $-\pi/6$, $\pi/3$ and $-\pi/6$, respectively. Notice that only in groups B and C the relative phases of the first row can be predicted (mod π) to be independent of θ^ν , θ^e and δ^e . Furthermore, case C1 stands out since it is, out of these relevant cases, the only one which survives the constraints on the magnitudes of the PMNS matrix elements given in eqs. (3.10) and (3.11). Finally, $\chi_{\min}^2 \approx 7$ for both mass orderings.

• **Case C2:** $|(U_{\text{PMNS}})_{\mu 1}| = 1/2$ ($P_e = P_{213}$, $P_\nu = P_{123}$). The correlations between the mixing parameters obtained in this case for NO are summarised in Fig. 6 (the results for IO are very similar). This case accounts for the whole 3σ range of $\sin^2 \theta_{13}$, but constrains the values of the two other angles. Namely, we find $\sin^2 \theta_{12} \in [0.285, 0.354]$ and $\sin^2 \theta_{23} \in [0.381, 0.524]$. This case enjoys the sum rule for $\cos \delta$ given in eq. (3.37), since $|(U_{\text{PMNS}})_{\mu 1}| = 1/2$ as it was also in case A1. As a consequence, we find δ to be constrained: $\delta \in (-0.38\pi, 0.38\pi)$. Both Majorana phases are distributed in relatively narrow intervals around π : $\alpha_{21} \in (0.85\pi, 1.15\pi)$ and $\alpha_{31} \in [0.91\pi, 1.09\pi]$. The phase δ is correlated with each of the two Majorana phases in a similar way. The latter in turn are correlated linearly between themselves. Overall, NO is slightly preferred over IO in this case. The corresponding values of χ_{\min}^2 read 4.5 and 5.5, respectively.

• **Case C3:** $|(U_{\text{PMNS}})_{\tau 1}| = 1/2$ ($P_e = P_{321}$, $P_\nu = P_{123}$). This case shares some of the predictions of case C2. Namely, the whole 3σ range of $\sin^2 \theta_{13}$ is allowed, and the ranges of α_{21} and α_{31} are the same as in the preceding case, as can be seen from Fig. 7, in which we present the results for the IO neutrino mass spectrum. The interval of values of $\sin^2 \theta_{12}$

differs somewhat from that of case C2 and reads $\sin^2 \theta_{12} \in [0.279, 0.354]$. The predictions for $\sin^2 \theta_{23}$ and δ , however, are very different from those of case C2. The allowed values of $\sin^2 \theta_{23}$ are concentrated mostly in the upper octant, $\sin^2 \theta_{23} \in [0.475, 0.636]$. The sum rule for $\cos \delta$ in eq. (3.40) is valid in this case, since $|(U_{\text{PMNS}})_{\tau 1}| = 1/2$, and we find the values of δ to be symmetrically distributed around π in the interval $[0.60\pi, 1.40\pi]$. The pairwise correlations between the CPV phases are of the same type as in case C2 (taking into account an approximate shift of δ by π , as suggested by Figs. 6 and 7). Due to the predicted range of $\sin^2 \theta_{23}$, this case is favoured by the data for IO, for which $\chi_{\text{min}}^2 \approx 1.5$, while for NO we find $\chi_{\text{min}}^2 \approx 8.5$.

• **Case C4:** $|(U_{\text{PMNS}})_{\mu 2}| = 1/2$ ($P_e = P_\nu = P_{213}$). From eqs. (3.10) and (3.11) it follows that the value of $|(U_{\text{PMNS}})_{\mu 2}| = 1/2$ is allowed at 3σ only for IO. Thus, below we present results obtained in the IO case. In the case under consideration there are no constraints on the ranges of $\sin^2 \theta_{12}$ and $\sin^2 \theta_{13}$. The atmospheric angle is, in turn, found to lie in the upper octant, $\sin^2 \theta_{23} \in (0.505, 0.636]$. As can be seen in Fig. 8, $\delta \in [-0.54\pi, 0.54\pi]$, which is a consequence of the following correlation between $\cos \delta$ and the mixing angles:

$$\cos \delta = \frac{4 \cos^2 \theta_{12} \cos^2 \theta_{23} + 4 \sin^2 \theta_{12} \sin^2 \theta_{23} \sin^2 \theta_{13} - 1}{2 \sin 2\theta_{12} \sin 2\theta_{23} \sin \theta_{13}}, \quad (3.57)$$

obtained from $|(U_{\text{PMNS}})_{\mu 2}| = 1/2$. There is also a peculiar correlation between $\sin^2 \theta_{23}$ and δ . The phases $\alpha_{21} \in [0.73\pi, 1.27\pi]$ and $\alpha_{31} \in [-0.18\pi, 0.18\pi]$. The values of all the three phases are highly correlated among themselves. The predicted values of $\sin^2 \theta_{23}$ in the upper octant lead to $\chi_{\text{min}}^2 \approx 8.5$ for NO (see footnote 13), which is bigger than that of $\chi_{\text{min}}^2 \approx 2$ for IO.

• **Case C5:** $|(U_{\text{PMNS}})_{\tau 2}| = 1/2$ ($P_e = P_{321}$, $P_\nu = P_{213}$). The last case of this group, analogously to case C4, does not constrain the ranges of $\sin^2 \theta_{12}$ and $\sin^2 \theta_{13}$. Moreover, it leads to almost the same allowed ranges of α_{21} and α_{31} as in the previous case, $\alpha_{21} \in (0.74\pi, 1.26\pi)$ and $\alpha_{31} \in [-0.16\pi, 0.16\pi]$. The differences are in predictions for $\sin^2 \theta_{23}$ and δ . Now the atmospheric angle lies in the lower octant, namely, for NO we find $\sin^2 \theta_{23} \in [0.381, 0.494]$. The condition $|(U_{\text{PMNS}})_{\tau 2}| = 1/2$ gives rise to the following sum rule:

$$\cos \delta = \frac{1 - 4 \cos^2 \theta_{12} \sin^2 \theta_{23} - 4 \sin^2 \theta_{12} \cos^2 \theta_{23} \sin^2 \theta_{13}}{2 \sin 2\theta_{12} \sin 2\theta_{23} \sin \theta_{13}}. \quad (3.58)$$

The allowed values of δ span the range $[0.51\pi, 1.49\pi]$. The correlations between the mixing parameters in this case are summarised in Fig. 9. Finally, we have $\chi_{\text{min}}^2 \approx 0.5$ for both NO and IO.

Group D: $\{G_e, G_\nu\} = \{Z_2^{TU}, Z_2^U \times H_{\text{CP}}^\nu\}$ with $H_{\text{CP}}^\nu = \{S, SU\}$. For this last group of cases, we find that the PMNS matrix takes the following form (up to permutations of rows and columns and the phases in the matrix Q_ν):

$$U_{\text{PMNS}}^{\text{D}} = \frac{1}{2\sqrt{3}} \begin{pmatrix} -\sqrt{3} e^{-\frac{i\pi}{6}} & \sqrt{3} (\sqrt{2} c^\nu + i s^\nu) e^{-\frac{i\pi}{6}} & \sqrt{3} (\sqrt{2} s^\nu - i c^\nu) e^{-\frac{i\pi}{6}} \\ 3 c^e e^{\frac{i\pi}{3}} & d_1 (\theta^\nu, \theta^e, \delta^e) & d_2 (\theta^\nu, \theta^e, \delta^e) \\ -3 s^e e^{\frac{i\pi}{3}} e^{i\delta^e} & d_3 (\theta^\nu, \theta^e, \delta^e) & d_4 (\theta^\nu, \theta^e, \delta^e) \end{pmatrix}, \quad (3.59)$$

where

$$d_1(\theta^\nu, \theta^e, \delta^e) = \left(\sqrt{2}c^\nu + i s^\nu\right) c^e e^{\frac{i\pi}{3}} + 2 \left(c^\nu - i\sqrt{2}s^\nu\right) s^e e^{-i\delta^e}, \quad (3.60)$$

$$d_2(\theta^\nu, \theta^e, \delta^e) = \left(\sqrt{2}s^\nu - i c^\nu\right) c^e e^{\frac{i\pi}{3}} + 2 \left(s^\nu + i\sqrt{2}c^\nu\right) s^e e^{-i\delta^e}, \quad (3.61)$$

$$d_3(\theta^\nu, \theta^e, \delta^e) = 2 \left(c^\nu - i\sqrt{2}s^\nu\right) c^e - \left(\sqrt{2}c^\nu + i s^\nu\right) s^e e^{\frac{i\pi}{3}} e^{i\delta^e}, \quad (3.62)$$

$$d_4(\theta^\nu, \theta^e, \delta^e) = 2 \left(s^\nu + i\sqrt{2}c^\nu\right) c^e - \left(\sqrt{2}s^\nu - i c^\nu\right) s^e e^{\frac{i\pi}{3}} e^{i\delta^e}. \quad (3.63)$$

Therefore, the absolute value of the fixed element of the neutrino mixing matrix yields $1/2$. Thus, we have again five potentially viable cases.

- **Case D1:** $|(U_{\text{PMNS}})_{e2}| = 1/2$ ($P_e = P_{123}$, $P_\nu = P_{213}$). In this case we find

$$\sin^2 \theta_{13} = \frac{3 - \cos 2\theta^\nu}{8}, \quad (3.64)$$

which implies that $\sin^2 \theta_{13}$ can have values between $1/4$ and $1/2$. Thus, this case is ruled out.

- **Case D2:** $|(U_{\text{PMNS}})_{\mu 1}| = 1/2$ ($P_e = P_{213}$, $P_\nu = P_{123}$). This case allows for the whole 3σ range of $\sin^2 \theta_{13}$ and, in the case of NO, for the following ranges of $\sin^2 \theta_{12}$ and $\sin^2 \theta_{23}$: $\sin^2 \theta_{12} \in [0.284, 0.354]$ and $\sin^2 \theta_{23} \in [0.381, 0.512]$. The sum rule for $\cos \delta$ in eq. (3.37) holds, since $|(U_{\text{PMNS}})_{\mu 1}| = 1/2$. We find $\delta \in [-0.37\pi, 0.37\pi]$. What concerns the Majorana phases, α_{21} spans a relatively broad interval $[0.25\pi, 1.75\pi]$, while $\alpha_{31} \in [-0.48\pi, 0.48\pi]$. There are very particular correlations between $\alpha_{21(31)}$ and all the other mixing parameters in this case, as can be seen in Fig. 10, in which we summarise the results for NO. Finally, $\chi_{\text{min}}^2 \approx 4.5$ for NO, and it is slightly higher, $\chi_{\text{min}}^2 \approx 5.5$, for IO.

- **Case D3:** $|(U_{\text{PMNS}})_{\tau 1}| = 1/2$ ($P_e = P_{321}$, $P_\nu = P_{123}$). As in the previous case, the whole 3σ range of $\sin^2 \theta_{13}$ gets reproduced. The allowed ranges of $\sin^2 \theta_{12}$, α_{21} and α_{31} are very similar to those of case D2. Namely, in the case of IO spectrum we have $\sin^2 \theta_{12} \in [0.279, 0.354]$, $\alpha_{21} \in [0.21\pi, 1.79\pi]$ and $\alpha_{31} \in (-0.53\pi, 0.53\pi)$. Instead, the values of $\sin^2 \theta_{23}$ occupy mostly the upper octant, $\sin^2 \theta_{23} \in [0.488, 0.636]$. The sum rule in eq. (3.40), which holds in this case since $|(U_{\text{PMNS}})_{\tau 1}| = 1/2$, leads to the values of δ distributed around π in a rather broad range of $(0.59\pi, 1.41\pi)$. The correlations between the Majorana phases and δ are as in the previous case, but again with an approximate shift of δ by π (see Fig. 11). The minimal value $\chi_{\text{min}}^2 \approx 1.5$ in the IO case, while for the NO spectrum we get approximately 8.5. This difference is due to the allowed values of $\sin^2 \theta_{23}$.

- **Case D4:** $|(U_{\text{PMNS}})_{\mu 2}| = 1/2$ ($P_e = P_\nu = P_{213}$). This case can account only for a part of the 3σ range of $\sin^2 \theta_{13}$, namely, $\sin^2 \theta_{13} \in [0.0214, 0.0240(2)]$ for NO (IO) spectrum. The constraints on two other angles are more severe. We find that only a narrow region of the values of $\sin^2 \theta_{23}$, which falls outside its present 2σ range, is allowed, namely, $\sin^2 \theta_{23} \in [0.505, 0.512]$. For the solar mixing angle we have $\sin^2 \theta_{12} \in [0.345, 0.354]$, which is also outside the current 2σ range of this parameter. The sum rule in eq. (3.57), which is also valid in this case, constrains δ to lie in a narrow interval around 0: $\delta \in [-0.11\pi, 0.11\pi]$. The Majorana phases instead are distributed in narrow intervals around π . Namely, $\alpha_{21} \in (0.83\pi, 1.17\pi)$

and $\alpha_{31} \in [0.92\pi, 1.08\pi]$. However, the global minimum of χ^2 is somewhat large in this case for both NO and IO orderings. Namely, we find $\chi_{\min}^2 \approx 22$ (19) for NO (IO), i.e., this case is disfavoured at more than 4σ by the current global data.

• **Case D5:** $|(U_{\text{PMNS}})_{\tau 2}| = 1/2$ ($P_e = P_{321}$, $P_\nu = P_{213}$). This last case shares the predicted ranges for $\sin^2 \theta_{12}$, $\sin^2 \theta_{13}$, α_{21} and α_{31} with case D4. Therefore, this case is also not compatible with the 2σ range of the values of $\sin^2 \theta_{12}$. For $\sin^2 \theta_{23}$ instead we find the narrow interval in the lower octant, $\sin^2 \theta_{23} \in [0.488, 0.495]$, which lies outside the 2σ range of $\sin^2 \theta_{23}$. We find $\cos \delta$ to satisfy the sum rule in eq. (3.58), which in this case gives us the values of δ in a narrow interval around π , $\delta \in [0.89\pi, 1.11\pi]$. Thus, all the three CPV phases are concentrated in narrow ranges around π . Finally, we find $\chi_{\min}^2 \approx 18.5$ (15) for NO (IO), which implies that this case is also disfavoured by the latest global neutrino oscillation data.

The PMNS matrix in case A2 is related with that in case A1 by the permutation matrix P_{312} as $U_{\text{PMNS}}^{\text{A2}} = P_{312} U_{\text{PMNS}}^{\text{A1}}$. Given that $P_{312} = P_{132} P_{321}$, one can see that these matrices are related by $\mu - \tau$ interchange, after an unphysical exchange of the first and third rows of $U_{\text{PMNS}}^{\text{A1}}$ has been performed (which amounts to a redefinition of the free parameter θ^e , as shown in eq. (3.21)). The same also holds for the following pairs of cases: (B1, B2), (B3, B4), (C2, C3), (C4, C5), (D2, D3) and (D4, D5). As can be seen from the discussion above and Figs. 1–4 and 6–11, cases inside a pair share some qualitative features. Namely, i) the predicted ranges of $\sin^2 \theta_{12}$, $\sin^2 \theta_{13}$, α_{21} and α_{31} are approximately the same; ii) the predicted range of $\sin^2 \theta_{23}$ gets approximately reflected around $1/2$, i.e., $\sin^2 \theta_{23} \rightarrow 1 - \sin^2 \theta_{23}$; iii) the predicted range of the CPV phase δ experiences an approximate shift by π , i.e., $\delta \rightarrow \delta + \pi$.

In Tables 3 and 4 we summarise the predicted ranges of the mixing parameters obtained in all the phenomenologically viable cases discussed above. The corresponding best fit values together with χ_{\min}^2 are presented in Tables 5 and 6. Finally, in Table 7 we show whether the cases compatible with the 3σ ranges of the three mixing angles are also compatible with their corresponding 2σ ranges.

The results shown in Tables 3–6 allow to assess the possibilities to critically test the predictions of the viable cases of the model and to distinguish between them. We recall that the current 1σ uncertainties on the measured values of $\sin^2 \theta_{12}$, $\sin^2 \theta_{13}$ and $\sin^2 \theta_{23}$ are [24] 5.8%, 4.0% and 9.6%, respectively. These uncertainties are foreseen to be further reduced by the currently active and/or future planned experiments. The Daya Bay collaboration plans to determine $\sin^2 \theta_{13}$ with 1σ uncertainty of 3% [42]. The uncertainties on $\sin^2 \theta_{12}$ and $\sin^2 \theta_{23}$ are planned to be reduced significantly. The parameter $\sin^2 \theta_{12}$ is foreseen to be measured with 1σ relative error of 0.7% in the JUNO experiment [43]. In the proposed upgrading of the currently taking data T2K experiment [44], for example, θ_{23} is estimated to be determined with a 1σ error of 1.7° , 0.5° and 0.7° if the best fit value of $\sin^2 \theta_{23} = 0.50$, 0.43 and 0.60 , respectively. This implies that for these three values of $\sin^2 \theta_{23}$ the absolute 1σ error would be 0.0297, 0.0086 and 0.0120. This error on $\sin^2 \theta_{23}$ will be further reduced in the future planned T2HK [45] and DUNE [46] experiments. If $\delta = 3\pi/2$, the CP-conserving case of $\sin \delta = 0$ would be disfavoured for the NO mass spectrum in the same experiment at least at 3σ C.L. Higher precision measurements of δ are planned to be performed in the T2HK and DUNE experiments.

We turn now to the possibilities to discriminate experimentally between the different cases listed in Tables 3–6 using the prospective data on $\sin^2 \theta_{12}$, $\sin^2 \theta_{13}$, $\sin^2 \theta_{23}$ and δ . The first

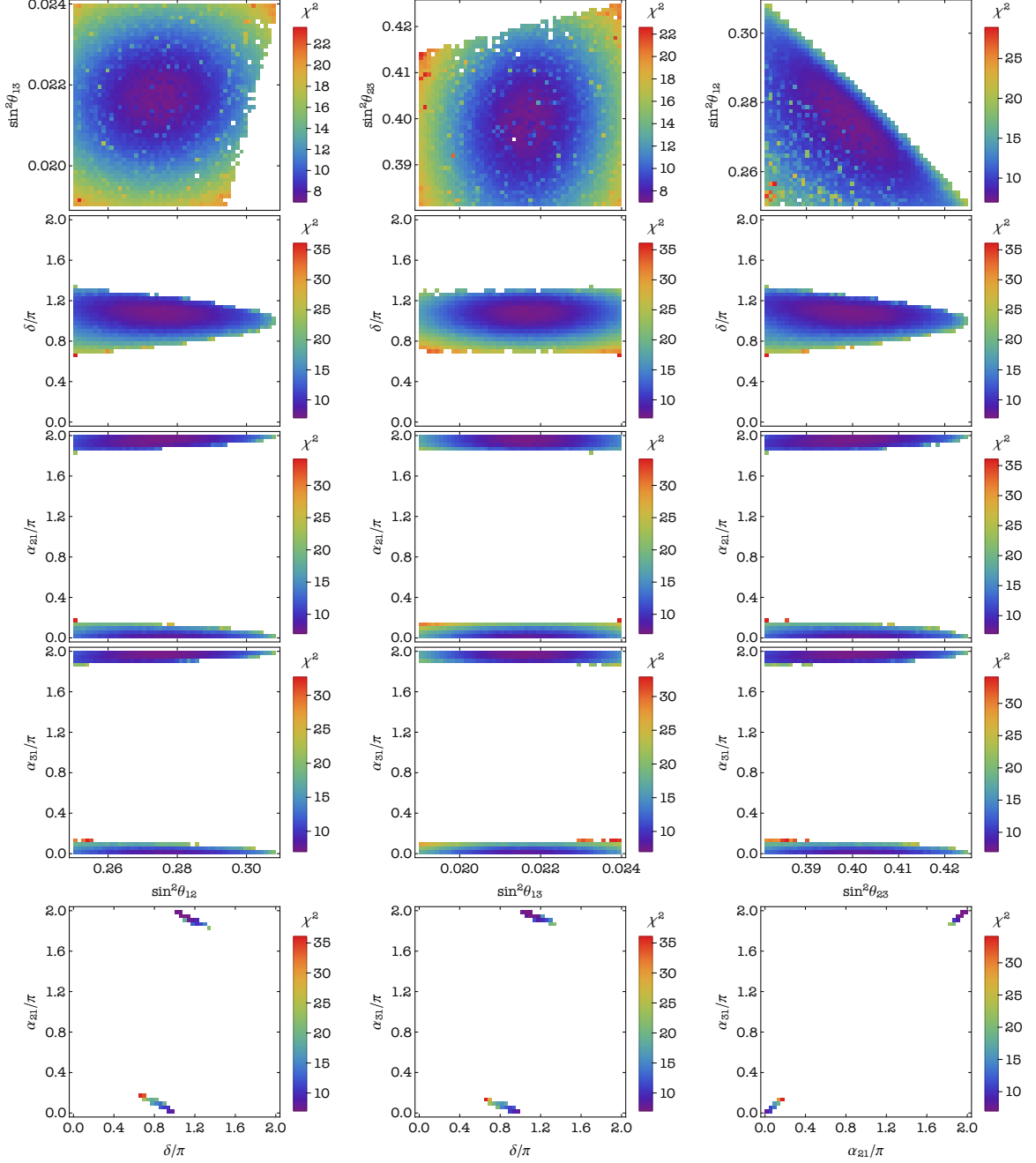


Figure 1: Correlations between the neutrino mixing parameters in case B1. The values of all the three mixing angles are required to lie in their respective 3σ ranges. Colour represents values of χ^2 for the NO neutrino mass spectrum.

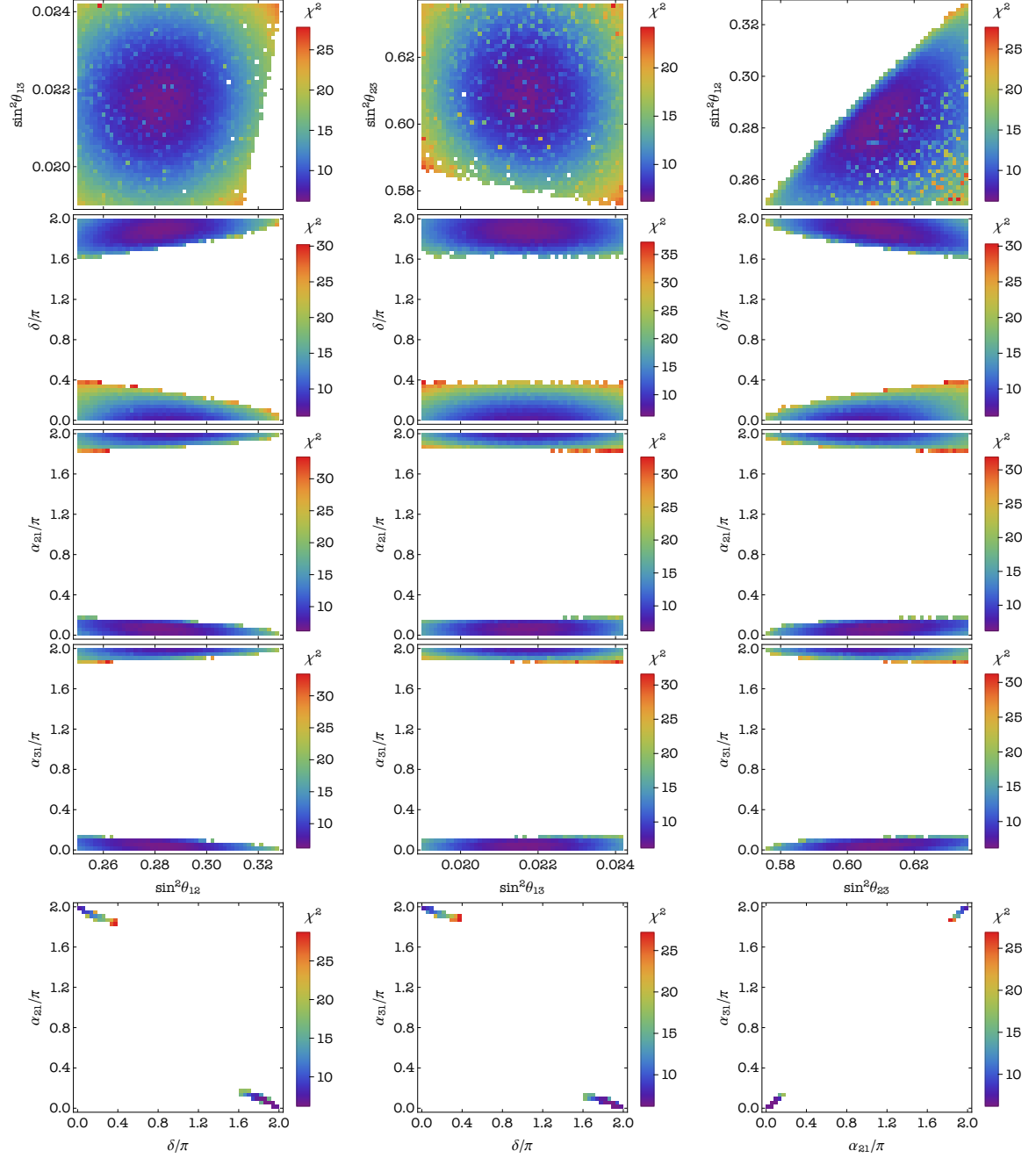


Figure 2: Correlations between the neutrino mixing parameters in case B2. The values of all the three mixing angles are required to lie in their respective 3σ ranges. Colour represents values of χ^2 for the IO neutrino mass spectrum.

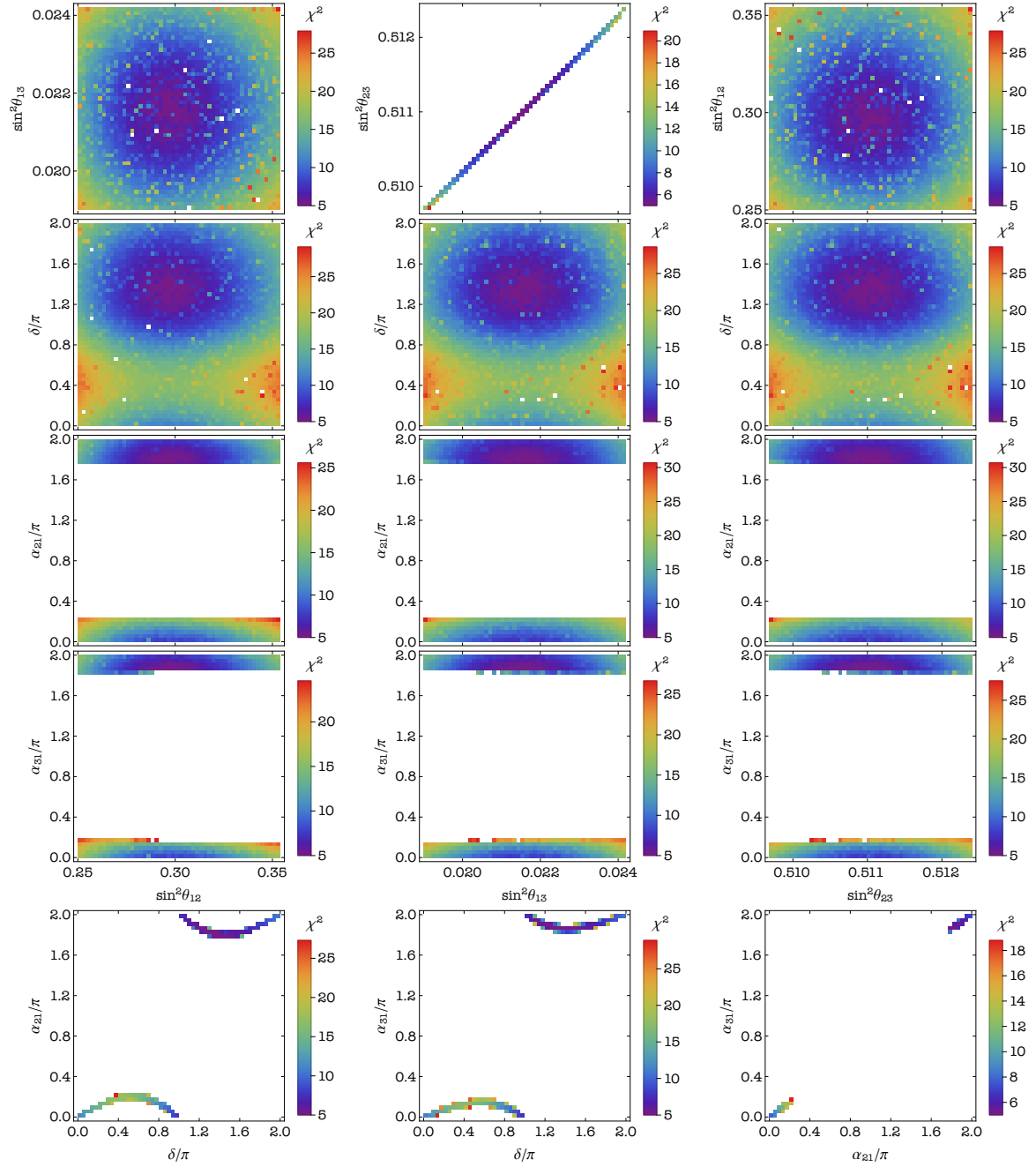


Figure 3: Correlations between the neutrino mixing parameters in case B3. The values of all the three mixing angles are required to lie in their respective 3σ ranges. Colour represents values of χ^2 for the IO neutrino mass spectrum. Note that this case is not compatible with the 2σ range of $\sin^2\theta_{23}$.

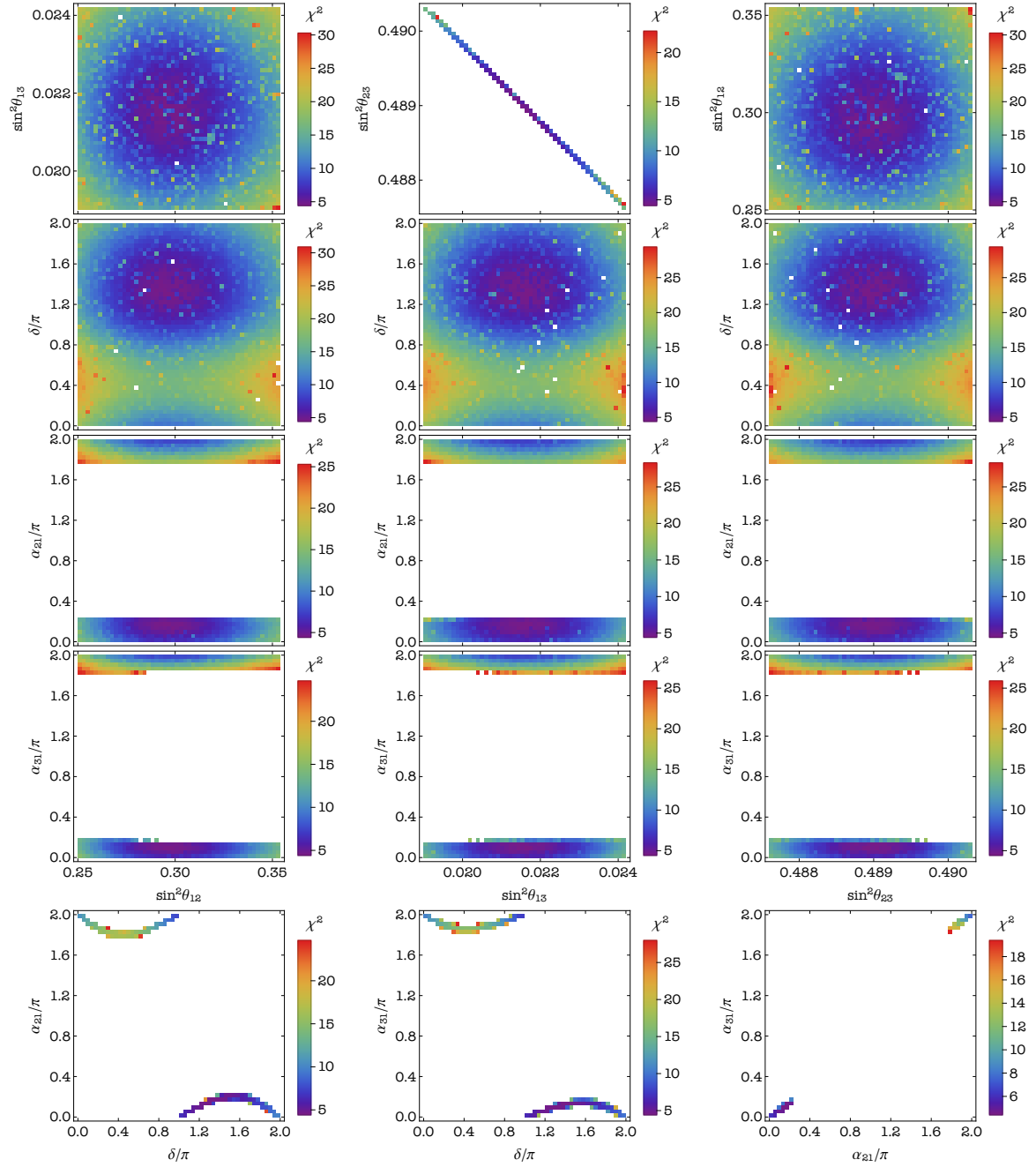


Figure 4: Correlations between the neutrino mixing parameters in case B4. The values of all the three mixing angles are required to lie in their respective 3σ ranges. Colour represents values of χ^2 for the IO neutrino mass spectrum. Note that this case is not compatible with the 2σ range of $\sin^2 \theta_{23}$.

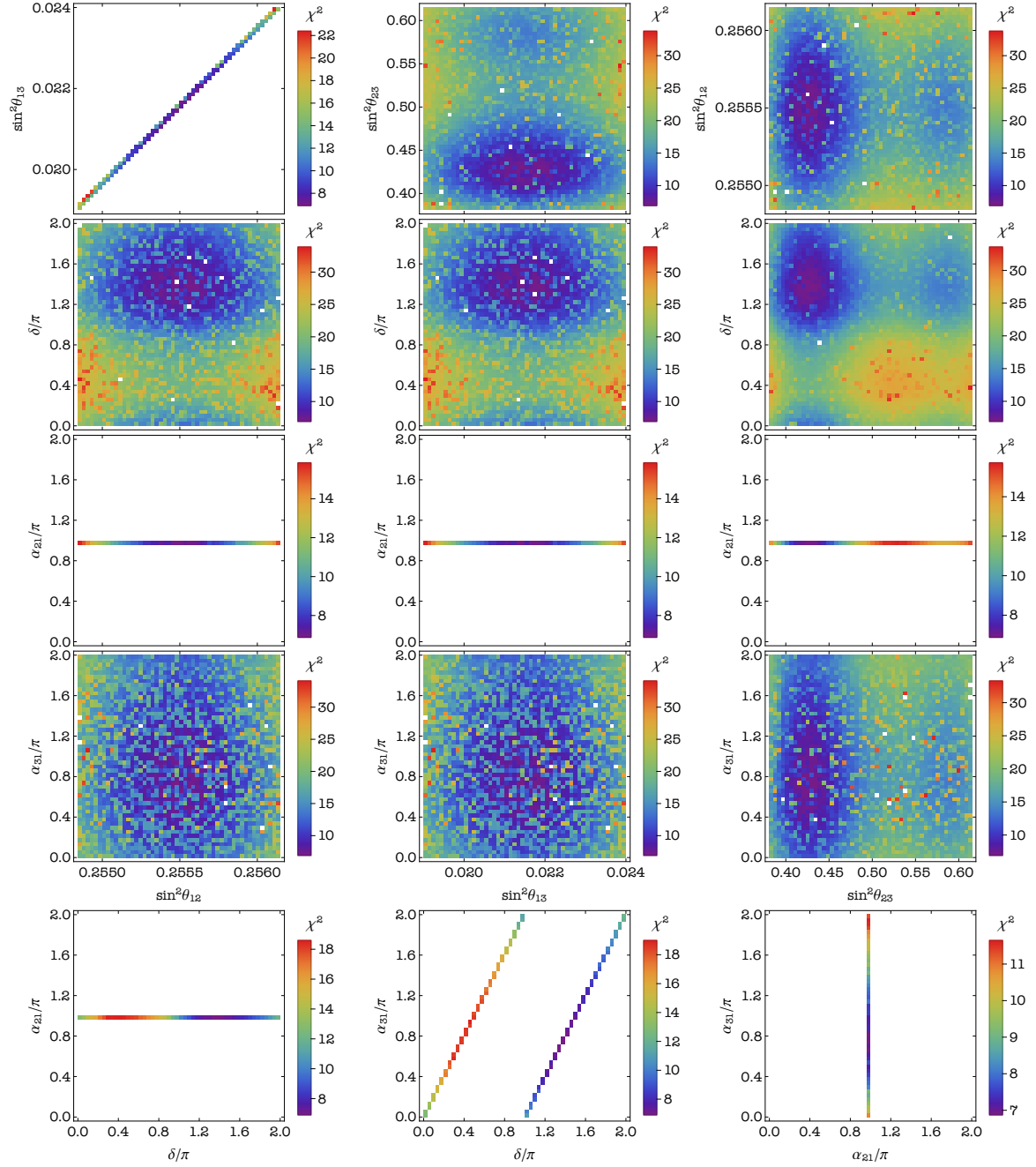


Figure 5: Correlations between the neutrino mixing parameters in case C1. The values of all the three mixing angles are required to lie in their respective 3σ ranges. Colour represents values of χ^2 for the NO neutrino mass spectrum. Note that this case is not compatible with the 2σ range of $\sin^2\theta_{12}$.

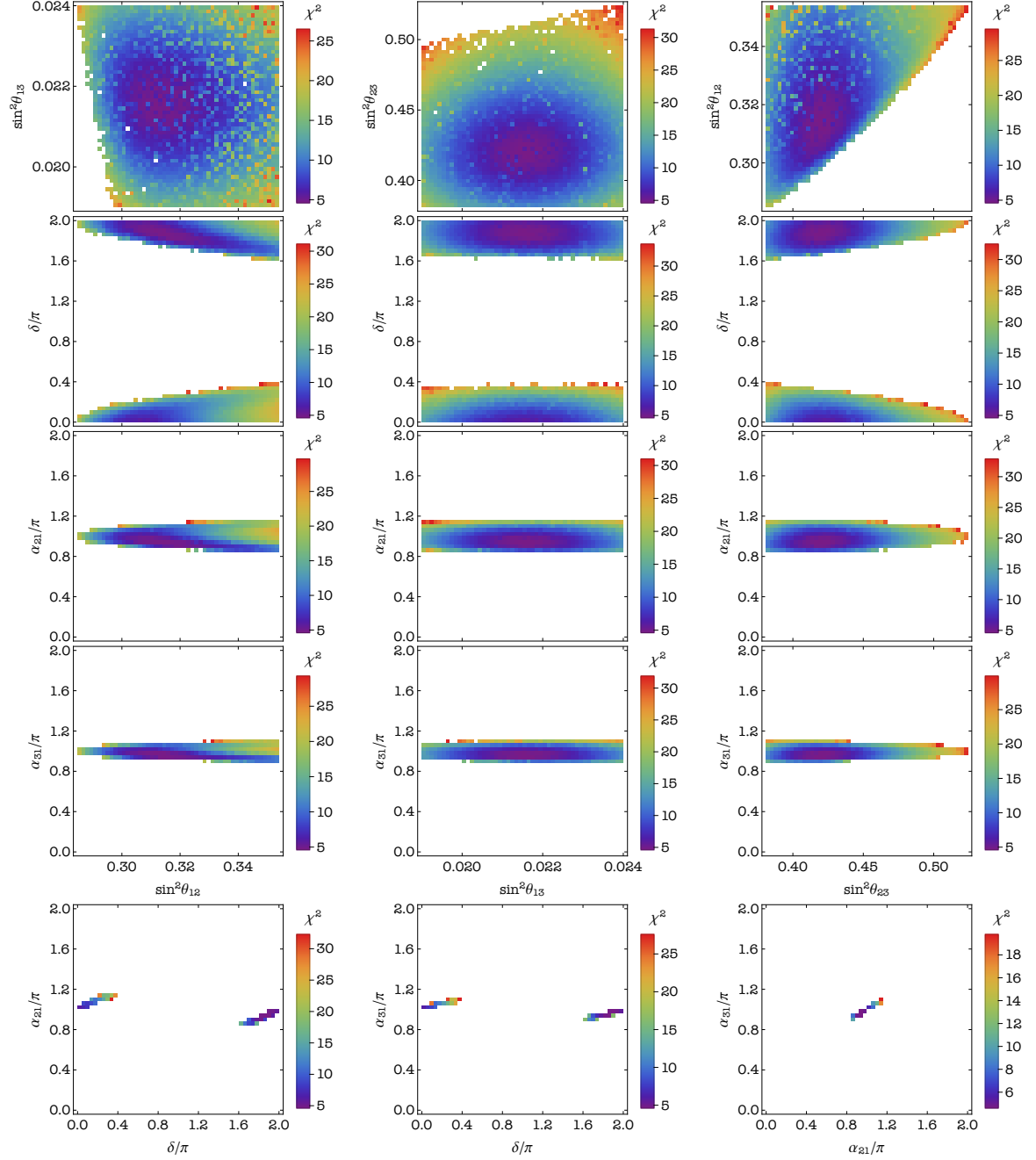


Figure 6: Correlations between the neutrino mixing parameters in case C2. The values of all the three mixing angles are required to lie in their respective 3σ ranges. Colour represents values of χ^2 for the NO neutrino mass spectrum.

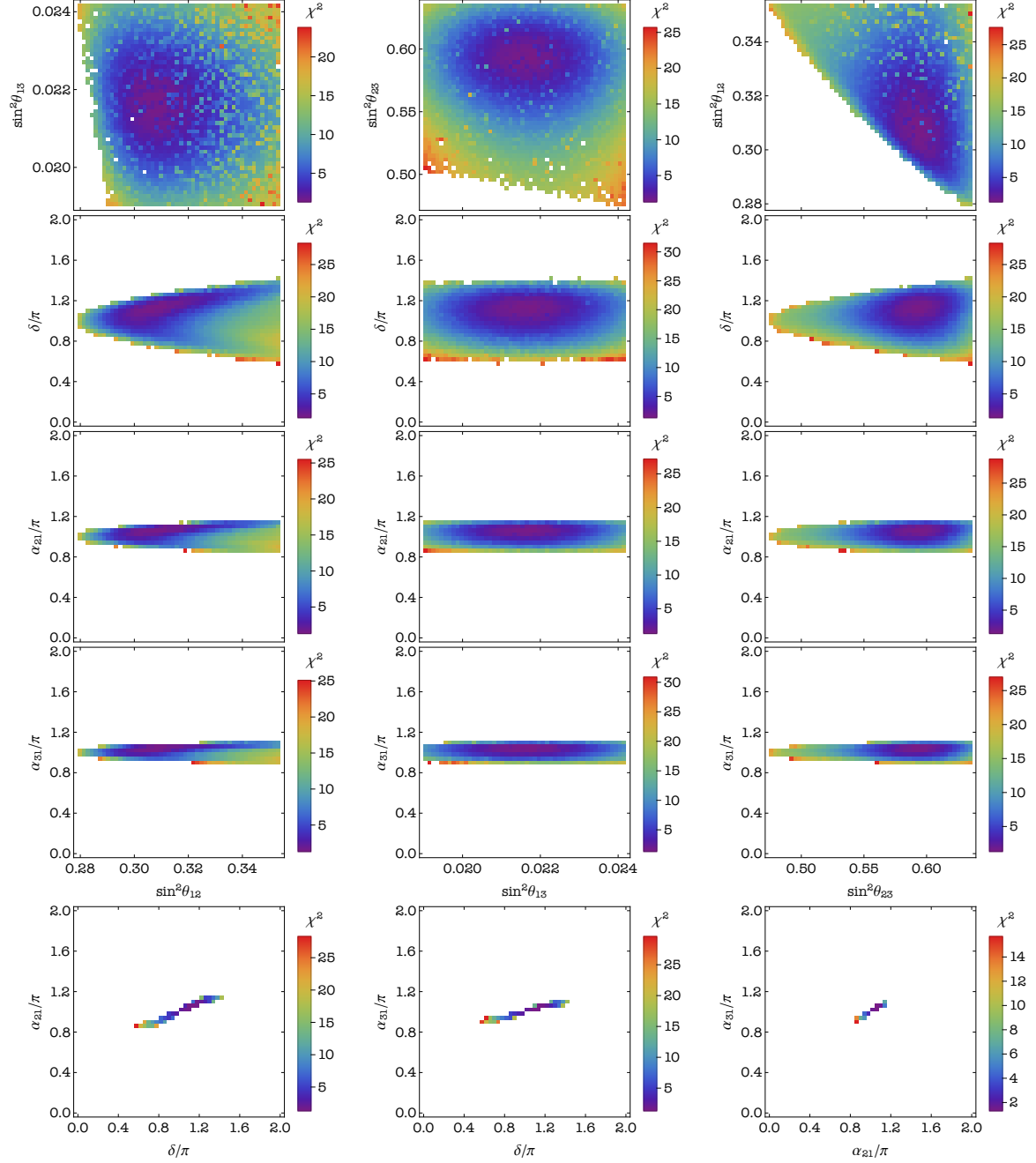


Figure 7: Correlations between the neutrino mixing parameters in case C3. The values of all the three mixing angles are required to lie in their respective 3σ ranges. Colour represents values of χ^2 for the IO neutrino mass spectrum.

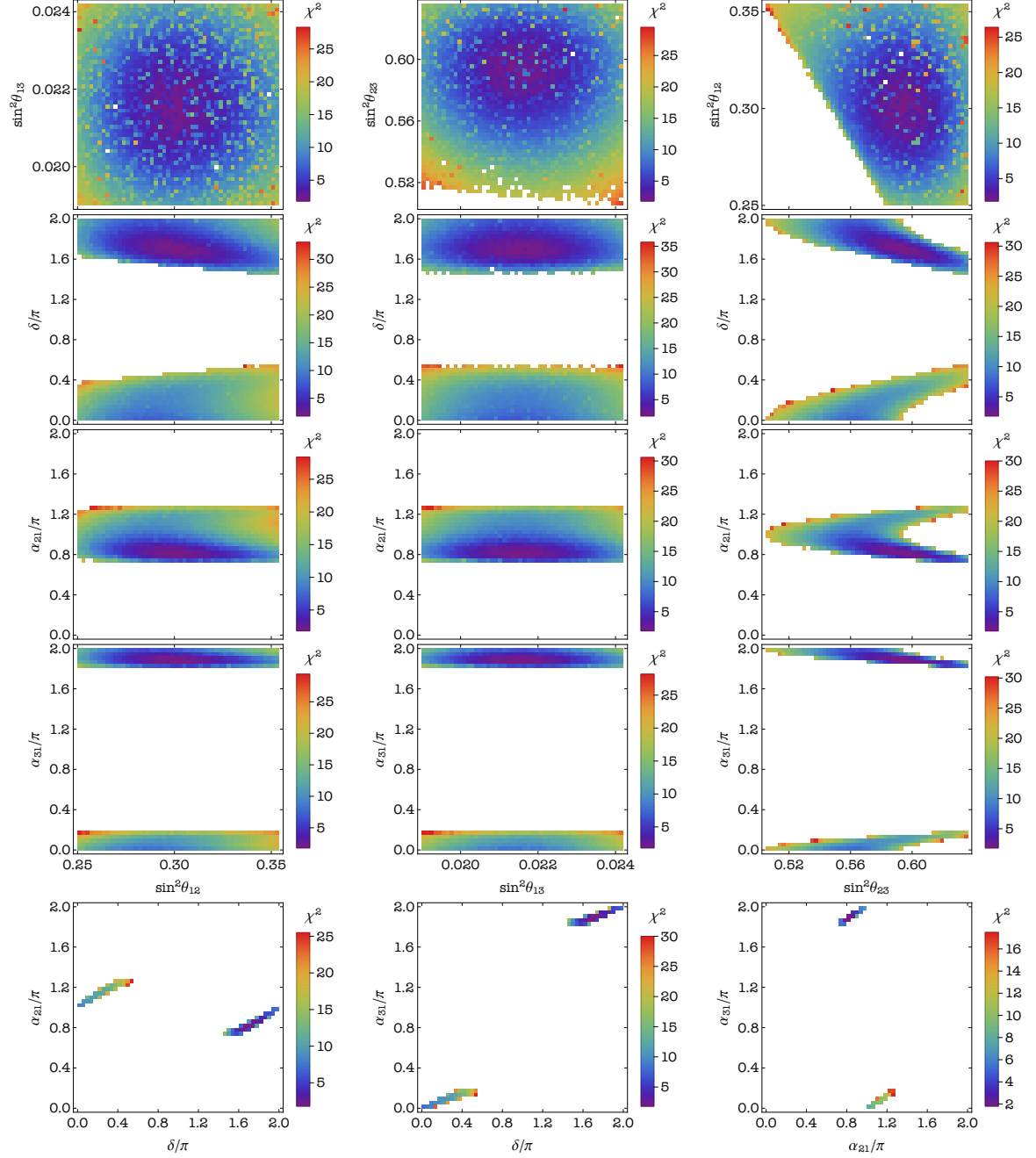


Figure 8: Correlations between the neutrino mixing parameters in case C4. The values of all the three mixing angles are required to lie in their respective 3σ ranges. Colour represents values of χ^2 for the IO neutrino mass spectrum.

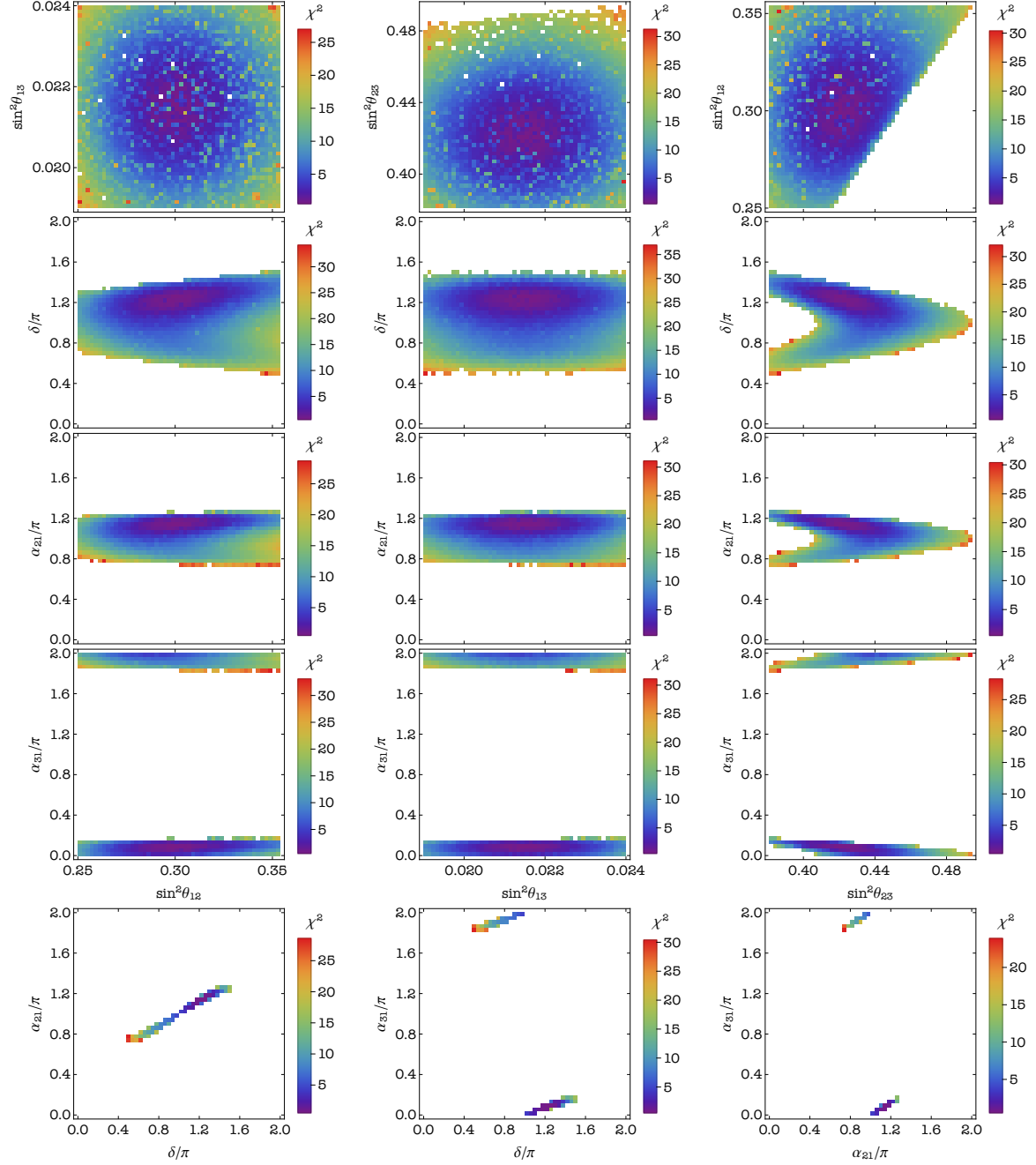


Figure 9: Correlations between the neutrino mixing parameters in case C5. The values of all the three mixing angles are required to lie in their respective 3σ ranges. Colour represents values of χ^2 for the NO neutrino mass spectrum.

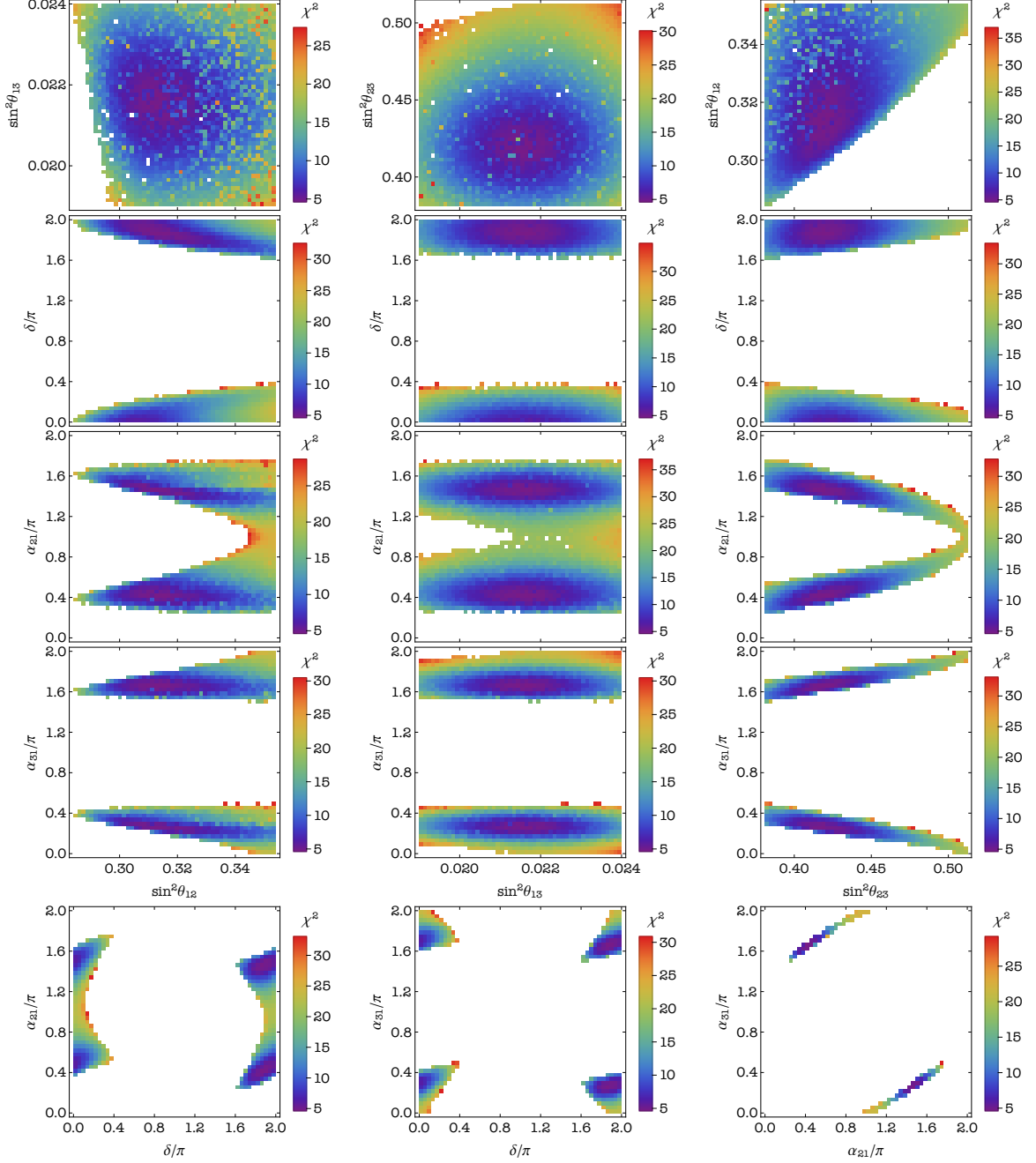


Figure 10: Correlations between the neutrino mixing parameters in case D2. The values of all the three mixing angles are required to lie in their respective 3σ ranges. Colour represents values of χ^2 for the NO neutrino mass spectrum.

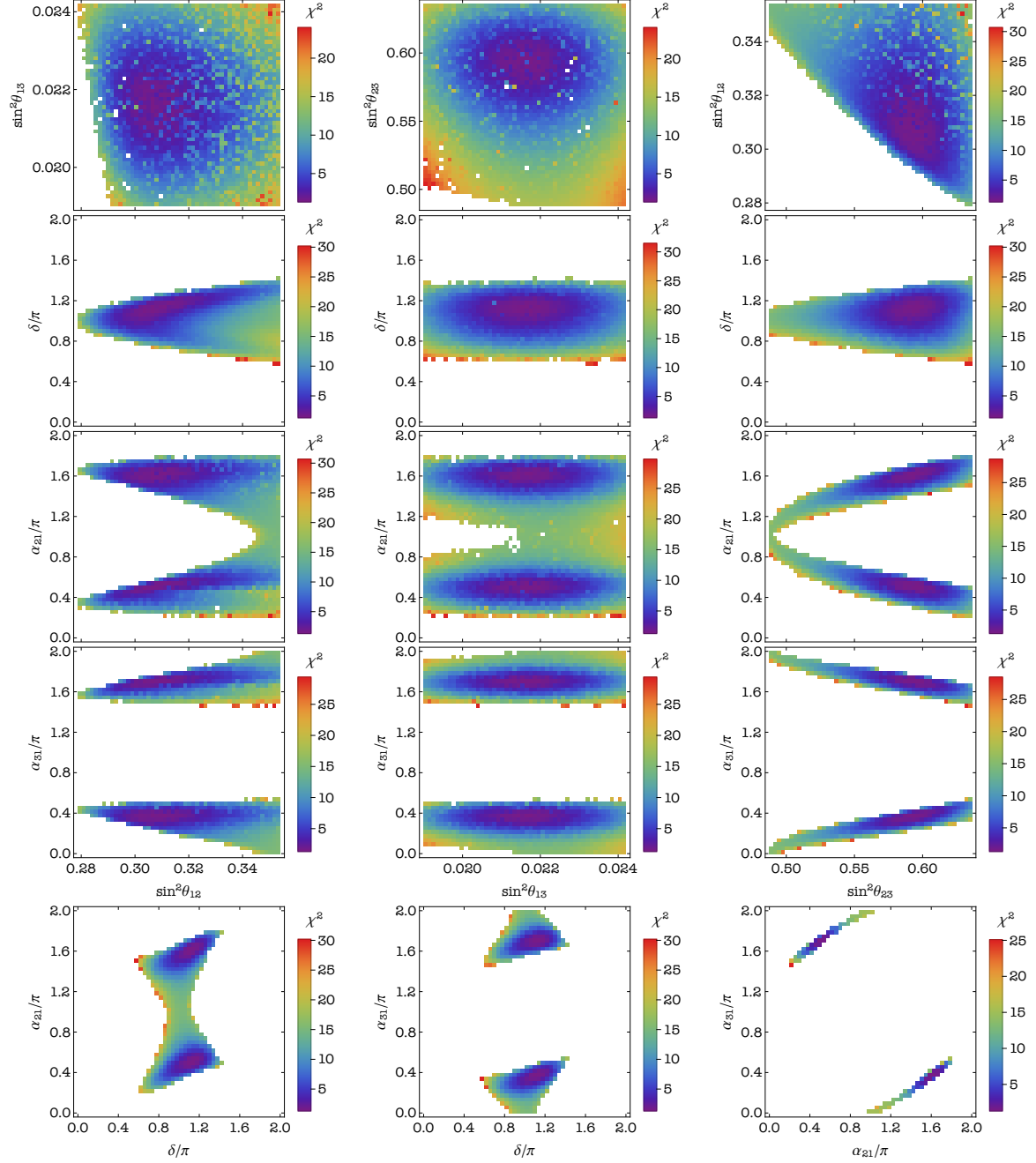


Figure 11: Correlations between the neutrino mixing parameters in case D3. The values of all the three mixing angles are required to lie in their respective 3σ ranges. Colour represents values of χ^2 for the IO neutrino mass spectrum.

thing to notice is that the predicted ranges for $\sin^2 \theta_{12}$, $\sin^2 \theta_{13}$, $\sin^2 \theta_{23}$ and δ in cases A1 and A2 practically coincide with the predictions respectively in cases D4 and D5. However, cases A1, D4 and cases A2, D5 are strongly disfavoured by the current data: for the NO (IO) neutrino mass spectrum A1 and D4 are disfavoured at 4.7σ (4.4σ), while A2 and D5 are disfavoured at 4.3σ (3.9σ). In all these cases $\sin^2 \theta_{12}$, in particular, is predicted to lie in the interval $(0.345, 0.354)$ compatible with the current 3σ range and, given the current best fit value of $\sin^2 \theta_{12}$ and prospective JUNO precision on $\sin^2 \theta_{12}$, it is very probable that future more precise data on $\sin^2 \theta_{12}$ will rule out completely these scenarios. We will not discuss them further in this subsection.

It follows also from Tables 5 and 6 that the combined results on the best fit values of $\sin^2 \theta_{12}$, $\sin^2 \theta_{23}$ and δ we have obtained in the different viable cases (excluding A1, A2, D4 and D5) differ significantly. Assuming, for example, that the experimentally determined best fit values of $\sin^2 \theta_{12}$ and $\sin^2 \theta_{23}$ will coincide with those found by us for a given viable case, it is not difficult to convince oneself inspecting Tables 5 and 6 that the cited prospective 1σ errors on $\sin^2 \theta_{12}$ and $\sin^2 \theta_{23}$ will allow to discriminate between the different viable cases identified in our study. More specifically, considering as an example only the case of NO neutrino mass spectrum, the prospective high precision measurement of $\sin^2 \theta_{12}$ will allow to discriminate between case C1 and all other cases B1–B4, C2–C5, D2 and D3. The same measurement will make it possible to distinguish i) between case B1 and all the other cases except B2, ii) between case B2 and all the other cases except B1, B3 and B4, and similarly iii) between case B3 and all the other cases except B2, B4, C4 and C5. However, the differences between the best fit values of $\sin^2 \theta_{23}$ in cases B1, B2 and B3 (or B4) are sufficiently large, which would permit to distinguish between these three cases if $\sin^2 \theta_{23}$ were measured with the prospective precision. It follows from Table 5, however, that it would be very challenging to discriminate between cases B3 and B4: it will require extremely high precision measurement of $\sin^2 \theta_{23}$. These two cases would be ruled out, however, if the experimentally determined best fit value of $\sin^2 \theta_{23}$ differs significantly from the results for $\sin^2 \theta_{23}$, namely, 0.511 and 0.489, we have obtained for $\sin^2 \theta_{23}$ in the B3 and B4 cases.

In the remaining cases C2–C5 and D2–D3, the results we have obtained for $\sin^2 \theta_{12}$, as Table 6 shows, are very similar. However, the predictions for the pair $\sin^2 \theta_{23}$ and δ differ significantly in cases C2 or D2, and C3 or D3. The cases within each pair would be ruled out if the experimentally determined values of $\sin^2 \theta_{23}$ and δ differ significantly from the predicted best fit values.

Thus, the planned future high precision measurements of $\sin^2 \theta_{12}$ and $\sin^2 \theta_{23}$, together with more precise data on the Dirac phase δ , will make it possible to critically test the predictions of the cases listed in Tables 3–6. A comprehensive analysis of the possibilities to distinguish between the different viable cases found in our work in the considered S_4 model can only be done when more precise data first of all on $\sin^2 \theta_{12}$ and $\sin^2 \theta_{23}$, and then on δ , will be available.

We schematically summarise in Fig. 12 the predicted 3σ allowed regions in the plane $(\sin^2 \theta_{23}, \sin^2 \theta_{12})$ for all currently viable cases from Figs. 1–11. In this figure we also present the best fit point in each case used in the preceding discussion. When future more precise data on $\sin^2 \theta_{23}$ and $\sin^2 \theta_{12}$ become available, the experimentally allowed region in the $(\sin^2 \theta_{23}, \sin^2 \theta_{12})$ plane will shrink, and only a limited number of cases, if any, will remain viable. It will be possible to distinguish further between some or all of the remaining viable cases with a high precision measurement of δ .

Finally, we note that the sum rules for $\sin^2 \theta_{23}$ ($\sin^2 \theta_{12}$ in case C1) and/or $\cos \delta$ obtained in

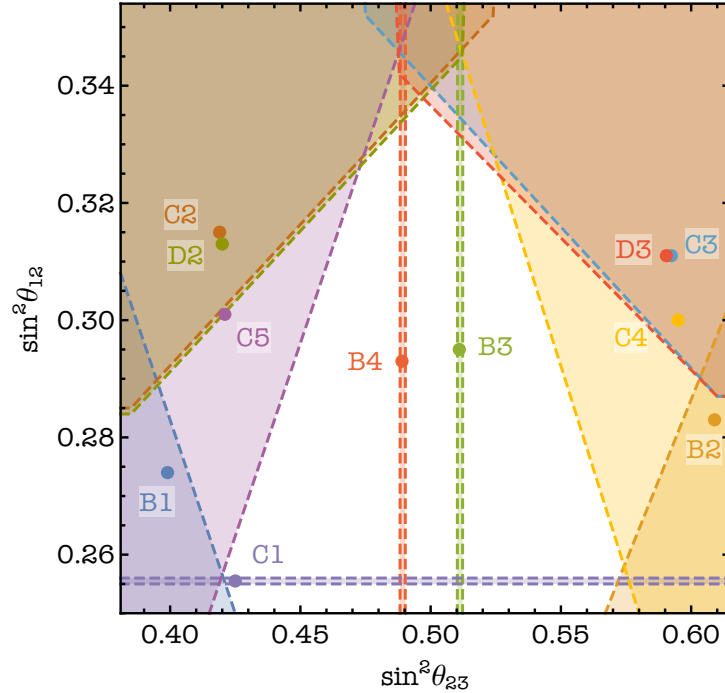


Figure 12: Summary of the predicted allowed regions in the $(\sin^2 \theta_{23}, \sin^2 \theta_{12})$ plane and the corresponding best fit points in cases B1–B4, C1–C5, D2 and D3 for the NO neutrino mass spectrum. The values of all the three mixing angles are required to lie in their respective current 3σ ranges.

the present study follow from those derived in [7] for certain values of the parameters $\sin^2 \theta_{ij}^o$, fixed by $G_f = S_4$ and the residual $Z_2^{g_e}$ and $Z_2^{g_\nu}$ flavour symmetries, and the additional constraints provided by the GCP symmetry H_{CP}^ν . Note that in [7] only flavour symmetry, without imposing a GCP symmetry, has been considered. As we have seen in subsection 2.1, a GCP symmetry does not allow for a free phase δ^ν coming from the neutrino sector, which is present otherwise. This, in turn, leads to the fact that in certain cases the parameter $\sin \hat{\theta}_{ij}^\nu$ (see eq. (213) in [7]), which is free in [7], gets fixed by the GCP symmetry. Thus, we find additional correlations between θ_{ij} and between θ_{ij} and $\cos \delta$ in these cases. We provide the correspondence between the phenomenologically viable cases of the present study and the cases considered in [7] in Appendix D.

H_{CP}^ν	Case (p.f.e.)	$\frac{\sin^2 \theta_{12}}{10^{-1}}$	$\frac{\sin^2 \theta_{13}}{10^{-2}}$	$\frac{\sin^2 \theta_{23}}{10^{-1}}$	δ/π	α_{21}/π (mod 1)	α_{31}/π (mod 1)
$\{1, S\}$	A1	3.45 – 3.54	2.13 – 2.40	5.11 – 5.12	0 – 0.11 \oplus 1.89 – 2	0 – 0.07 \oplus 0.93 – 1	0 – 1
	(μ 3)	3.44 – 3.54	2.13 – 2.42	5.11 – 5.12	0 – 0.12 \oplus 1.88 – 2	0 – 0.07 \oplus 0.93 – 1	0 – 1
	A2	3.45 – 3.54	2.13 – 2.40	4.88 – 4.89	0.89 – 1.11	0 – 0.07 \oplus 0.93 – 1	0 – 1
	(τ 3)	3.44 – 3.54	2.13 – 2.42	4.88 – 4.89	0.88 – 1.12	0 – 0.07 \oplus 0.93 – 1	0 – 1
$\{U, SU\}$	B1	2.50 – 3.08	Full 3σ	3.81 – 4.25	0.68 – 1.32	0 – 0.16 \oplus 0.84 – 1	0 – 0.13 \oplus 0.88 – 1
	(μ 2)	2.50 – 3.06	Full 3σ	3.84 – 4.25	0.69 – 1.31	0 – 0.16 \oplus 0.84 – 1	0 – 0.12 \oplus 0.88 – 1
	B2	2.50 – 3.03	Full 3σ	5.76 – 6.15	0 – 0.30 \oplus 1.70 – 2	0 – 0.16 \oplus 0.84 – 1	0 – 0.12 \oplus 0.88 – 1
	(τ 2)	2.50 – 3.28	Full 3σ	5.76 – 6.36	0 – 0.38 \oplus 1.61 – 2	0 – 0.17 \oplus 0.83 – 1	0 – 0.13 \oplus 0.87 – 1
	B3	Full 3σ	Full 3σ	5.10 – 5.12	0 – 2	0 – 0.23 \oplus 0.77 – 1	0 – 0.18 \oplus 0.83 – 1
	(μ 3)	Full 3σ	Full 3σ	5.10 – 5.12	0 – 2	0 – 0.23 \oplus 0.77 – 1	0 – 0.18 \oplus 0.82 – 1
	B4	Full 3σ	Full 3σ	4.88 – 4.90	0 – 2	0 – 0.23 \oplus 0.77 – 1	0 – 0.17 \oplus 0.83 – 1
	(τ 3)	Full 3σ	Full 3σ	4.88 – 4.90	0 – 2	0 – 0.23 \oplus 0.77 – 1	0 – 0.18 \oplus 0.82 – 1

Table 3: Ranges of the mixing parameters for the viable cases, i.e., those cases for which the predicted values of all the three mixing angles lie inside their respective 3σ allowed ranges. The cases presented here correspond to $G_e = Z_2^{g_e}$ and $G_\nu = Z_2^{g_\nu} \times H_{\text{CP}}^\nu$ with $\{g_e, g_\nu\} = \{TU, S\}$, for which the magnitude of the fixed element is $1/\sqrt{2}$ (p.f.e. denotes its position in U_{PMNS}). For each case, the upper and lower rows refer to NO and IO, respectively.

H_{CP}^ν	Case (p.f.e.)	$\frac{\sin^2 \theta_{12}}{10^{-1}}$	$\frac{\sin^2 \theta_{13}}{10^{-2}}$	$\frac{\sin^2 \theta_{23}}{10^{-1}}$	δ/π	α_{21}/π (mod 1)	α_{31}/π (mod 1)
$\{1, U\}$	C1	2.55 – 2.56	Full 3σ	Full 3σ	0 – 2	0 (exactly)	0 – 1
	(e2)	2.55 – 2.56	Full 3σ	Full 3σ	0 – 2	0 (exactly)	0 – 1
	C2	2.85 – 3.54	Full 3σ	3.81 – 5.24	0 – 0.38 \oplus 1.62 – 2	0 – 0.15 \oplus 0.85 – 1	0 – 0.09 \oplus 0.91 – 1
	(μ 1)	2.86 – 3.54	Full 3σ	3.84 – 5.25	0 – 0.37 \oplus 1.63 – 2	0 – 0.15 \oplus 0.85 – 1	0 – 0.09 \oplus 0.91 – 1
	C3	2.87 – 3.54	Full 3σ	4.75 – 6.15	0.63 – 1.37	0 – 0.15 \oplus 0.86 – 1	0 – 0.09 \oplus 0.91 – 1
	(τ 1)	2.79 – 3.54	Full 3σ	4.75 – 6.36	0.60 – 1.40	0 – 0.15 \oplus 0.85 – 1	0 – 0.09 \oplus 0.91 – 1
	C4	Full 3σ	Full 3σ	5.06 – 6.15	0 – 0.48 \oplus 1.52 – 2	0 – 0.25 \oplus 0.75 – 1	0 – 0.16 \oplus 0.84 – 1
	(μ 2)	Full 3σ	Full 3σ	5.05 – 6.36	0 – 0.54 \oplus 1.45 – 2	0 – 0.27 \oplus 0.73 – 1	0 – 0.18 \oplus 0.82 – 1
	C5	Full 3σ	Full 3σ	3.81 – 4.94	0.51 – 1.49	0 – 0.26 \oplus 0.74 – 1	0 – 0.17 \oplus 0.84 – 1
	(τ 2)	Full 3σ	Full 3σ	3.84 – 4.94	0.52 – 1.48	0 – 0.25 \oplus 0.74 – 1	0 – 0.16 \oplus 0.84 – 1
$\{S, SU\}$	D2	2.84 – 3.54	Full 3σ	3.81 – 5.12	0 – 0.38 \oplus 1.63 – 2	0 – 1	0 – 0.48 \oplus 0.52 – 1
	(μ 1)	2.85 – 3.54	Full 3σ	3.84 – 5.12	0 – 0.37 \oplus 1.63 – 2	0 – 1	0 – 0.48 \oplus 0.52 – 1
	D3	2.87 – 3.54	Full 3σ	4.88 – 6.15	0.63 – 1.37	0 – 1	0 – 0.47 \oplus 0.52 – 1
	(τ 1)	2.79 – 3.54	Full 3σ	4.88 – 6.36	0.59 – 1.41	0 – 1	0 – 1
	D4	3.45 – 3.54	2.14 – 2.40	5.05 – 5.12	0 – 0.11 \oplus 1.89 – 2	0 – 0.16 \oplus 0.83 – 1	0 – 0.08 \oplus 0.92 – 1
	(μ 2)	3.45 – 3.54	2.14 – 2.42	5.05 – 5.12	0 – 0.11 \oplus 1.89 – 2	0 – 0.17 \oplus 0.83 – 1	0 – 0.08 \oplus 0.91 – 1
D5	3.45 – 3.54	2.13 – 2.40	4.88 – 4.95	0.89 – 1.11	0 – 0.16 \oplus 0.83 – 1	0 – 0.08 \oplus 0.92 – 1	
(τ 2)	3.45 – 3.54	2.13 – 2.42	4.88 – 4.95	0.88 – 1.11	0 – 0.17 \oplus 0.83 – 1	0 – 0.09 \oplus 0.91 – 1	

Table 4: The same as in Table 3, but for $G_e = Z_2^{g_e}$ and $G_\nu = Z_2^{g_\nu} \times H_{\text{CP}}^\nu$ with $\{g_e, g_\nu\} = \{TU, U\}$. In this case the magnitude of the fixed element is 1/2.

H_{CP}^ν	Case (p.f.e.)	$\frac{\sin^2 \theta_{12}}{10^{-1}}$	$\frac{\sin^2 \theta_{13}}{10^{-2}}$	$\frac{\sin^2 \theta_{23}}{10^{-1}}$	δ/π	α_{21}/π (mod 1)	α_{31}/π (mod 1)	χ_{min}^2
$\{1, S\}$	A1	3.54	2.18	5.11	1.96	0.97	0.43	22.0
	($\mu 3$)	3.53	2.19	5.11	1.95	0.97	0.89	19.0
	A2	3.54	2.18	4.89	1.05	0.03	0.01	18.5
	($\tau 3$)	3.53	2.20	4.89	1.04	0.02	0.67	15.0
$\{U, SU\}$	B1	2.74	2.17	3.99	1.09	0.94	0.96	7.0
	($\mu 2$)	2.75	2.18	4.01	1.07	0.96	0.97	7.0
	B2	2.83	2.17	6.09	1.89	0.07	0.05	12.5
	($\tau 2$)	2.83	2.17	6.09	1.89	0.07	0.05	6.0
	B3	2.95	2.15	5.11	1.36	0.80	0.85	8.5
	($\mu 3$)	2.95	2.15	5.11	1.36	0.80	0.85	5.0
	B4	2.93	2.16	4.89	1.38	0.19	0.13	6.5
	($\tau 3$)	2.97	2.16	4.89	1.31	0.16	0.11	4.5

Table 5: Best fit values of the mixing parameters and the corresponding value of the χ^2 function, χ_{min}^2 , for the viable cases, i.e., those cases for which the predicted values of all the three mixing angles lie inside their respective 3σ allowed ranges. The cases presented here correspond to $G_e = Z_2^{g_e}$ and $G_\nu = Z_2^{g_\nu} \times H_{\text{CP}}^\nu$ with $\{g_e, g_\nu\} = \{TU, S\}$, for which the magnitude of the fixed element is $1/\sqrt{2}$ (p.f.e. denotes its position in U_{PMNS}). For each case, the upper and lower rows refer to NO and IO, respectively.

H_{CP}^ν	Case (p.f.e.)	$\frac{\sin^2 \theta_{12}}{10^{-1}}$	$\frac{\sin^2 \theta_{13}}{10^{-2}}$	$\frac{\sin^2 \theta_{23}}{10^{-1}}$	δ/π	α_{21}/π (mod 1)	α_{31}/π (mod 1)	χ_{min}^2
$\{1, U\}$	C1	2.56	2.16	4.25	1.32	0	0.64	7.0
	(e2)	2.56	2.16	5.85	1.36	0	0.73	7.0
	C2	3.15	2.16	4.19	1.86	0.93	0.96	4.5
	(μ 1)	3.14	2.16	4.24	1.88	0.94	0.96	5.5
	C3	3.11	2.16	5.92	1.15	0.07	0.05	8.5
	(τ 1)	3.08	2.17	5.93	1.13	0.06	0.04	1.5
	C4	3.00	2.14	5.95	1.69	0.81	0.88	8.5
	(μ 2)	3.00	2.14	5.95	1.69	0.81	0.88	2.0
	C5	3.01	2.15	4.21	1.25	0.15	0.10	0.5
	(τ 2)	2.99	2.17	4.26	1.22	0.13	0.09	0.5
$\{S, SU\}$	D2	3.13	2.15	4.20	1.88	0.43	0.65	4.5
	(μ 1)	3.15	2.17	4.23	1.87	0.43	0.66	5.5
	D3	3.11	2.17	5.91	1.14	0.61	0.38	8.5
	(τ 1)	3.06	2.16	5.96	1.12	0.50	0.69	1.5
	D4	3.54	2.18	5.11	1.96	0.97	0.98	22.0
	(μ 2)	3.53	2.20	5.11	1.95	0.97	0.98	19.0
	D5	3.54	2.19	4.89	1.05	0.03	0.02	18.5
	(τ 2)	3.53	2.19	4.89	1.04	0.03	0.01	15.0

Table 6: The same as in Table 5, but for $G_e = Z_2^{g_e}$ and $G_\nu = Z_2^{g_\nu} \times H_{\text{CP}}^\nu$ with $\{g_e, g_\nu\} = \{TU, U\}$. In this case the magnitude of the fixed element is $1/2$.

		A1	A2	B1	B2	B3	B4	C1	C2	C3	C4	C5	D2	D3	D4	D5
3σ	NO	✓	✓	✓	✓	✓	✓	✓	✓	✓	✓	✓	✓	✓	✓	✓
	IO	✓	✓	✓	✓	✓	✓	✓	✓	✓	✓	✓	✓	✓	✓	✓
2σ	NO	✗	✗	✓	✗	✗	✗	✗	✓	✗	✗	✓	✓	✗	✗	✗
	IO	✗	✗	✓	✓	✗	✗	✗	✓	✓	✓	✓	✓	✓	✗	✗

Table 7: Compatibility of the cases under consideration with the 3σ and 2σ experimentally allowed ranges of the three neutrino mixing angles for both types of the neutrino mass spectrum.

4 Neutrinoless Double Beta Decay

As we have seen, in the class of models investigated in the present article the Dirac and Majorana CPV phases, δ and α_{21} , α_{31} , are (statistically) predicted to lie in specific, in most cases relatively narrow, intervals and their values are strongly correlated. The only exception is case C1, in which the exact predictions $\alpha_{21} = 0$ or π and $(\alpha_{31} - 2\delta) = 0$ or π hold.

These results make it possible to derive predictions for the absolute value of the neutrinoless double beta ($(\beta\beta)_{0\nu}$ -) decay effective Majorana mass, $\langle m \rangle$ (see, e.g., refs. [1, 40, 41]), as a function of the lightest neutrino mass. As is well known, information about $|\langle m \rangle|$ is provided by the experiments on $(\beta\beta)_{0\nu}$ -decay of even-even nuclei ^{48}Ca , ^{76}Ge , ^{82}Se , ^{100}Mo , ^{116}Cd , ^{130}Te , ^{136}Xe , ^{150}Nd , etc., $(A, Z) \rightarrow (A, Z + 2) + e^- + e^-$, in which the total lepton charge changes by two units, and through the observation of which the possible Majorana nature of massive neutrinos can be revealed. If the light neutrinos with definite mass ν_j are Majorana fermions, their exchange between two neutrons of the initial nucleus (A, Z) can trigger the process of $(\beta\beta)_{0\nu}$ -decay. In this case the $(\beta\beta)_{0\nu}$ -decay amplitude has the following general form (see, e.g., refs. [40, 41]): $A((\beta\beta)_{0\nu}) = G_{\text{F}}^2 \langle m \rangle M(A, Z)$, with G_{F} , $\langle m \rangle$ and $M(A, Z)$ being respectively the Fermi constant, the $(\beta\beta)_{0\nu}$ -decay effective Majorana mass and the nuclear matrix element (NME) of the process. All the dependence of $A((\beta\beta)_{0\nu})$ on the neutrino mixing parameters is contained in $\langle m \rangle$. The current best limits on $|\langle m \rangle|$ have been obtained by the KamLAND-Zen [47] and GERDA Phase II [48] experiments searching for $(\beta\beta)_{0\nu}$ -decay of ^{136}Xe and ^{76}Ge , respectively:

$$|\langle m \rangle| < (0.061 - 0.165) \text{ eV} \quad [47] \quad \text{and} \quad |\langle m \rangle| < (0.15 - 0.33) \text{ eV} \quad [48], \quad (4.1)$$

both at 90% C.L., where the intervals reflect the estimated uncertainties in the relevant NMEs used to extract the limits on $|\langle m \rangle|$ from the experimentally obtained lower bounds on the ^{136}Xe and ^{76}Ge $(\beta\beta)_{0\nu}$ -decay half-lives (for a review of the limits on $|\langle m \rangle|$ obtained in other $(\beta\beta)_{0\nu}$ -decay experiments and a detailed discussion of the NME calculations for $(\beta\beta)_{0\nu}$ -decay and their uncertainties see, e.g., [49]). It is important to note that a large number of experiments of a new generation aims at a sensitivity to $|\langle m \rangle| \sim (0.01 - 0.05) \text{ eV}$, which will allow to probe the whole range of the predictions for $|\langle m \rangle|$ in the case of IO neutrino mass spectrum [50] (see, e.g., [49, 51] for reviews of the currently running and future planned $(\beta\beta)_{0\nu}$ -decay experiments and their prospective sensitivities).

The predictions for $|\langle m \rangle|$ (see, e.g., [36, 40, 41]),

$$\begin{aligned} |\langle m \rangle| &= \left| \sum_{i=1}^3 m_i U_{ei}^2 \right| \\ &= \left| m_1 \cos^2 \theta_{12} \cos^2 \theta_{13} + m_2 \sin^2 \theta_{12} \cos^2 \theta_{13} e^{i\alpha_{21}} + m_3 \sin^2 \theta_{13} e^{i(\alpha_{31} - 2\delta)} \right|, \end{aligned} \quad (4.2)$$

$m_{1,2,3}$ being the light Majorana neutrino masses, depend on the values of the Majorana phase α_{21} and on the Majorana-Dirac phase difference $(\alpha_{31} - 2\delta)$. For the normal hierarchical (NH), inverted hierarchical (IH) and quasi-degenerate (QD), neutrino mass spectra $|\langle m \rangle|$ is given

by (see, e.g., [1, 52]):

$$|\langle m \rangle| \cong \left| \sqrt{\Delta m_{21}^2} \sin^2 \theta_{12} \cos^2 \theta_{13} e^{i\alpha_{21}} + \sqrt{\Delta m_{31}^2} \sin^2 \theta_{13} e^{i(\alpha_{31} - 2\delta)} \right| \quad (\text{NH}), \quad (4.3)$$

$$|\langle m \rangle| \cong \sqrt{\Delta m_{23}^2} \cos^2 \theta_{13} |\cos^2 \theta_{12} + \sin^2 \theta_{12} e^{i\alpha_{21}}| \quad (\text{IH}), \quad (4.4)$$

$$|\langle m \rangle| \cong m_0 |\cos^2 \theta_{12} + \sin^2 \theta_{12} e^{i\alpha_{21}}| \quad (\text{QD}), \quad (4.5)$$

where $m_0 \cong m_{1,2,3}$. We recall that the NH spectrum corresponds to $m_1 \ll m_2 < m_3$, and thus, $m_2 = (m_1^2 + \Delta m_{21}^2)^{\frac{1}{2}} \cong (\Delta m_{21}^2)^{\frac{1}{2}} \cong 8.6 \times 10^{-3}$ eV, $m_3 = (m_3^2 + \Delta m_{31}^2)^{\frac{1}{2}} \cong (\Delta m_{31}^2)^{\frac{1}{2}} \cong 0.0506$ eV. The IH spectrum corresponds to $m_3 \ll m_1 < m_2$, and therefore, $m_1 = (m_3^2 + \Delta m_{23}^2 - \Delta m_{21}^2)^{\frac{1}{2}} \cong (\Delta m_{23}^2 - \Delta m_{21}^2)^{\frac{1}{2}} \cong 0.0497$ eV, $m_2 = (m_3^2 + \Delta m_{23}^2)^{\frac{1}{2}} \cong (\Delta m_{23}^2)^{\frac{1}{2}} \cong 0.0504$ eV. In the case of QD spectrum we have: $m_1 \cong m_2 \cong m_3 \cong m_0$, $m_j^2 \gg \Delta m_{31(23)}^2$, $m_0 \gtrsim 0.10$ eV. In eqs. (4.3) and (4.4) we have assumed that the contributions respectively $\propto m_1$ and $\propto m_3$ are negligible, while in eq. (4.5) we have neglected corrections $\propto \sin^2 \theta_{13}$ ¹⁵ and $\propto \Delta m_{31(23)}^2/m_0^2$. Clearly, the values of the phases ($\alpha_{31} - \alpha_{21} - 2\delta$) and α_{21} determine the ranges of possible values of $|\langle m \rangle|$ in the cases of NH and IH (QD) spectra, respectively. Using the 3σ ranges of the allowed values of the neutrino oscillation parameters from Table 1, we find that:

- i) 0.79×10^{-3} eV $\lesssim |\langle m \rangle| \lesssim 4.33 \times 10^{-3}$ eV in the case of NH spectrum;
- ii) $\sqrt{\Delta m_{23}^2} \cos^2 \theta_{13} \cos 2\theta_{12} \lesssim |\langle m \rangle| \lesssim \sqrt{\Delta m_{23}^2} \cos^2 \theta_{13}$, or 1.4×10^{-2} eV $\lesssim |\langle m \rangle| \lesssim 5.1 \times 10^{-2}$ eV in the case of IH spectrum;
- iii) $m_0 \cos 2\theta_{12} \lesssim |\langle m \rangle| \lesssim m_0$, or 2.9×10^{-2} eV $\lesssim |\langle m \rangle| \lesssim m_0$ eV, $m_0 \gtrsim 0.10$ eV, in the case of QD spectrum, where we have used the fact that at 3σ C.L., $\cos 2\theta_{12} \geq 0.29$.

In what follows, we obtain predictions for $|\langle m \rangle|$ using the phenomenologically viable neutrino mixing patterns found in subsection 3.4. In Figs. 13–16 we present $|\langle m \rangle|$ as a function of the lightest neutrino mass m_{\min} ($m_{\min} = m_1$ for the NO spectrum and $m_{\min} = m_3$ for the IO spectrum) in cases B1–B4, C1–C3, C4 and C5, and D2 and D3. The solid and dashed lines limit the found allowed regions of $|\langle m \rangle|$ calculated using the predicted ranges for θ_{12} , θ_{13} , α_{21} , ($\alpha_{31} - 2\delta$). In the left panels we require the predicted values of $\sin^2 \theta_{12}$, $\sin^2 \theta_{13}$ and $\sin^2 \theta_{23}$ to lie in their corresponding experimentally allowed 3σ intervals, while in the right panels we require them to be inside the corresponding 2σ ranges. The mass squared differences Δm_{21}^2 and $\Delta m_{31(23)}^2$ in the case of NO (IO) spectrum are varied in their appropriate ranges given in Table 1. The light-blue (light-red) areas in the left and right panels are obtained varying the neutrino oscillation parameters θ_{12} , θ_{13} , Δm_{21}^2 and $\Delta m_{31(23)}^2$ in their full 3σ and 2σ NO (IO) ranges, respectively, and varying the phases α_{21} and ($\alpha_{31} - 2\delta$) in the interval $[0, 2\pi)$. The horizontal brown and grey bands indicate the current most stringent upper limits on $|\langle m \rangle|$, given in eq. (4.1), set by KamLAND-Zen and GERDA Phase II, respectively. The vertical grey line represents the prospective upper limit on $m_{\min} \lesssim 0.2$ eV from the KATRIN experiment [53].

¹⁵The term $\propto \sin^2 \theta_{13}$ gives a subleading contribution because even in the case of $\alpha_{21} = \pi$, when the leading term $\propto (\cos^2 \theta_{12} - \sin^2 \theta_{12})$ has a minimal value, $\sin^2 \theta_{13} \ll \cos 2\theta_{12}$ since $\sin^2 \theta_{13} \leq 0.0242$ while $\cos 2\theta_{12} \geq 0.29$ at 3σ .

Several comments are in order. Firstly, for given values of (k_1, k_2) and a given ordering we find $|\langle m \rangle|$ to be inside of a band, which occupies a certain part of the allowed parameter space. Secondly, we note that most cases are compatible with both 3σ and 2σ ranges of all the mixing angles for both neutrino mass orderings (see Table 7). There are several exceptions. Namely, cases B2, C3, C4 and D3, in which, due to the correlations imposed by the employed symmetry, the predictions for $\sin^2 \theta_{23}$ for the NO spectrum are not compatible with its 2σ allowed range (see Tables 3 and 4). Moreover, there is incompatibility for both orderings of cases B3 and B4 with the allowed 2σ ranges of $\sin^2 \theta_{23}$ (see Table 3), and of case C1 with the 2σ range of $\sin^2 \theta_{12}$ (see Table 4). Thirdly, the predictions for $|\langle m \rangle|$ compatible with the 3σ ranges of all the mixing angles are almost the same for the following pairs of cases: (B1, B2), (B3, B4), (C2, C3), (C4, C5) and (D2, D3). As discussed at the end of subsection 3.4, the cases in each pair share some qualitative features, in particular, the allowed ranges of θ_{12} , θ_{13} , α_{21} and $(\alpha_{31} - 2\delta)$ are approximately equal. We note also that case C1 stands out by having relatively narrow bands for $|\langle m \rangle|$ due to the predicted values of $\alpha_{21} = k_1 \pi$ and $(\alpha_{31} - 2\delta) = k_2 \pi$. Finally, the results shown in Figs. 13–16 and derived using the predictions for the CPV phases and the mixing angles θ_{12} and θ_{13} in the case when the predicted values of all the three mixing angles θ_{12} , θ_{13} and θ_{23} are compatible with their respective 3σ experimentally allowed ranges, can be obtained analytically in the limiting cases of NH, IH and QD spectra using eqs. (4.3)–(4.5), the values of Δm_{21}^2 and $\Delta m_{31(23)}^2$ quoted in Table 1 and the results on $\sin^2 \theta_{12}$, $\sin^2 \theta_{13}$, δ , α_{21} and α_{31} given in Tables 3 and 4.

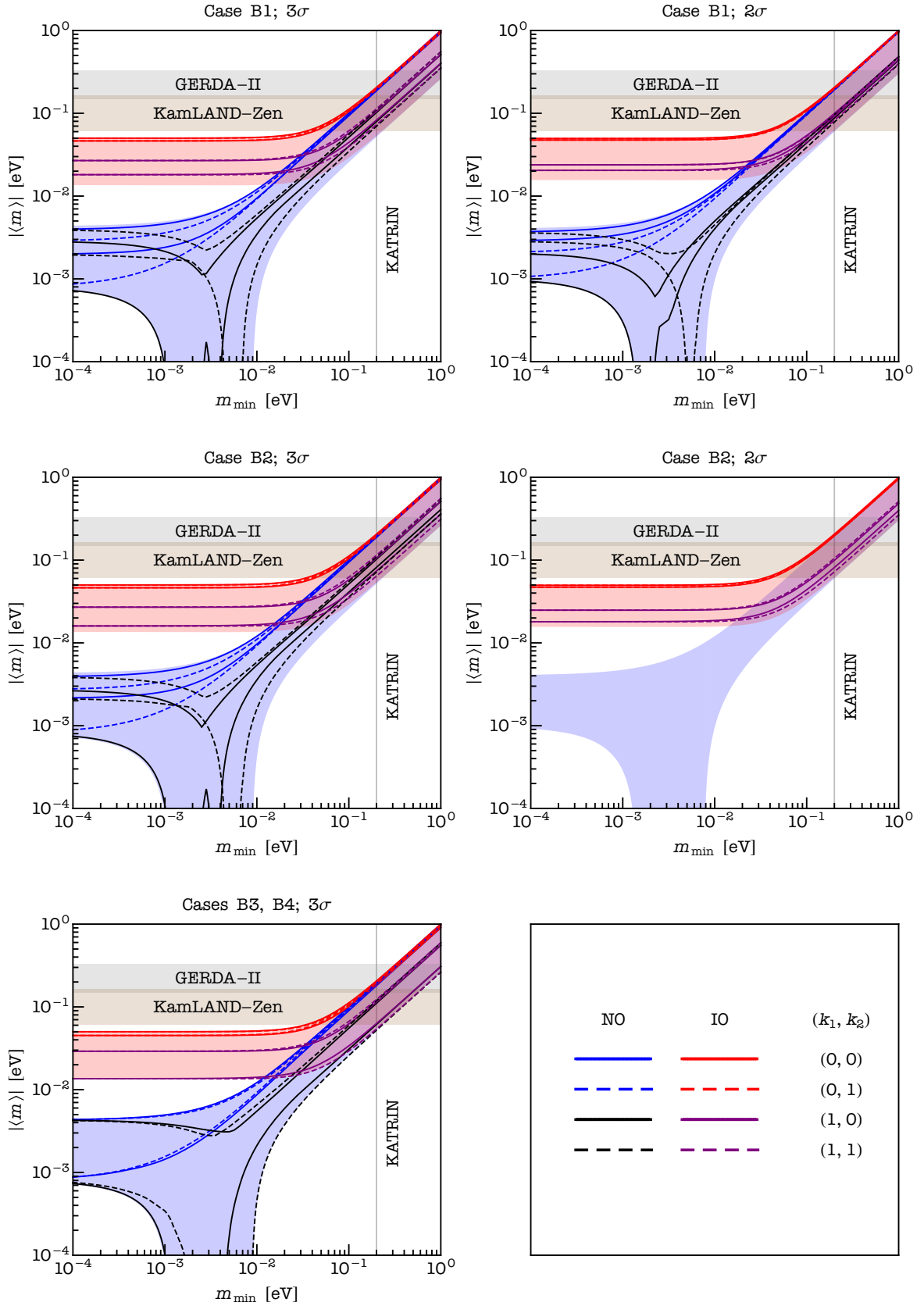


Figure 13: The magnitude of the effective Majorana mass $|\langle m \rangle|$ versus the lightest neutrino mass m_{\min} . The *lines* limit the allowed regions of $|\langle m \rangle|$ calculated using the predictions for the relevant mixing angles and the CPV phases obtained in cases B1 – B4 and compatible with the 3σ (left panels) and 2σ (right panels) ranges of all the three mixing angles. The *light-blue* (*light-red*) areas are obtained varying the neutrino oscillation parameters θ_{12} , θ_{13} , Δm_{21}^2 and $\Delta m_{31(23)}^2$ for NO (IO) in their allowed 3σ and 2σ ranges in the left and right panels, respectively, and the phases α_{21} and $(\alpha_{31} - 2\delta)$ in the interval $[0, 2\pi)$. The *horizontal brown* and *grey bands* indicate the current upper bounds on $|\langle m \rangle|$ quoted in eq. (4.1) set by KamLAND-Zen [47] and GERDA Phase II [48], respectively. The *vertical grey line* represents the prospective upper limit on $m_{\min} \lesssim 0.2$ eV from KATRIN [53]. Cases B3 and B4 are compatible with the 3σ ranges of the mixing angles, but not with their 2σ ranges.

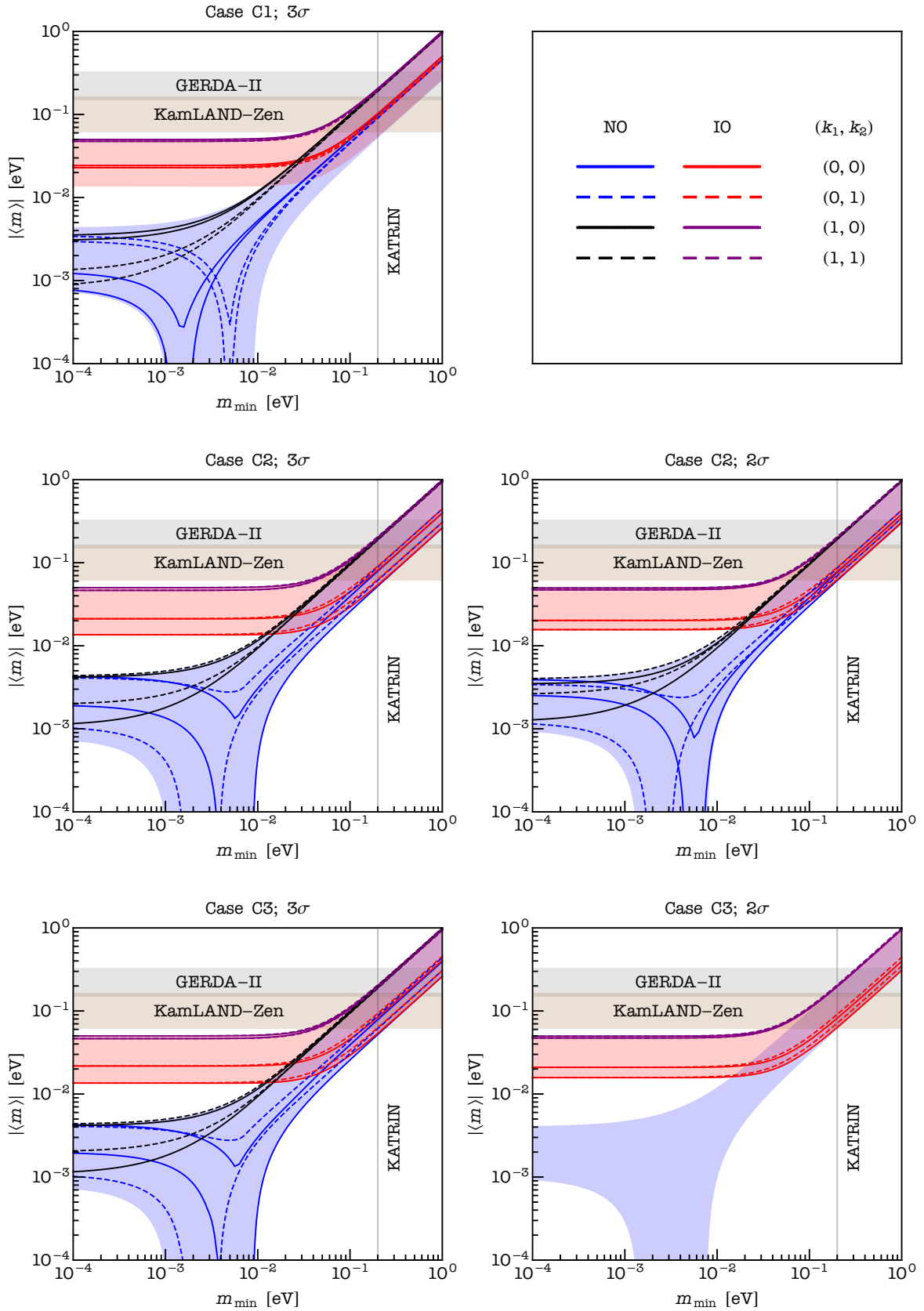


Figure 14: The same as in Fig. 13, but for cases C1–C3. Case C1 is compatible with the 3σ ranges of the mixing angles, but not with their 2σ ranges.

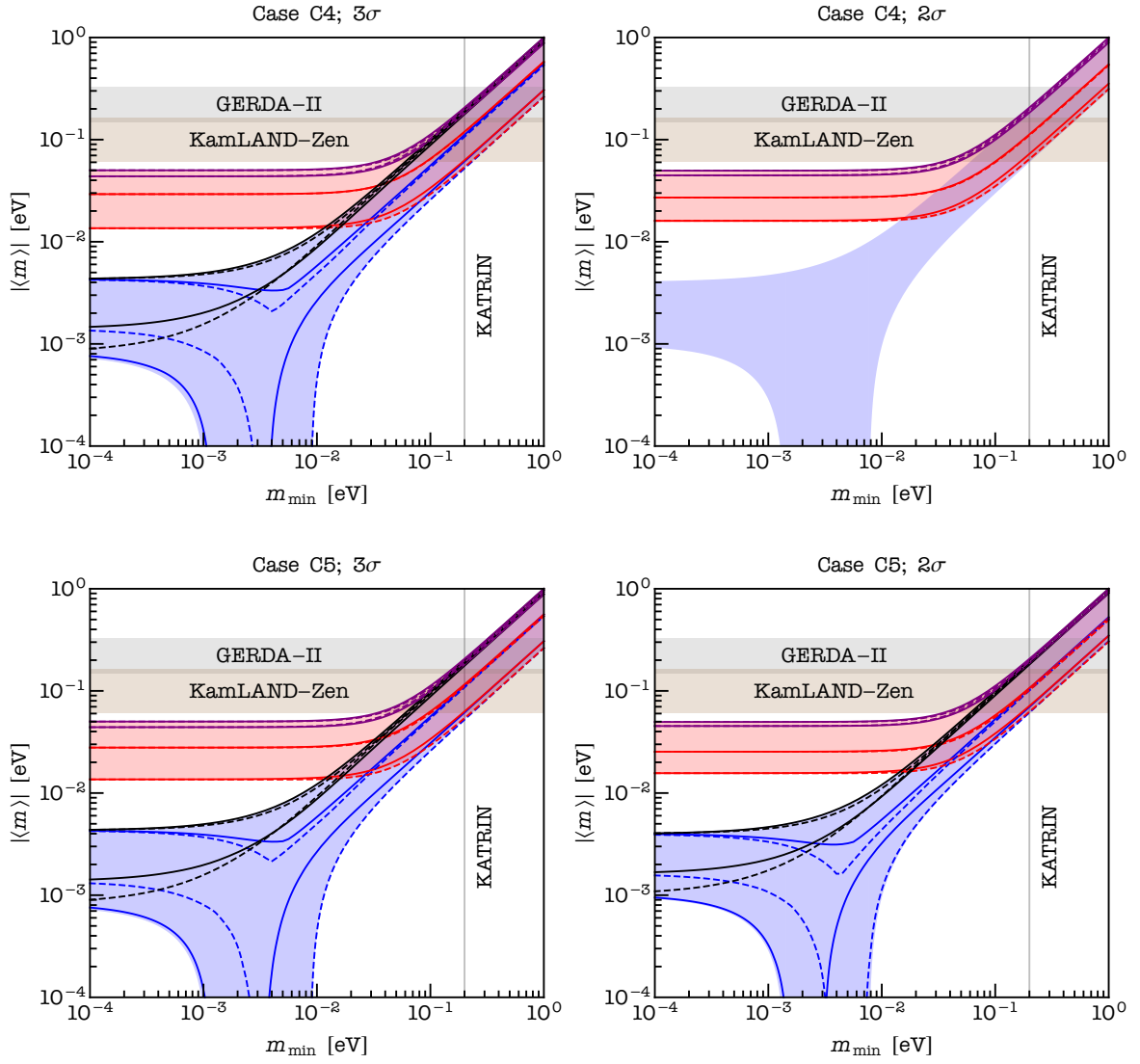


Figure 15: The same as in Fig. 13, but for cases C4 and C5.

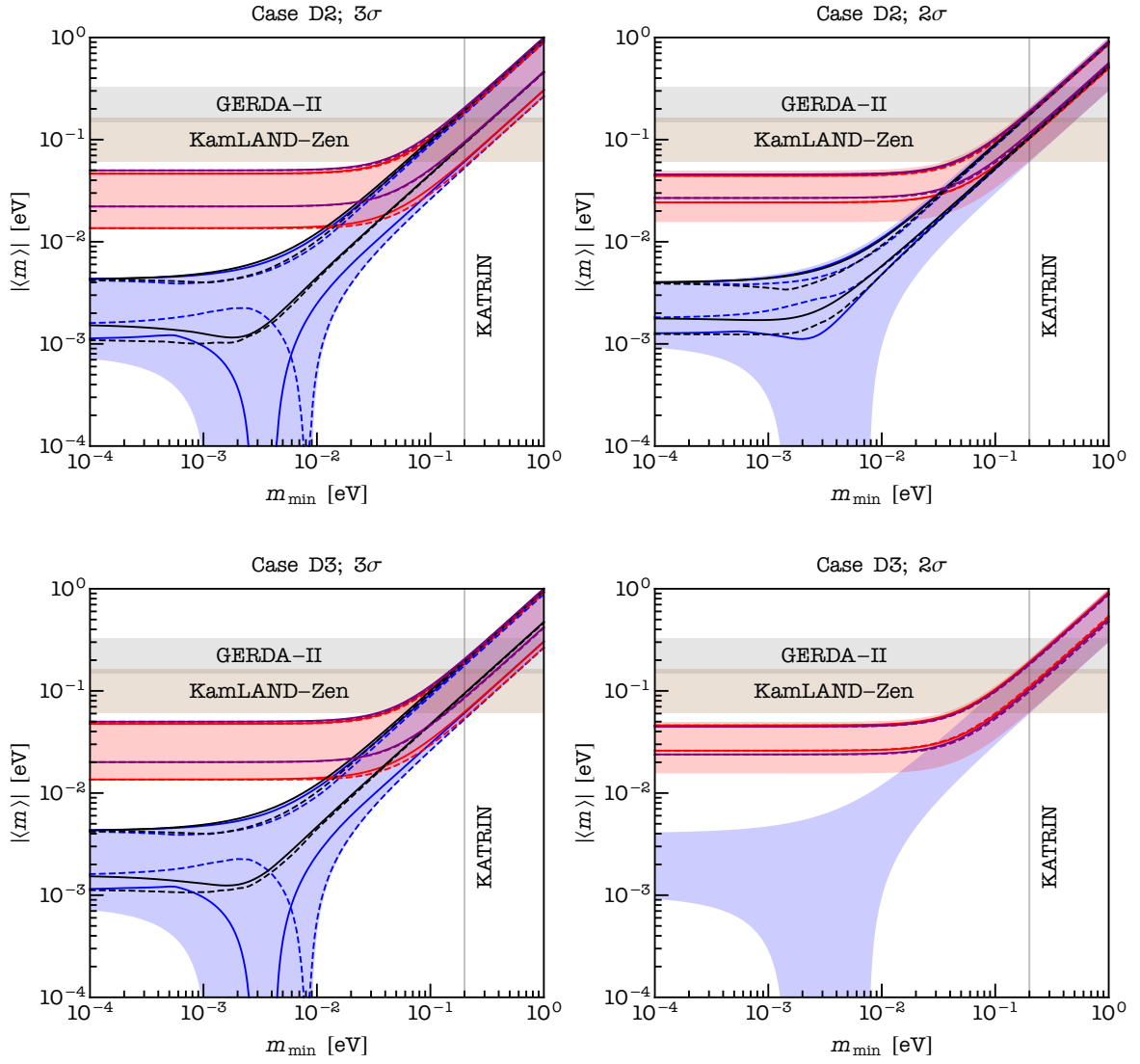


Figure 16: The same as in Fig. 13, but for cases D2 and D3.

5 Summary and Conclusions

In the present article we have derived predictions for the 3-neutrino (lepton) mixing and leptonic Dirac and Majorana CP violation in a class of models based on S_4 lepton flavour symmetry combined with a generalised CP (GCP) symmetry H_{CP} , which are broken to residual $Z_2^{g_e}$ and $Z_2^{g_\nu} \times H_{\text{CP}}^\nu$ symmetries in the charged lepton and neutrino sectors, respectively, where $Z_2^{g_e} = \{1, g_e\}$, $Z_2^{g_\nu} = \{1, g_\nu\}$ and $H_{\text{CP}}^\nu = \{X_\nu\}$, 1 being the unit element of S_4 . The massive neutrinos are assumed to be Majorana particles with their masses generated by the neutrino Majorana mass term of the left-handed (LH) flavour neutrino fields $\nu_{lL}(x)$, $l = e, \mu, \tau$. We show that in this class of models the three neutrino mixing angles, θ_{12} , θ_{23} and θ_{13} , the Dirac and the two Majorana CP violation (CPV) phases, δ and α_{21} , α_{31} , are functions of altogether three parameters — two mixing angles and a phase, θ^e , θ^ν and δ^e .

The S_4 group has 9 different Z_2 subgroups. Assuming that the LH flavour neutrino and charged lepton fields, $\nu_{lL}(x)$ and $l_L(x)$, $l = e, \mu, \tau$, transform under a triplet irreducible unitary representation of S_4 , we prove that there are only 3 pairs of subgroups $Z_2^{g_e}$ and $Z_2^{g_\nu}$ which can lead to different viable (i.e., compatible with the current data) predictions for the lepton mixing. For these three pairs, $\{g_e, g_\nu\} = \{S, TU\}$, $\{TU, S\}$ and $\{TU, U\}$, where S , T and U are the generators of S_4 (see eq. (3.1)) taken here in the triplet representation of S_4 (eq. (3.12)). In what concerns the residual GCP symmetry in the neutrino sector, $H_{\text{CP}}^\nu = \{X_\nu\}$, we show that the constraints on X_ν (following from the conditions of consistency between $Z_2^{g_e}$ and H_{CP}^ν and of having non-degenerate neutrino mass spectrum, $X_\nu = X_\nu^T$) are satisfied in the following cases:

- i) for $g_\nu = S$, if $H_{\text{CP}}^\nu = \{1, S\}$, $\{U, SU\}$ or $\{TST^2U, T^2STU\}$;
- ii) for $g_\nu = U$, if $H_{\text{CP}}^\nu = \{1, U\}$ or $\{S, SU\}$;
- iii) for $g_\nu = TU$, if $H_{\text{CP}}^\nu = \{U, T\}$ or $\{STS, T^2STU\}$.

However, $H_{\text{CP}}^\nu = \{U, SU\}$ and $H_{\text{CP}}^\nu = \{TST^2U, T^2STU\}$ in the case of $g_\nu = S$, and $H_{\text{CP}}^\nu = \{U, T\}$ and $H_{\text{CP}}^\nu = \{STS, T^2STU\}$ in the case of $g_\nu = TU$, are shown to lead to the same predictions for the PMNS neutrino mixing matrix. Thus, we have found that effectively there are 4 distinct groups of cases to be considered. We have analysed them case by case and have classified all phenomenologically viable mixing patterns they lead to. In all four groups of cases the PMNS neutrino mixing matrix is predicted to contain one constant element which does not depend on the three basic parameters, θ^e , θ^ν and δ^e . The magnitude of this element is equal to $1/\sqrt{2}$ in the ‘‘Group A’’ cases of $\{G_e, G_\nu\} = \{Z_2^{TU}, Z_2^S \times H_{\text{CP}}^\nu\}$ with $H_{\text{CP}}^\nu = \{1, S\}$, and in the ‘‘Group B’’ cases of $\{G_e, G_\nu\} = \{Z_2^{TU}, Z_2^S \times H_{\text{CP}}^\nu\}$ with $H_{\text{CP}}^\nu = \{U, SU\}$; and it is equal to $1/2$ in the ‘‘Group C’’ cases of $\{G_e, G_\nu\} = \{Z_2^{TU}, Z_2^U \times H_{\text{CP}}^\nu\}$ with $H_{\text{CP}}^\nu = \{1, U\}$, and in the ‘‘Group D’’ cases of $\{G_e, G_\nu\} = \{Z_2^{TU}, Z_2^U \times H_{\text{CP}}^\nu\}$ with $H_{\text{CP}}^\nu = \{S, SU\}$. In the approach to the neutrino mixing based on S_4 flavour and GCP symmetries employed by us, the PMNS matrix is determined up to permutations of columns and rows. This implies that theoretically any of the elements of the PMNS matrix can be equal by absolute value to $1/\sqrt{2}$ in the Group A and Group B cases, and to $1/2$ in the Group C and Group D cases. However, the data on the neutrino mixing angles and the Dirac phase δ imply that, taking into account the currently allowed 3σ ranges of the PMNS matrix elements (see eqs. (3.10) and (3.11)), only 4 elements, namely, $(U_{\text{PMNS}})_{\mu 2}$, $(U_{\text{PMNS}})_{\mu 3}$, $(U_{\text{PMNS}})_{\tau 2}$ or $(U_{\text{PMNS}})_{\tau 3}$, can have an absolute value equal to $1/\sqrt{2} \approx 0.707$, and only 5 elements, namely, $(U_{\text{PMNS}})_{e 2}$,

$(U_{\text{PMNS}})_{\mu 1}$, $(U_{\text{PMNS}})_{\tau 1}$, $(U_{\text{PMNS}})_{\mu 2}$ or $(U_{\text{PMNS}})_{\tau 2}$, can have an absolute value equal to $1/2$. It should be added that i) $|(U_{\text{PMNS}})_{\tau 2}| = 0.707$ lies outside the respective currently allowed 3σ range in the case of NO neutrino mass spectrum, ii) $|(U_{\text{PMNS}})_{\mu 2}| = 0.707$ is slightly outside the 3σ allowed range for the IO spectrum, and that iii) the value of $|(U_{\text{PMNS}})_{\mu 2}| = 1/2$ is allowed at 3σ only for the IO spectrum.

We have derived predictions for the six parameters of the PMNS matrix, θ_{12} , θ_{23} and θ_{13} , δ , α_{21} and α_{31} , in the potentially viable cases of Groups A–D. This was done for both NO and IO neutrino mass spectra in the cases compatible at 3σ with the existing data. We have performed also a statistical analysis of the predictions for the neutrino mixing angles and CPV phases for each of these cases. We have found that in certain cases the predicted values of the neutrino mixing angles are ruled out, or are strongly disfavoured, by the existing data (see subsection 3.4 for details). These are:

- i) in Group A, the cases of $|(U_{\text{PMNS}})_{\mu 3}| = 1/\sqrt{2}$ (strongly disfavoured), and $|(U_{\text{PMNS}})_{\tau 3}| = 1/\sqrt{2}$ (strongly disfavoured);
- ii) in Group D, the cases of $|(U_{\text{PMNS}})_{e 2}| = 1/2$ (ruled out), $|(U_{\text{PMNS}})_{\mu 2}| = 1/2$ (strongly disfavoured), and $|(U_{\text{PMNS}})_{\tau 2}| = 1/2$ (strongly disfavoured).

The results of the statistical analysis in the viable cases are presented graphically in Figs. 1–11. The predicted ranges of the neutrino mixing parameters and the their corresponding best fit values are summarised in Tables 3–6.

Given the difference in the currently allowed 2σ ranges of $\sin^2 \theta_{23}$ (see Table 1), the prediction for the allowed values of $\sin^2 \theta_{23}$ in certain phenomenologically viable cases makes the IO (NO) spectrum statistically somewhat more favourable than the NO (IO) spectrum. At the same time, we have found that in a large number of viable cases the results we have obtained for the NO and IO spectra are very similar.

As a consequence of the fact that, in the class of models we consider, the six PMNS matrix parameters, θ_{12} , θ_{23} , θ_{13} , δ , α_{21} and α_{31} , are fitted with the three basic parameters, θ^e , θ^ν and δ^e , it is not surprising that we have found that there are strong correlations i) between the values of the Dirac phase δ and the values of the two Majorana phases α_{21} and α_{31} , which in turn are correlated between themselves (Figs. 1, 2, 6–9), and depending on the case ii) either between the values of θ_{12} and θ_{13} (Fig. 5), or between the values of θ_{23} and θ_{13} (Figs. 3 and 4) or else between the values of θ_{12} and θ_{23} (Figs. 1, 2, 6–11). In certain cases our results showed strong correlations between the predicted values of θ_{23} and the Dirac phase δ and/or the Majorana phases $\alpha_{21,31}$ (Figs. 8–11).

In the cases of i) Group B with $|(U_{\text{PMNS}})_{\mu 2}| = 1/\sqrt{2}$, or $|(U_{\text{PMNS}})_{\tau 2}| = 1/\sqrt{2}$, ii) Group C with $|(U_{\text{PMNS}})_{\mu 1}| = 1/2$, or $|(U_{\text{PMNS}})_{\tau 1}| = 1/2$, or $|(U_{\text{PMNS}})_{\mu 2}| = 1/2$, or $|(U_{\text{PMNS}})_{\tau 2}| = 1/2$, and iii) Group D with $|(U_{\text{PMNS}})_{\mu 1}| = 1/2$, or $|(U_{\text{PMNS}})_{\tau 1}| = 1/2$, the cosine of the Dirac phase δ satisfies a sum rule by which it is expressed in terms of the three neutrino mixing angles θ_{12} , θ_{23} and θ_{13} . Taking into account the ranges and correlations of the predicted values of the three neutrino mixing angles, δ is predicted to lie in certain, in most of the discussed cases rather narrow, intervals (subsection 3.4). In the remaining viable cases of Groups B and C, $\cos \delta$ was shown to satisfy sum rules which depend explicitly, in addition to θ_{12} , θ_{23} and θ_{13} , on one of the three basic parameters of the class of models considered, θ^e or θ^ν . In these cases, as we have shown, $\cos \delta$ can take any value.

We have derived also predictions for the Majorana CPV phases α_{21} and α_{31} in all viable cases of Groups B, C and D (subsection 3.4). With one exception — the case of $|(U_{\text{PMNS}})_{e 2}| =$

1/2 of Group C — the values of α_{21} and α_{31} , as we have indicated earlier, are strongly correlated between themselves. In case C1 there is a strong linear correlation between α_{31} and δ .

Using the predictions for the Dirac and Majorana CPV phases allowed us to derive predictions for the magnitude of the neutrinoless double beta decay effective Majorana mass, $|\langle m \rangle|$, as a function of the lightest neutrino mass for all the viable cases belonging to Groups B, C and D. They are presented graphically in Figs. 13–16.

All viable cases in the class of S_4 models investigated in the present article have distinct predictions for the set of observables $\sin^2 \theta_{12}$, $\sin^2 \theta_{23}$, $\sin^2 \theta_{13}$, the Dirac phase δ and the absolute value of one element of the PMNS neutrino mixing matrix. Using future more precise data on $\sin^2 \theta_{12}$, $\sin^2 \theta_{23}$, $\sin^2 \theta_{13}$ and the Dirac phase δ , which will allow also to determine the absolute values of the elements of the PMNS matrix with a better precision, will make it possible to test and discriminate between the predictions of all the cases found by us to be compatible with the current data on the neutrino mixing parameters.

Future data will show whether Nature followed the $S_4 \times H_{\text{CP}}$ flavour + GCP symmetry “three-parameter path” for fixing the values of the three neutrino mixing angles and of the Dirac (and Majorana) CP violation phases of the PMNS neutrino mixing matrix. We are looking forward to these data.

Acknowledgements

We would like to thank F. Capozzi, E. Lisi, A. Marrone, D. Montanino and A. Palazzo for kindly sharing with us the data files for one-dimensional χ^2 projections. This work was supported in part by the INFN program on Theoretical Astroparticle Physics (TASP), by the research grant 2012CPPYP7 under the program PRIN 2012 funded by the Italian Ministry of Education, University and Research (MIUR), by the European Union Horizon 2020 research and innovation programme under the Marie Skłodowska-Curie grants 674896 and 690575, and by the World Premier International Research Center Initiative (WPI Initiative), MEXT, Japan (S.T.P.).

A Symmetry of X_ν

If the neutrino sector respects a residual GCP symmetry $H'_{\text{CP}} = \{X_\nu\}$, the neutrino mass matrix satisfies eq. (2.12), namely,

$$X_\nu^T M_\nu X_\nu = M_\nu^*. \quad (\text{A.1})$$

The GCP transformation matrices X_ν must be unitary due to the GCP invariance of the neutrino kinetic term. In what follows we show that these matrices are additionally constrained to be symmetric if the neutrino mass spectrum is non-degenerate, as is known to be the case.

Expressing M_ν from eq. (2.14) and substituting it in eq. (A.1) yields

$$d_\nu \tilde{X} = \tilde{X}^* d_\nu, \quad (\text{A.2})$$

where $d_\nu \equiv \text{diag}(m_1, m_2, m_3)$ and $\tilde{X} \equiv U_\nu^\dagger X_\nu U_\nu^*$ is unitary.

Being 3×3 unitary, \tilde{X} can be parametrised as the product of three complex rotations U_{ij} and a diagonal matrix of phases Ψ as follows:

$$\tilde{X} = \Psi U_{23}(\vartheta_{23}, \delta_{23}) U_{13}(\vartheta_{13}, \delta_{13}) U_{12}(\vartheta_{12}, \delta_{12}), \quad (\text{A.3})$$

where $\Psi = \text{diag}(e^{i\psi_1}, e^{i\psi_2}, e^{i\psi_3})$ and the $U_{ij}(\vartheta_{ij}, \delta_{ij})$ are complex rotations in the i - j plane. Explicitly,

$$U_{23}(\vartheta_{23}, \delta_{23}) = \begin{pmatrix} 1 & 0 & 0 \\ 0 & \cos \vartheta_{23} & \sin \vartheta_{23} e^{-i\delta_{23}} \\ 0 & -\sin \vartheta_{23} e^{i\delta_{23}} & \cos \vartheta_{23} \end{pmatrix}, \quad (\text{A.4})$$

with a straightforward generalisation to $(ij) = (12), (13)$.

Imposing eq. (A.2) produces the following relations:

$$e^{i(\psi_1 - \delta_{13})} m_1 \sin \vartheta_{13} = e^{-i(\psi_1 - \delta_{13})} m_3 \sin \vartheta_{13}, \quad (\text{A.5})$$

$$e^{i(\psi_2 - \delta_{23})} m_2 \cos \vartheta_{13} \sin \vartheta_{23} = e^{-i(\psi_2 - \delta_{23})} m_3 \cos \vartheta_{13} \sin \vartheta_{23}, \quad (\text{A.6})$$

$$e^{i(\psi_1 - \delta_{12})} m_1 \cos \vartheta_{13} \sin \vartheta_{12} = e^{-i(\psi_1 - \delta_{12})} m_2 \cos \vartheta_{13} \sin \vartheta_{12}. \quad (\text{A.7})$$

From the non-degeneracy of the neutrino mass spectrum it follows that $\sin \vartheta_{13} = \sin \vartheta_{23} = \sin \vartheta_{12} = 0$. Thus, \tilde{X} is constrained to be diagonal and hence symmetric, $\tilde{X}^T = \tilde{X}$. This finally implies that also $X_\nu^T = X_\nu$, i.e., a phenomenologically relevant X_ν must be symmetric.

B Conjugate Pairs of S_4 Elements

As detailed in subsection 2.2, residual flavour symmetries $Z_2^{g_e}$ and $Z_2^{g_\nu}$ which are conjugate to each other lead to the same form of the PMNS matrix. For $G_f = S_4$, there are nine group elements of order two, given in eqs. (3.2) and (3.3), which generate Z_2 subgroups. The resulting 81 pairs of elements $\{g_e, g_\nu\}$ can themselves be partitioned, under the conjugacy relation of eq. (2.25), into the following nine equivalence classes:

- **$\{S, S\}$** , $\{TST^2, TST^2\}$, $\{T^2ST, T^2ST\}$;
- **$\{U, U\}$** , $\{SU, SU\}$, $\{T^2U, T^2U\}$, $\{TU, TU\}$, $\{ST^2SU, ST^2SU\}$, $\{STSU, STSU\}$;
- **$\{T^2ST, S\}$** , $\{TST^2, S\}$, $\{T^2ST, TST^2\}$, $\{S, T^2ST\}$, $\{S, TST^2\}$, $\{TST^2, T^2ST\}$;
- **$\{S, U\}$** , $\{S, SU\}$, $\{TST^2, T^2U\}$, $\{T^2ST, TU\}$, $\{TST^2, ST^2SU\}$, $\{T^2ST, STSU\}$;
- **$\{U, S\}$** , $\{SU, S\}$, $\{T^2U, TST^2\}$, $\{TU, T^2ST\}$, $\{ST^2SU, TST^2\}$, $\{STSU, T^2ST\}$;
- **$\{SU, U\}$** , $\{U, SU\}$, $\{ST^2SU, T^2U\}$, $\{STSU, TU\}$, $\{T^2U, ST^2SU\}$, $\{TU, STSU\}$;
- **$\{S, TU\}$** , $\{S, STSU\}$, $\{S, T^2U\}$, $\{TST^2, TU\}$, $\{S, ST^2SU\}$, $\{T^2ST, U\}$, $\{T^2ST, SU\}$, $\{TST^2, U\}$, $\{T^2ST, T^2U\}$, $\{TST^2, SU\}$, $\{T^2ST, ST^2SU\}$, $\{TST^2, STSU\}$;
- **$\{TU, S\}$** , $\{STSU, S\}$, $\{T^2U, S\}$, $\{TU, TST^2\}$, $\{ST^2SU, S\}$, $\{U, T^2ST\}$, $\{SU, T^2ST\}$, $\{U, TST^2\}$, $\{T^2U, T^2ST\}$, $\{SU, TST^2\}$, $\{ST^2SU, T^2ST\}$, $\{STSU, TST^2\}$;
- **$\{TU, U\}$** , $\{STSU, U\}$, $\{STSU, SU\}$, $\{TU, SU\}$, $\{T^2U, U\}$, $\{TU, T^2U\}$, $\{ST^2SU, U\}$, $\{U, TU\}$, $\{TU, ST^2SU\}$, $\{SU, STSU\}$, $\{U, T^2U\}$, $\{T^2U, TU\}$, $\{U, ST^2SU\}$, $\{SU, T^2U\}$, $\{SU, ST^2SU\}$, $\{T^2U, STSU\}$, $\{ST^2SU, STSU\}$, $\{ST^2SU, TU\}$, $\{STSU, ST^2SU\}$, $\{STSU, T^2U\}$, $\{SU, TU\}$, $\{ST^2SU, SU\}$, $\{T^2U, SU\}$, $\{U, STSU\}$;

where in boldface we have identified a representative pair of elements for each class, matching the choice made in eqs. (3.4) and (3.5).

C Equivalent Cases

A necessary condition for two matrices U_{PMNS} and U'_{PMNS} to be equivalent is the same magnitude of the fixed element. Indeed, in the four cases under consideration the absolute value of one element is $1/\sqrt{2}$. For $P_e = P'_e$ and $P_\nu = P'_\nu$, the two matrices U_{PMNS} and U'_{PMNS} would be equivalent, if the products $\Omega_e^\dagger \Omega_\nu$ and $\Omega_e'^\dagger \Omega'_\nu$ could be related in the following way:

$$\Omega_e^\dagger \Omega_\nu = \text{diag}(e^{i\phi_1}, e^{i\phi_2}, e^{i\phi_3}) U_{23}(\theta_\circ^e, \delta_\circ^e) \Omega_e'^\dagger \Omega'_\nu R_{23}(\theta_\circ^\nu) \text{diag}(1, i^k, i^k), \quad (\text{C.1})$$

with ϕ_i , δ_\circ^e and θ_\circ^e , θ_\circ^ν being fixed phases and angles, respectively, and k is allowed to be 0, 1, 2 or 3. Indeed, if this relation holds, from eq. (2.24) we have

$$\begin{aligned} U_{\text{PMNS}} &= P_e U_{23}(\theta^e, \delta^e) \text{diag}(e^{i\phi_1}, e^{i\phi_2}, e^{i\phi_3}) U_{23}(\theta_\circ^e, \delta_\circ^e) \Omega_e'^\dagger \Omega'_\nu R_{23}(\theta_\circ^\nu) \text{diag}(1, i^k, i^k) R_{23}(\theta^\nu) P_\nu Q_\nu \\ &= P_e \text{diag}(e^{i\phi_1}, e^{i\phi_2}, e^{i\phi_3}) U_{23}(\theta^e, \tilde{\delta}^e) U_{23}(\theta_\circ^e, \delta_\circ^e) \Omega_e'^\dagger \Omega'_\nu R_{23}(\hat{\theta}^\nu) P_\nu \hat{Q}_\nu, \end{aligned} \quad (\text{C.2})$$

with

$$\tilde{\delta}^e = \delta^e + \phi_2 - \phi_3, \quad \hat{\theta}^\nu = \theta_\circ^\nu + \theta^\nu \quad \text{and} \quad \hat{Q}_\nu = P_\nu^T \text{diag}(1, i^k, i^k) P_\nu Q_\nu. \quad (\text{C.3})$$

Now, using

$$U_{23}(\theta^e, \tilde{\delta}^e) U_{23}(\theta_\circ^e, \delta_\circ^e) = \text{diag}(1, e^{i\alpha}, e^{-i\alpha}) U_{23}(\hat{\theta}^e, \hat{\delta}^e), \quad (\text{C.4})$$

where (see Appendix B in [7])

$$\begin{aligned} \alpha &= \arg \left\{ \cos \theta^e \cos \theta_\circ^e - \sin \theta^e \sin \theta_\circ^e e^{i(\delta_\circ^e - \tilde{\delta}^e)} \right\}, \quad \beta = \arg \left\{ \sin \theta^e \cos \theta_\circ^e e^{-i\tilde{\delta}^e} + \cos \theta^e \sin \theta_\circ^e e^{-i\delta_\circ^e} \right\}, \\ \cos \hat{\theta}^e &= \left| \cos \theta^e \cos \theta_\circ^e - \sin \theta^e \sin \theta_\circ^e e^{i(\delta_\circ^e - \tilde{\delta}^e)} \right|, \quad \sin \hat{\theta}^e = \left| \sin \theta^e \cos \theta_\circ^e e^{-i\tilde{\delta}^e} + \cos \theta^e \sin \theta_\circ^e e^{-i\delta_\circ^e} \right| \\ &\quad \text{and} \quad \hat{\delta}^e = \alpha - \beta, \end{aligned}$$

we obtain

$$U_{\text{PMNS}} = Q_e P_e U_{23}(\hat{\theta}^e, \hat{\delta}^e) \Omega_e'^\dagger \Omega'_\nu R_{23}(\hat{\theta}^\nu) P_\nu \hat{Q}_\nu, \quad (\text{C.5})$$

with

$$Q_e = P_e \text{diag} \left(e^{i\phi_1}, e^{i(\phi_2 + \alpha)}, e^{i(\phi_3 - \alpha)} \right) P_e^T \quad (\text{C.6})$$

being the matrix of unphysical phases. Thus, up to this matrix, U_{PMNS} and U'_{PMNS} are the same.

Taking $\{G_e, G_\nu\} = \{Z_2^{TU}, Z_2^S \times H_{\text{CP}}^\nu\}$ with $H_{\text{CP}}^\nu = \{U, SU\}$ as a reference case and denoting the corresponding diagonalising matrices as Ω_e' and Ω'_ν , we find the values of ϕ_i , δ_\circ^e , θ_\circ^e , θ_\circ^ν and k for which eq. (C.1) holds, if Ω_e and Ω_ν are the diagonalising matrices in one of the three remaining cases under consideration. We summarise these values in Table 8.

D Correspondence with Earlier Results

The sum rules for $\cos \delta$ or $\sin^2 \theta_{23}$ ($\sin^2 \theta_{12}$ in case C1) can formally be obtained from the corresponding sum rules derived in [7]. In certain cases, this requires an additional input which is provided by the residual GCP symmetry H_{CP}^ν considered in the present article. Below we provide the correspondence between the phenomenologically viable cases of the present study and the cases considered in [7].

g_e	g_ν	H_{CP}^ν	S	TU	$\{U, T\}$	S	TU	$\{STS, T^2STU\}$	TU	S	$\{TST^2U, T^2STU\}$
ϕ_1				$\pi/6$				$-\pi/3$			$-\pi/2$
ϕ_2			$-\arctan \sqrt{1 + 2\sqrt{2}/3}$					$-\arctan(\sqrt{2} + \sqrt{3})$			$\text{arccot}(2)$
ϕ_3			$\arctan(3\sqrt{3} + 2\sqrt{6})$					$\text{arccot}(2\sqrt{2} + \sqrt{3})$			$\arctan(2)$
δ_\circ^e			$\text{arccot}(5/\sqrt{3})$					$\pi/3$			$\arctan((5\sqrt{3} - 6)/13)$
θ_\circ^e			$\arctan \sqrt{(11 - 6\sqrt{2})/7}$					$\arctan(\sqrt{2} + \sqrt{3})$			$\pi - \arctan(2/\sqrt{5})$
θ_\circ^ν			$\pi - \arctan(3 - 2\sqrt{2})$					$\pi/4$			$\pi/4$
k								0			1

Table 8: The values of the parameters ϕ_i , δ_\circ^e , θ_\circ^e , θ_\circ^ν and k for which eq. (C.1), proving the equivalence of the PMNS matrix in a given case to the PMNS matrix in the reference case of $\{G_e, G_\nu\} = \{Z_2^{TU}, Z_2^S \times H_{\text{CP}}^\nu\}$ with $H_{\text{CP}}^\nu = \{U, SU\}$, holds.

- i) Cases B1, C4 and D4 of the present study correspond to case C8 in [7], since for all these cases $(U_{\text{PMNS}})_{\mu 2}$ is fixed. The sum rule for $\cos \delta$ in case B1, eq. (3.46), follows from that of case C8 in [7] (see Table 4 therein) for $\sin^2 \theta_{23}^\circ = 1/2$, while the sum rule in eq. (3.57), valid in cases C4 and D4, can be obtained from the same sum rule found in [7], but for $\sin^2 \theta_{23}^\circ = 3/4$. As should be, these two values of $\sin^2 \theta_{23}^\circ$ follow from $G_f = S_4$, when it is broken to two different non-equivalent specific pairs of residual $\{Z_2^{g_e}, Z_2^{g_\nu}\}$ flavour symmetries (see Table 10 in [7]).
- ii) Cases B2, C5 and D5 correspond to case C1 in [7], since for all of them $(U_{\text{PMNS}})_{\tau 2}$ is fixed. The sum rule for $\cos \delta$ in case B2, eq. (3.47), follows from that of case C1 in [7] (see Table 4 therein) for $\sin^2 \theta_{23}^\circ = 1/2$, while the sum rule in eq. (3.58), valid in cases C5 and D5, can be obtained from the same sum rule found in [7], but for $\sin^2 \theta_{23}^\circ = 1/4$. Again, these values of $\sin^2 \theta_{23}^\circ$ are fixed uniquely by $G_f = S_4$ and the specific choice of the residual symmetries considered in the present article ¹⁶.
- iii) Cases A1 and B3 of the present study correspond to case C2 in [7], since for these cases $(U_{\text{PMNS}})_{\mu 3}$ is fixed. The expression for $\sin^2 \theta_{23}$ in eq. (3.35) follows from the corresponding expression for case C2 in Table 6 of [7] with $\sin^2 \theta_{23}^\circ = 1/2$. This value is in agreement with Table 10 of [7]. Moreover, the sum rule for $\cos \delta$ in eq. (3.37) in case A1 can be obtained from the sum rule for case C2 ¹⁷ in Table 4 of [7] with $\sin^2 \theta_{23}^\circ = 1/2$ and $\sin^2 \hat{\theta}_{12}^\nu = 1/2$. The value of $\sin^2 \hat{\theta}_{12}^\nu$, which was an arbitrary free parameter in [7], is fixed by the GCP symmetry employed in the present study. Finally, we note that the expression for $\cos \delta$ in eq. (3.49) valid in case B3 can formally be obtained from the corresponding expression in case C2 of Table 4 in [7] setting $\hat{\theta}_{12}^\nu = \theta^\nu - \pi/4$.
- iv) Analogously, cases A2 and B4 correspond to case C7 in [7]. Equation (3.38) can be obtained from the corresponding formula in Table 6 of [7] for $\sin^2 \theta_{23}^\circ = 1/2$, which

¹⁶Note that the value of $\sin^2 \theta_{23}^\circ = 1/2$ is not present in Table 10 of [7], since in this reference the best fit values of the mixing angles for the NO spectrum quoted in eqs. (6)–(8) therein have been used, and employing them, one obtains $\cos \delta \approx 2.76$.

¹⁷We would like to point out a typo in eq. (85) in [7]: $\cos^2 \theta_{23}^\circ$ should read $\cos \theta_{23}^\circ$. This typo, however, does not affect the corresponding sum rule for $\cos \delta$ in eq. (86) and in Table 4 of [7].

agrees with the result in Table 10 therein. The sum rule in eq. (3.40) follows from that in case C7 in Table 4 of [7] with $\sin^2 \theta_{23}^o = 1/2$ and $\sin^2 \hat{\theta}_{12}^\nu = 1/2$, where again the value of $\sin^2 \hat{\theta}_{12}^\nu$, which in [7] is a free parameter, here is fixed by the GCP symmetry. Similarly to the previous clause, eq. (3.51) can formally be derived from the corresponding expression in case C7 of Table 4 in [7] setting $\hat{\theta}_{12}^\nu = \theta^\nu - \pi/4$.

- v) Case C1 corresponds to case C5 in [7], in which all possible residual flavour symmetries $G_e = Z_2$ and $G_\nu = Z_2$ have been considered. The expression for $\sin^2 \theta_{12}$ in eq. (3.53) follows from that of case C5 in Table 6 in [7] with $\sin^2 \theta_{12}^o = 1/4$. This value of $\sin^2 \theta_{12}^o$ is found for $G_f = S_4$ and the specific choice of the residual symmetries (see Table 10 in [7]). Moreover, eq. (3.56) for $\cos \delta$ can formally be obtained from the corresponding formula in case C5 of Table 4 in [7] setting $\sin^2 \hat{\theta}_{23}^e = \sin^2 \theta^e$.
- vi) Cases C2 and D2 correspond to case C4 of [7]. The sum rule for $\cos \delta$ in eq. (3.37), valid in cases C2 and D2, follows from that of case C4 in [7] (see Table 4 therein) for $\sin^2 \theta_{12}^o = 1/4$, which is in agreement with Table 10 in [7].
- vii) Cases C3 and D3 correspond to case C3 in [7]. Equation (3.40) for $\cos \delta$, which holds in these cases, can be obtained from the corresponding sum rule for case C3 from Table 4 in [7] with $\sin^2 \theta_{13}^o = 1/4$. As it should be, we find this value in Table 10 of [7].

References

- [1] K. Nakamura and S. T. Petcov in C. Patrignani *et al.* [Particle Data Group Collaboration], *Chin. Phys. C* **40** (2016) 100001.
- [2] G. Altarelli and F. Feruglio, *Rev. Mod. Phys.* **82** (2010) 2701 [arXiv:1002.0211 [hep-ph]].
- [3] H. Ishimori *et al.*, *Prog. Theor. Phys. Suppl.* **183** (2010) 1 [arXiv:1003.3552 [hep-th]].
- [4] S. F. King *et al.*, *New J. Phys.* **16** (2014) 045018 [arXiv:1402.4271 [hep-ph]].
- [5] S. T. Petcov, *Nucl. Phys. B* **892** (2015) 400 [arXiv:1405.6006 [hep-ph]].
- [6] I. Girardi, S. T. Petcov and A. V. Titov, *Eur. Phys. J. C* **75** (2015) 345 [arXiv:1504.00658 [hep-ph]].
- [7] I. Girardi, S. T. Petcov, A. J. Stuart and A. V. Titov, *Nucl. Phys. B* **902** (2016) 1 [arXiv:1509.02502 [hep-ph]].
- [8] D. Marzocca, S. T. Petcov, A. Romanino and M. C. Sevilla, *JHEP* **1305** (2013) 073 [arXiv:1302.0423 [hep-ph]].
- [9] M. Tanimoto, *AIP Conf. Proc.* **1666** (2015) 120002.
- [10] P. Ballett *et al.*, *Phys. Rev. D* **89** (2014) 016016 [arXiv:1308.4314 [hep-ph]].
- [11] S. F. Ge, D. A. Dicus and W. W. Repko, *Phys. Rev. Lett.* **108** (2012) 041801 [arXiv:1108.0964 [hep-ph]]; *Phys. Lett. B* **702** (2011) 220 [arXiv:1104.0602 [hep-ph]].
- [12] S. Antusch, S. F. King, C. Luhn and M. Spinrath, *Nucl. Phys. B* **856** (2012) 328 [arXiv:1108.4278 [hep-ph]].

- [13] A. D. Hanlon, S. F. Ge and W. W. Repko, Phys. Lett. B **729** (2014) 185 [arXiv:1308.6522 [hep-ph]];
- [14] I. Girardi, S. T. Petcov and A. V. Titov, Nucl. Phys. B **894** (2015) 733 [arXiv:1410.8056 [hep-ph]]; Int. J. Mod. Phys. A **30** (2015) 1530035 [arXiv:1504.02402 [hep-ph]].
- [15] S. M. Bilenky, J. Hosek and S. T. Petcov, Phys. Lett. B **94** (1980) 495.
- [16] G. C. Branco, L. Lavoura and M. N. Rebelo, Phys. Lett. B **180** (1986) 264.
- [17] F. Feruglio, C. Hagedorn and R. Ziegler, JHEP **1307** (2013) 027 [arXiv:1211.5560 [hep-ph]].
- [18] M. Holthausen, M. Lindner and M. A. Schmidt, JHEP **1304** (2013) 122 [arXiv:1211.6953 [hep-ph]].
- [19] G. J. Ding, S. F. King, C. Luhn and A. J. Stuart, JHEP **1305** (2013) 084 [arXiv:1303.6180 [hep-ph]].
- [20] G. J. Ding, S. F. King and A. J. Stuart, JHEP **1312** (2013) 006 [arXiv:1307.4212 [hep-ph]].
- [21] C. C. Li and G. J. Ding, JHEP **1505** (2015) 100 [arXiv:1503.03711 [hep-ph]].
- [22] A. Di Iura, C. Hagedorn and D. Meloni, JHEP **1508** (2015) 037 [arXiv:1503.04140 [hep-ph]].
- [23] P. Ballett, S. Pascoli and J. Turner, Phys. Rev. D **92** (2015) no.9, 093008 [arXiv:1503.07543 [hep-ph]].
- [24] F. Capozzi *et al.*, Phys. Rev. D **95** (2017) no.9, 096014 [arXiv:1703.04471 [hep-ph]].
- [25] I. Esteban *et al.*, JHEP **1701** (2017) 087 [arXiv:1611.01514 [hep-ph]].
- [26] C. Y. Yao and G. J. Ding, Phys. Rev. D **94** (2016) no.7, 073006 [arXiv:1606.05610 [hep-ph]].
- [27] I. Girardi, A. Meroni, S. T. Petcov and M. Spinrath, JHEP **1402** (2014) 050 [arXiv:1312.1966 [hep-ph]].
- [28] J. Turner, Phys. Rev. D **92** (2015) no.11, 116007 [arXiv:1507.06224 [hep-ph]].
- [29] I. Girardi, S. T. Petcov and A. V. Titov, Nucl. Phys. B **911** (2016) 754 [arXiv:1605.04172 [hep-ph]].
- [30] J. N. Lu and G. J. Ding, Phys. Rev. D **95** (2017) no.1, 015012 [arXiv:1610.05682 [hep-ph]].
- [31] C. Hagedorn, S. F. King and C. Luhn, JHEP **1006** (2010) 048 [arXiv:1003.4249 [hep-ph]].
- [32] C. C. Li and G. J. Ding, JHEP **1508** (2015) 017 [arXiv:1408.0785 [hep-ph]].
- [33] Private communication with F. Capozzi.

- [34] S. F. King and C. Luhn, Nucl. Phys. B **820** (2009) 269 [arXiv:0905.1686 [hep-ph]].
- [35] P. I. Krastev and S. T. Petcov, Phys. Lett. B **205** (1988) 84.
- [36] S. M. Bilenky, S. Pascoli and S. T. Petcov, Phys. Rev. D **64** (2001) 053010 [hep-ph/0102265].
- [37] J. F. Nieves and P. B. Pal, Phys. Rev. D **36** (1987) 315.
- [38] J. A. Aguilar-Saavedra and G. C. Branco, Phys. Rev. D **62** (2000) 096009 [hep-ph/0007025].
- [39] J. F. Nieves and P. B. Pal, Phys. Rev. D **64** (2001) 076005 [hep-ph/0105305].
- [40] S. M. Bilenky and S. T. Petcov, Rev. Mod. Phys. **59** (1987) 671.
- [41] W. Rodejohann, Int. J. Mod. Phys. E **20** (2011) 1833 [arXiv:1106.1334 [hep-ph]]; S. T. Petcov, Adv. High Energy Phys. **2013** (2013) 852987 [arXiv:1303.5819 [hep-ph]].
- [42] J. Ling [Daya Bay Collaboration], PoS ICHEP **2016** (2016) 467.
- [43] F. An *et al.* [JUNO Collaboration], J. Phys. G **43** (2016) no.3, 030401 [arXiv:1507.05613 [physics.ins-det]]; Y. F. Li, Int. J. Mod. Phys. Conf. Ser. **31** (2014) 1460300 [arXiv:1402.6143 [physics.ins-det]].
- [44] K. Abe *et al.* [T2K Collaboration], PTEP **2015** (2015) no.4, 043C01 [arXiv:1409.7469 [hep-ex]]; arXiv:1609.04111 [hep-ex].
- [45] K. Abe *et al.*, PTEP **2015** (2015) 053C02 [arXiv:1502.05199 [hep-ex]].
- [46] R. Acciarri *et al.* [DUNE Collaboration], arXiv:1512.06148; arXiv:1601.05471; arXiv:1601.02984.
- [47] A. Gando *et al.* [KamLAND-Zen Collaboration], Phys. Rev. Lett. **117** (2016) no.8, 082503; Addendum: Phys. Rev. Lett. **117** (2016) no.10, 109903 [arXiv:1605.02889 [hep-ex]].
- [48] M. Agostini *et al.* [GERDA Collaboration], Nature **544** (2017) 47 [arXiv:1703.00570 [nucl-ex]].
- [49] J. D. Vergados, H. Ejiri and F. Šimkovic, Int. J. Mod. Phys. E **25** (2016) no.11, 1630007 [arXiv:1612.02924 [hep-ph]].
- [50] S. Pascoli and S. T. Petcov, Phys. Lett. B **544** (2002) 239 [hep-ph/0205022]; Phys. Lett. B **580** (2004) 280 [hep-ph/0310003].
- [51] S. Dell’Oro, S. Marcocci, M. Viel and F. Vissani, Adv. High Energy Phys. **2016** (2016) 2162659 [arXiv:1601.07512 [hep-ph]].
- [52] S. T. Petcov, Nucl. Phys. B **908** (2016) 279.
- [53] K. Eitel, Nucl. Phys. Proc. Suppl. **143** (2005) 197.